INSPECTION OF HISTORIC STEEL BRIDGES USING ULTRASONIC PHASED ARRAY

A Thesis

by

ALEJANDRA LUCIA ROLDAN ARCOS

Submitted to the Office of Graduate and Professional Studies of
Texas A&M University
in partial fulfillment of the requirements for the degree of

MASTER OF SCIENCE

Chair of Committee,	Stefan Hurlebaus
Committee Members,	Gary Fry
	Robert Warden
Head of Department,	Robin Autenrieth

May 2014

Major Subject: Civil Engineering

ABSTRACT

The use of ultrasonic phased array (UPA) technology for inspection of the trunnion bearing pin of the 100-year old Salmon Bay Bascule Bridge is the focus of this research. To thoroughly investigate the bearing pin, two main objectives are addressed: the development of a UPA system, including the design of a case that uses a Poly Methyl Meth Acrylate (PMMA) material to house the transducer, and the implementation of the system in the field to test the feasibility of the UPA system and its application as a nondestructive testing unit.

Two different testing settings are carried out in this research. The first study is performed in a lab-based setting on a mock-up model pin. This model is used as a reference to provide the calibration of the UPA system using the exterior edge, two keyholes, and three diagonal interior grease holes. The second study is performed in a field-based setting on the authentic trunnion bearing pin taken out of service from the Salmon Bay Bridge in Seattle, Washington, currently residing at the Riverside Campus. This pin has three similar diagonal holes, keyholes, and unknown internal defects. Real-time measurements using the UPA system is used to identify the exterior surfaces and the keyholes of the original pin.

The results of the inspection of the pins using the UPA system indicate the accuracy of the real-time data taken from the probe measurements. It was limited to seeing perpendicular defects and exterior sides, and could not identify the diagonal grease hole within both pin parts. It did, however, identify the keyholes, and was later verified by visual inspection once the sleeves were removed. The original pin showed no internal defects.

For future research in nondestructive testing used in historic trunnion pins, it is recommended to combine this technology with an automatic system that allows the reduction of human interaction with the inspection. A membrane-like surface adaptable

to rough faces, along with a constant flow of water between the wedge and surface, would facilitate the need to remove the PMMA case out of the pin to re-apply couplant for inspections. Finally, a modified angled wedge could also be applied within the PMMA case to search for different angled cracking.

DEDICATION

To my grandmothers, Isabel Roldan Cornejo and Emperatriz Arcos Alarcon.

ACKNOWLEDGEMENTS

I would like to thank my committee chair, Dr. Hurlebaus, for his patience and guidance throughout all of my research endeavors. I would also like to thank my committee members, Prof. Warden for getting me involved with historic preservation, and Dr. Fry for his encouragement and aid throughout the course of this research.

Thanks also to Dr. Story for all of his insight in the Salmon Bay Bridge and his bascule bridge knowledge. A special thanks to Jae Baik for all of the help with phased arrays and the set-up of my testing, and Josh White for helping me with the design of the PMMA case model. Thank you to the workers from Riverside Campus with the removal of the pin sleeves. Also, thanks to many of the faculty at Texas A&M who have pushed me to excel in my research and my academic career.

Thanks to my family and friends for their love and support during my graduate and research years. The constant encouragement of my parents, Edwin and Lucy Roldan, and my brothers, Francisco, Rodrigo, and Fernando, will never be forgotten. A special thank you to Pierre Brandicourt whose willingness to listen and to provide words of encouragement always brought me peace and motivation to finish.

Finally, thank you Lord Jesus for your love throughout everything.

TABLE OF CONTENTS

LIST OF FIGURES

LIST OF TABLES

TABLE Page

1. INTRODUCTION

Through civil engineering, structures are able to beautify their surroundings while also providing a service to civilians. ASCE acknowledges that bridges are a visible icon of the civil engineer's art (DeLony and Klein, 2005). Bridges display the creative and ingenious designs of the past, provide safe and viable transportation for the society, and carry on part of the nation's engineering identity for future generations. Each bridge becomes embedded in a community's history and has a valuable story of its coming into existence, but not all bridges are officially acknowledged as "historic." The National Park Service and the Secretary of the Interior's Standards recognize historic properties as an important asset to the nation's identity, but they cannot cover all properties and many individuals or companies are hesitant to register their property because the recognition limits a property's maintenance. Bridges that are not recognized officially as "historic" may still possess cultural and historic values important to the engineering society. The Secretary of Interior's Standards for the Treatment of Historic Properties can provide a good guideline for bridge rehabilitation projects to all types of bridges, even though the standards may not be a requirement. These bridges still need to be maintained to safely and properly function as a crossing for civilians.

Many of America's bridges are in danger of losing their functional value. ASCE's 2009 Report Card for America's Infrastructure rated the nation's transportation bridge faction a mediocre "C" commenting that 12.1% of the bridges were structurally deficient, and 14.8% functionally obsolete (ASCE, 2009). The most recent ASCE 2013 Report Card rated the transportation a "C+," but the percentages are about the same as in 2009, with the exception that the percent of structurally deficient bridges increased to 24.9% in the nation (ASCE, 2013). The low rates of the nation's bridges affect which new, renovation, or reconstruction public bridge projects take precedence over others. Bridge inspection facilitates this concern, in which the symptoms of structural or mechanical

wearing can be detected and treated properly before a critical problem develops. Early detection through inspection can also minimize future structural failure costs.

As America's infrastructure ages, faster and reliable inspection and evaluation methods are required. In order to provide efficient inspection, non-destructive evaluation (NDE) has become a generally accepted practice because it allows for inspection without altering the structure. A type of non-destructive testing (NDT) system is ultrasonics, which provide many advantages, including its surface sensitivity, single-side access, minimal part preparation, and detailed images.

NDT systems have been implemented in various bridge inspections and are very popular in historic bridges. A typical example of NDT in historic bridges has been in the analysis of Aramid fiber reinforced polymers (AFRP) strengthening implementation on the historic cast-iron Corona Bridge in Venice, Italy. The research group preferred to use ultrasonics due to its better sensitivity, even though it was more time consuming (Bastianini et al., 2004). Because not all AFRP reinforcement would be reachable for visual inspection, the bridge would benefit from the ultrasonic pulse echo amplitude-based NDT. Their testing technique differs from the standard United States echo testing technique, which is based on the delay time of the echoes rather than the amplitude (Bastianini et al., 2004). This case study is still a well-presented project in which the flexibility of ultrasonic testing is distinguishable.

An emerging system which provides more flexibility in inspection compared to conventional ultrasonic systems is the ultrasound phased array systems. Conventional ultrasonic transducers allow for a pulse reading, where it produces a single voltage pulse which is then received back in the system. Phased arrays can use multiple elements, following a user-specified focus law, to detect imperfections. This allows for a sweep scan through different angles with a single probe, covering more area than a conventional ultrasonic pulse velocity at a faster rate. Companies like WINS: WavesinSolids LLC, TÜV Rheinland Industrial Solutions, and EWI are taking advantage of ultrasonic phased array

(UPA) testing to inspect steel bridge pins and other components. Their bridge inspection techniques adequately provide valuable insight, but documentation on the inspection of movable bridge parts are still limited. There is still a need to challenge the usage of phased array ultrasonic through the inspection of these parts, especially because some of these parts, like the trunnion bearings, are vital to the operation of the bridge, and also because limited documentation is available.

1.1 Literature Review

The objective of non-destructive testing is to identify cracking and other deformities in places that are difficult to view by eyesight. Conventional ultrasonic testing is based on acoustics, or time-varying deformations or vibrations in materials introduced through longitudinal and shear waves. A conventional transducer is made of a single piezoelectric (PZT) element (Song et al., 2000) that can generate a pulse and receive a voltage signal to identify deformations. The PZT element can deform by receiving an electrical signal, or vice versa, can receive an electric signal and deform accordingly. The conventional transducers typically use a conventional wedge for inspection to protect the sensitivity of the elements, but primarily to allow for the angle beam diffraction. Pospisil et al. (2005) remark that NDT is a fast and cheap way to evaluate bridges. Rens and Kim (2006) and Wood and Rens (2006) consider NDT as a valuable tool because of the various techniques it offers. The most frequent methods include ultrasound, infrared camera, radar, electric potential measurement, radiography, and vibration analysis (Pospisil et al., 2005). For steel inspections, AASHTO (1998) lists x-ray radiography, magnetic particle, eddy current, dye penetrant, and ultrasonic as applicable techniques. The use of ultrasonic testing has been seen in the Lawrence Street Bridge (Wood and Rens, 2006) and the Quebec Bridge (Rens and Kim, 2006). Both inspections applied the Ultrasonic Pulse Velocity (UPV) method to test for the elastic properties of concrete pier caps. Melewski et al. (2009) mentions the inspection of steel members on the historic Poughkeepsie-Highland Railroad Bridge using non-destructive ultrasonic thick gauging. Sparks (2008) suggests

the use of conventional ultrasonic transducers using longitudinal waves to inspect steel pins in historic bridges.

The AASHTO Inspection Manual (AASHTO, 1998) also suggests the use of NDT to supplement visual inspection methods to identify internal cracks as an assessment of various structural and electrical components. Table 1.1, partly reproduced from Table C2.10.1-1 of the AASHTO manual, shows the different test methods encouraged by AASHTO (1998) to be used on steel testing. Especially for in-depth inspection where cracks are suspected, nondestructive means are encouraged and should be performed by experienced technicians. Ultrasonic testing can be performed longitudinally, radially, or at various angles to locate cracks, forging flaws, and other interior defects in the material resulted from fabrication, stress, or impact (AASHTO, 1998). The AASHTO Manual for Condition Evaluation of Bridges also shows the capabilities of different NDE with respect to the defect detections, reproduced in Table 1.2. AASHTO (1994) notes that the major advantages of ultrasonics as its portability, sensitivity, and ability to detect the location of cracks or defects in depth. Examining Table 1.2 indicates that ultrasonic capabilities are flexible compared to the rest of the nondestructive testings. Its faults, as commented by AASHTO (1994), are its sensitivity because the observer may see irrelevant information to the inspection, like grain size in metals; its inability to inspect surface defects well; and its dependence on the operator skill.

Table 1.1: List of Test Methods (AASHTO, 1998)

Test Material	Method Description	Comments
Steel	X-ray Radiography	Radiation hazard during test.
	Magnetic Particle	May leave permanent magnetism.
	Eddy Current	Only good for simple geometry.
	Dye Penetrant	Only good for surface defects.
	Ultrasonic	Small defects not detectable.

Table 1.2: Capacity of Nondestructive Examination Techniques for Detecting Defects in Steel Structures in Field Use, taken from AASHTO (1994).

Method Based on		Minute Surface Cracks	Deeper Surface Cracks	Internal Cracks	Fatigue Cracks	Internal Voids	Porosity and Slag in Welds	Thickness	Stress Corrosion	Blistering	Corrosion Pits
Radiography		N	F	F	P	G	G	F	F	P	G
Magnetic Particle (A.C.)	Wet	G	G	N	G	N	N	N	G	N	N
	Dry	F	G	N	G	N	N	N	F	N	P
Eddy Current		F	G	N	N	N	P	P	N	N	N
Dye Penetrants		F	G	N	G	N	N	N	G	N	F
Ultrasonics		P	G	G	G	G	F	G	F	F	P
G=Good;F=Fair;P=Poor;N=Not suitable.											

Because of the advantages of ultrasonic as a strong NDT, and because of the encouragement for more research to be undertaken to make ultrasonics more widely applicable in the field of steel bridge examination from AASHTO (1994), then it is a feasible argument to use ultrasonic testing to inspect the trunnion bearing pins for this research.

Different types of NDT for steel structures have been investigated because of their many advantages over other inspection techniques. Dynamic thermography using inductive heating (Walle and Netzelmann, 2006) was used to detect perpendicular and slanted surface cracks in steel components. Alternative current (AC) thermography methods were also applied to rail axle inspection, while also combining phased array ultrasonic technology to inspect the internal surface of the axle (Rudlin et al., 2012). Acoustic emission methods have also been conducted as a diagnostic means (Pospisil et al., 2005). For curved surfaces different ways of inspection have been researched. Rudlin et al. (2012) scans the surface from within the hollow cylindral axle, whereas Kappes et al. (2006)

inspected a solid axle using ultrasonic phased arrays.

Many systems used to inspect hollow shafts are stationary, or fixed, in a lab. Zhang et al. (2012) mentioned a new design for inspecting large diameter hollow shafts using ultrasonic NDT, but the system is large and difficult to transport as an inspection instrument to a site.

Inspection time and cost can be reduced by the advancement of UPA technology. UPA is an emerging technology which consists of multiple transducer elements and provides means to focus the ultrasonic beam at different locations. The UPA can be steered on the inspected material to locate defects. It also provides 2D sound imaging that can be adjusted by increasing the transmitting energy. This causes an increase of sensitivity to noise, but it can still allow for easier defect identification.

Titanium billets, raw material used to manufacture airplane engine parts, are similar to shafts and have also used phased array ultrasonic inspections. Lacroix et al. (2002) chose to use UPA to improve the probability of detection (POD) and reduce the number of probes needed for the billets inspection. The inspection is performed by a helicoid-type mechanical sequence, where the phased array transducer is rotated around the exterior of the billet and moved laterally from one end to the other. The calibration billet used had flat-bottom holes that are very difficult to detect without a perpendicular ultrasonic beam to the flat surface. Lacroix et al. (2002) used phased array probes with segmented rings, as well as a dynamic depth focusing (DDF) technique which allows for dynamic modification of the focus law for different depths.

Similarly, Zimmer et al. (2010) shows the usage of radial tangential scans in the evolution of ultrasonic inspection for heavy forgings from the exterior. Figure 1.1 contrasts the inspection of the forgings with a conventional ultrasound on the left, where all of the black arrays are each a separate inspection, with the inspection using ultrasonic phased array on the right, where all of the red arrays are from one single inspection. Originally in the 1960s, fixed-angled conventional ultrasonics were used to create multiple scans, but

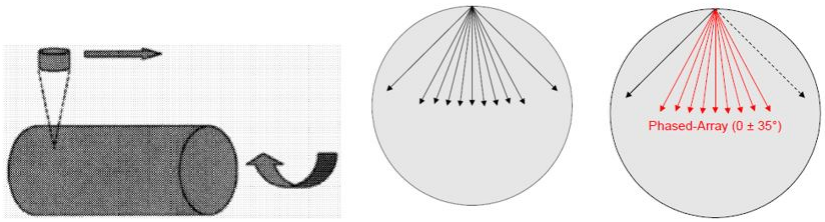

Figure 1.1: (Left) Helicoid mechanical sequence used in Lacroix et al. (2002). (Right) Radial tangential scans with conventional ultrasound, and the single scan position for phased array ultrasound used in Zimmer et al. (2010).

with UPA a multi-channel inspection from one point is possible. The inspection, though, consists of a fixed location outside of the shaft, with a requirement of disassembling the system to obtain the shaft alone.

Although phased array provides a beam spread to inspect more area, Ginzel and Thompson (2013) suggest that the errors from inspecting a curved surface with phased-array contoured wedge introduce uncertainties that are not possible to calibrate. The differences in curved and flat wedges also cause differences in delay time and sensitivity. This requires the user to calibrate the NDT system for accuracy, which will be addressed in this research.

Long and Cawley (2007) proposed two different approaches to inspect irregular surfaces. The first was using a flexible contact array purchased, and the second was a new design they created that replaced the conventional wedge with a fluid encapsulated by an elastomer membrane. Their results showed that both systems were comparable and consistent. This shows the adaptability of UPA for different surface types.

The UPA technology is more flexible in its application as well. Song et al. (2000) uses UPA to modify a medical ultrasonic diagnostic system, and Shan and Ou (2005) acknowledge UPA usage in weld inspection, turbine blade inspection, and train axle inspection. In train axle, Rudlin et al. (2012) introduce the idea of a phased array bore inspection where the ultrasonic rotates within the hollow axle to identify cracking,

similar to the inspection done for this research. This is also shown in Figure 1.2. Jemec et al. (2007) realized the rapid testing and the reliability of phased array technique for inspecting carriage axles, but considered it inapplicable for current application because of the high cost of the equipment. For movable bridges maintenance cost is already higher than that of fixed bridges (Catbas et al., 2009), but because a minor malfunction can cause an unexpected failure of the bridge operation and may affect both land and water traffic, it is necessary to provide a complete and thorough inspection to minimize the risk of any hazard.

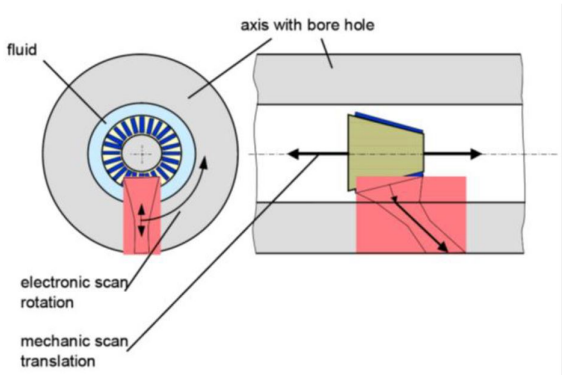

Figure 1.2: Phased Array Bore Inspection introduced by Rudlin et al. (2012).

JFE Group (2012) provides areas where ultrasonic phased array method for steel structures can be applicable. They list blast furnace, crane, rolling mills, wide flange mills, and other examples inspected for crack and weld points. They also mention the inspection of shafts, even shafts with different diameters, through the application of phased arrays from the shaft end (JFE Group, 2012). This method is similar to the work performed by Story et al. (2010) for the inspection of a trunnion bearing pin in a bascule bridge using conventional transducers. Story et al. (2010) positioned the transducer on the face of the pin to measure the propagation distance to the opposite pin. Similarly, this has been the common industrial way to inspect bridge pins, as seen in companies

like WINS and EWI. AASHTO (1998) also specifies ultrasonic testing using longitudinal testing for shafts, and it is recommended to test from both sides to detect shadow flaws.

Phased array technology is slowly becoming popular in the inspection of bridges. In 2005 the Edison Welding Institute, Inc. (EWI) was awarded a project to adapt its phased array ultrasonic inspection technology to inspect the pins and the eyebars of the Queensboro Bridge in New York City (ASM International, 2005). It was suggested that their inspection method was similar to the traditional scanning from one pin side to the other, as mentioned earlier. Sugiyama et al. (2010) considered a compound method for inspecting orthotropic steel decks to detect fatigue damages. Because the cracking to be inspected cannot be found by visual inspection, three NDE techniques were applied: infrared, eddy current, and phased array. In order to provide an economic method of inspection, infrared and eddy current technologies were used first to identify major cracking locations, and UPA was used afterwards to provide a more detailed investigation of the cracks (Sugiyama et al., 2010).

As commented by Zimmer et al. (2010), phased array technology applied for industrial applications is slowly maturing. The basic principal of phased array had already been proposed in the late 60's, and it has taken more than 20 years to be applied in the industry. Even now conventional ultrasonic is preferred over UPA because of the cost difference. But, because of the multiple advantages phased array technology has over conventional ultrasonic, UPA has the potential to surpass its competitor if more research is done on its extended application, and its advantages become better known. Future advancements of UPA consist of 3-D volumetric images through different algorithms, as seen in work by Song and Kim (2002) and Quaegebeur and Masson (2012).

1.2 Technical Needs

It is apparent that much research has been conducted using non-destructive ultrasonic technology for the inspection of various components. Specifically for ultrasonic phased array technology, its application and new advances are continuing to develop. However,

little research relating to the inspection of the components on historic movable steel bridges is available.

In addition to addressing historic bridges, more research applications using UPA is necessary to continue industrial acceptance of phased array technology as an accurate and well-developed method for the inspection of bridges. An approach to this is to provide an economical way to use UPA. The number of elements in a phased array transducer dictates the cost and the accuracy of inspection. The state of the inspected structure, meaning the state of corrosion of the material or the wearing of the components, may also affect the accuracy of inspection.

1.3 Objectives

The primary goal of this research is to develop a simple and accurate way to inspect the trunnion bearings of bascule bridges while also respecting the historical integrity of the bridge components. The intent of this research is also aligned with the integrity of preserving "living" historic structures by protecting their functionality values through the use of new inspection techniques. Specifically, a nondestructive ultrasonic phased array system is used for the inspection of a trunnion bearing pin of a 100-year old heel-trunnion bascule bridge. The bridge, known originally as Bridge No. 4 and later as the Salmon Bay Bridge, is surrounded by the cultural integrity of the community in Seattle, Washington. The ultrasonic phased array technology is applied to lab testing on a mock-up trunnion pin with known details, and field testing on the original parts of the trunnion pin taken out of service. The research project addresses: (a) the preservation integrity through nondestructive inspection, (b) the application of ultrasonic phased array technology in movable bridges, and (c) the usage of phased array with curved surface and its accuracy.

1.4 Structure of Thesis

The thesis consists of a brief introduction to nondestructive testing applications in historic bridges and past research conducted with ultrasonic technology. The second

chapter is dedicated to a background of bascule bridges to understand their civil engineering heritage value to the nation and introduces the preservation motivation. The following chapter delves into the history of the Salmon Bay Bridge used in this research, as well as the two trunnion bearing pins used for the lab and field inspection testing. The fourth chapter explains the usage of the phased array probe, the experimental set up, the Poly Methyl Meth Acrylate (PMMA) case designed for this project, and the calibration set-up used for the new case. This section also provides the lab and field testing of the pins. Finally, the findings are concluded with future research suggestions.

2. MOTIVATION FOR HISTORIC PRESERVATION

2.1 History of Bascule Bridges

Throughout the ages movable bridges have been used for military purposes to neglect passageway for enemies, and for efficient travel to allow both water and road traffic. As early as 480 B.C. the pontoon bridges used by the armies of Darius and Xerxes were a floating, temporary structure that swung out of the way for water traffic (Brown, 1993; Koglin, 2003). Medieval castles that contained a drawbridge at its entrance were popular protective devices over the moats of medieval castles (Koglin, 2003; Hool and Kinne, 1923).

During the Renaissance period, Leonardo Da Vinci developed plans for an asymmetric swing bridge for a trunnion bascule, and even designed a vertical lift span (Koglin, 2003; Weingardt, 2010). The heel trunnion type bridge and the rolling lift bridge were also developed around that time. During the invention of the steam engine, water traffic began to conflict with road traffic, and thus many types of movable bridges were developed (Koglin, 2003). Due to the high popularity of movable bridges, engineers devised numerous systems for lifting, dropping, folding, rotating and retracting a bridge span to provide temporary clearance for shipping (Tilly and Gifford and Partners, 2002).

In the late 19th century, the movable bridges progressed rapidly due to advances in mechanical, electrical, and civil engineering, initially dominated by swing span bridges and after the early 1890s by bascule bridges (Lichtenstein Consulting Engineers, Inc., 2002). The Van Buren Street Bridge in Chicago, a rolling lift bascule bridge developed and patented by William Scherzer (1858-1893) is traditionally held to be the beginning of the modern era of the bascule bridge in the U.S. (Lichtenstein Consulting Engineers, Inc., 2002; Hool and Kinne, 1923). From the 1890s to the early 1920s one competitor after the other patented a new design of bascule bridges. Finally, in 1902 the city of

Chicago's engineering department advocated an unpatented design by building its first simple trunnion bascule bridge (Lichtenstein Consulting Engineers, Inc., 2002).

The trunnion bridges became more popular at the beginning of the twentieth century. Having a patent on movable bridge types was considered a valuable marketing tool (Koglin, 2003). At this time many bridge variations arose, some of which were built but were less practical for construction (Hool and Kinne, 1923) and most only existed in drawings. At this time the Heel Trunnion design bridges were built to allow the construction of very large and long bascule spans. An example of a Heel Trunnion is shown in Figure 2.1. In 1919 the St. Charles Air Line Bridge, a two-track railroad bridge, was built over the South Branch of the Chicago River, measuring 260 feet from heel to toe. In the 1950s a single-track heel trunnion bascule railroad bridge was built in Cleveland, Ohio to replace an older bascule bridge in order to provide a larger span.

Figure 2.1: The Salmon Bay Bridge is a heel-trunnion bascule bridge in Seattle, WA. (Photo taken by Dr. Gary Fry.)

After World War I the trucking industry developed, which resulted in a decline in waterway commercial freight (Koglin, 2003). Nowadays, most movable bridges are being maintained for transportation uses but also as a historic site. For example, the famous Tower Bridge in London is both a transporter bridge as well as a touristic landmark (Brown, 1993).

The numbers of movable bridges are diminishing as uses of inland waterways change, and the bridges are either being demolished or fixed in position (Tilly and Gifford and Partners, 2002). Due to this development, there is a need to carry conservation work on some of the more significant survivors.

2.2 Types of Movable Bridges and Components

There are similar components that all movable bridges share that are important for them to function. These are the foundations, substructure, superstructure, ballast, and deck. The foundation loading from a movable bridge is essential as any movement or settlement of foundations may impact upon the operation of the bridge (Tilly and Gifford and Partners, 2002). The substructure may experience normal or abnormal collisions, which are loading conditions the bridge can sustain without significant damage and more severe loading conditions, respectively. The ballast is the counterweight that balances the self-weight of the superstructure (Tilly and Gifford and Partners, 2002), and the deck is the level of the bridge used for transportation.

New engineering designs arose to solve different problems, which led to three main bridge type categories, summarized Table 2.1.

The bascule bridge is the most common bridge that exists and is still operating in the U.S. "Bascule" is a French word for "seesaw," or balance. The bridge rotates in a vertical plane around a horizontal axis (Brown, 1993) and does not require clear turning radius, unlike the swing span bridge. There are two types of bascule bridges–a trunnion and a rolling, excluding the Rall bascule, which is a variant of the rolling bascule (Tilly and Gifford and Partners, 2002). According to Koglin (2003), a true trunnion is merely

Table 2.1: Types of Bridges and their Variations

Type of Bridge	Definition	Variation
Swing Span Bridge	All movable bridges that open by pivoting about a vertical axis.	Center Bearing, Rim Bearing, Combined Bearing, Bobtail Swing, Double Swing, Double Deck
Bascule Bridge	All movable bridges that are counterbalanced and open by pivoting about a horizontal axis.	Simple Trunnion, Heel Trunnion, Articulated Counterweight, Rolling Lift, Non-counterweighted, Double Deck
Vertical Lift Bridge	All movable bridges that open by lifting, without rotating or translating horizontally.	Span Drive, Tower Drive, Span-Tower Drive, Non-counterweighted, Strauss/Rall/Strobel, Double Deck

a pivot and never rotates more than a fraction of a turn. A simple trunnion bridge is one that consists of a bridge leaf with a counterweight rigidly attached to a rear portion of the main support members, supported near its center of gravity by trunnions that rest on bearings.

2.2.1 Heel Trunnion Bascule

Since about 1925 the most popular movable bridge type built has been the Strauss type bascule bridges (Malvern et al., 1985; Reichmann, 1924) in which the essential feature of the design is the direct balance of the opening leaf with the attached counterweight (Anon, 1908; Wallner and Pircher, 2007). It uses a parallelogram connection that allows for the equilibrium between the leaf span and the counterweight (Anon, 1908; Hool and Kinne, 1923; Reichmann, 1924). The trunnion in the bascule bridge is a horizontal steel pivot that supports the entire weight of the bridge when it is in operation or in the open position (Lichtenstein Consulting Engineers, Inc., 2002). The counterweight trunnion, located at the intersection of the top chord and the end post (Johnson, 1991), is vital for the bridge to maintain its functionality and must be carefully inspected. Good lubri-

cation is important (Hovey, 1927) for its flexibility. Regular maintenance inspection is required to keep the trunnions functional. The inspection of the bearing pins are challenging because they are difficult to inspect with mere eyesight due to its location (Story et al., 2010).

Sometimes called a Strauss bascule, the heel trunnion bascule is not a true bascule bridge because the movable leaf itself is a simple span and not balanced. This type of bascule bridge allows the pivot point to be placed considerably forward on the bascule pier, unlike the simple trunnion bascule, which allows for a shorter bridge leaf to span the same width of the navigation channel (Koglin, 2003). The shorter the span the more economical it is to construct. It also minimizes the movable span length and eliminates the counterweight pit (Koglin, 2003). The counterweight of a heel trunnion bascule is mounted separately on its own pivot parallel to the pivot of the bridge span.

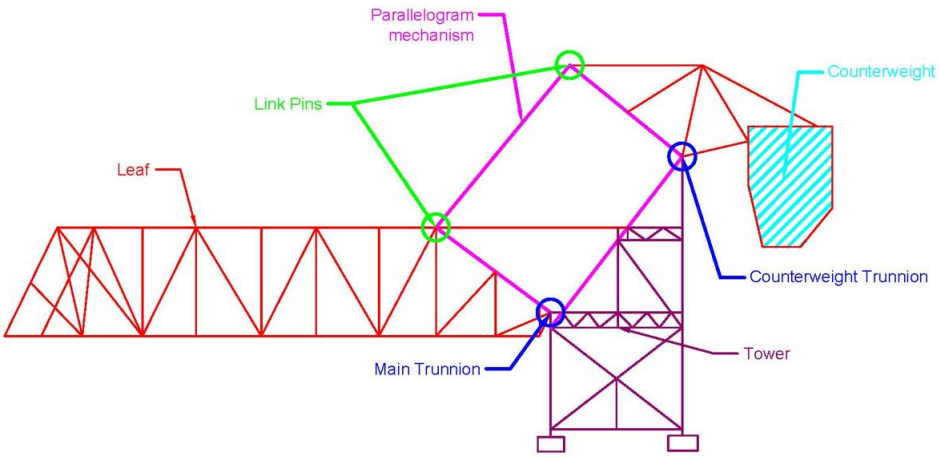

Figure 2.2: Heel Trunnion Bascule Bridge Components, modified from Story (2012).

The heel trunnion bascule bridge, as shown in Figure 2.2, is commonly used for railroad bridges. It is easy to see that the counterweight is connected to the bascule span by links. The main trunnion, or pivot section, is placed as a connection between the top

pier and the steel bridge. Also noted by Koglin (2003), not many single leaf heel trunnion bascule are built nowadays, so such existing bridges are historic sites that present past creative inventions of our time.

The heel trunnion bascule has had problems with fatigue of superstructure members that undergo stress reversal during operation, and with trunnion and other large bearings that have deteriorated and have been difficult to repair (Koglin, 2003).

The vocabulary definitions of the parts depicted in Figure 2.2 are shown in Table 2.2.

Table 2.2: Heel Trunnion Vocabulary (Koglin, 2003)

Vocabulary	Definition
Main Trunnion	The trunnions (pivots) at the heel of the bascule bridge.
Counterweight Trunnion	The trunnion that supports the counterweight.
Lower link pins	The connection points at the hinges between the bascule span and the connecting linkage.
Upper link pins	The connection points at the hinges between the counterweight structure and the connecting linkage.

2.2.2 Balancing Requirements

The moving portions of the bascule bridge must always be in balance to make the equipment as light as possible, and to focus on the inertia, friction, and wind as the only loads acting on the machinery (Hool and Kinne, 1923). In order to accomplish the balance of the span, a set of parallel lines are established, as shown in Figure 2.3. The line created by the center of gravity (COG) of the span with the main trunnion must be parallel with the line created by the COG of the counterweight with the counterweight trunnion. These two parallel lines must be true even when the span is lifted. The parallelogram linkage in the bridge design, created by the links and the trunnions, allows for the lines in red to maintain the parallel requirement. Malvern et al. (1985) develops the balancing idea of a trunnion-type bascule bridge, also noting that balancing the bascule leaf does not have

to have an optimal shape. The balance of the leaf can also be adjusted by the weight of the counterweight.

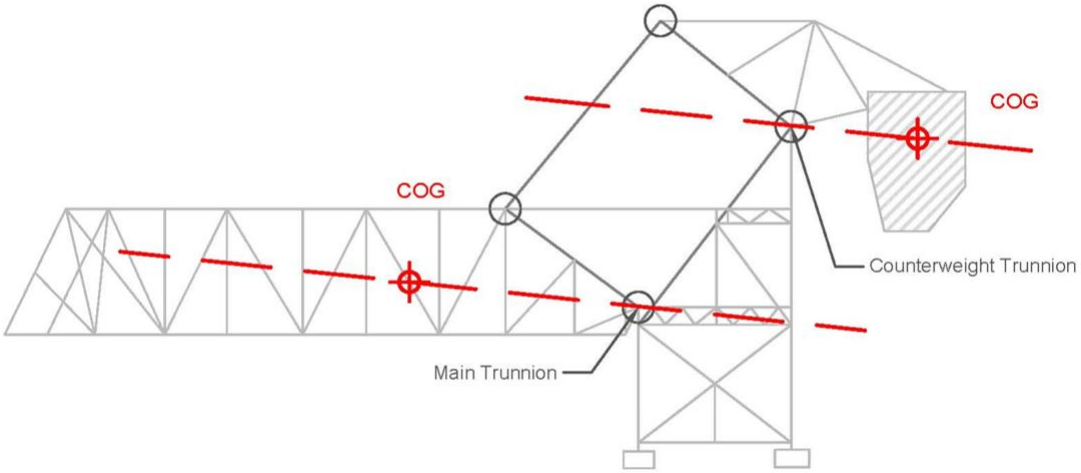

Figure 2.3: Balancing the Strauss type bascule.

2.2.3 Trunnion Pin

The trunnion bearing pin in a bascule bridge is subject to a balance of moments created by the weight of the counterweight used to lift up the bridge leaf, and the wind forces that cause a retarding moment about the main trunnion (Paine, 1929). Hovey (1927) provides the design aspects for the trunnion bearings to carry heavy load and rotate at small velocities. He also stresses on good lubrication for the trunnion to rotate.

2.3 Historic Preservation Motivation

Throughout the years construction projects in America have valued projects that are built cheap, fast, and efficient. This leaves small room for an embellishing perspective. Isohata (2005) also brings up the three civil fundamentals that are considered in any construction or preservation project: safety, durability, and utility. These three values are the main influence on an American engineer's decision to rehabilitate, reconstruct, or

restore a bridge project. These values have also influenced the advancement in technology for different structures.

Specifically in movable bridges, the improvement in technology arose because bridges needed to function appropriately for land and water traffic in a safe and satisfactory manner, but at a manageable cost. In the early 1900s bascule bridges were the preferred bridge for construction over the advancement of long-span vertical lift bridges. The American Bridge Type bascule bridge emerged as an ingenious solution in bridge engineering (Reichmann, 1924), contributing to the nation's engineering identity. Throughout the early American history of movable bridges, the advancement of its technology has been connected with daring designs by many engineers who pushed through the limits of their time. The notable John Alexander Lowe Waddell, albeit Canadian, proved to American engineers that long-span vertical lift spans were possible and better equipped to stabilize long spans than bascule and swing span bridges (Griggs, 2006). In general the kinetic mechanisms for movable bridges are complex and interesting to study.

Many of these movable bridges possess a rich historical background valuable for our cultural heritage, but some of these structures are still in use today for their intended purpose. America's infrastructure has aged, and the predictable physical threats to historic buildings have accelerated bridge deterioration rates in recent years (Saldibar III, 1997). These threats include deferred maintenance, harmful de-icing salts, and over-loading. The question of which values take priority over others in existing historic engineering structures has to be addressed to comprehend the importance placed on maintenance. The first fundamental canon from the Code of Ethics for Engineers to "hold paramount the safety, health, and welfare of the public." Because these movable bridges are still being used for transportation, the primary preservation value becomes utility, which incorporates the safety and durability aspects as well. If a structure such as a historic movable bridge then is valued for its utility, then it becomes a requirement to preserve its function by maintaining its counterparts.

The goal of conservation engineers is to stabilize with minimum intervention. The entire movable bridge inspection process should have the major goal of doing no damage to the existing structure, thus having a non-destructive inspection approach (Koglin, 2003). AASHTO (1998) comments on the importance of inspections used to evaluate the physical and functional condition of the structure. The information gathered from inspections provides assurance that the bridge is performing as properly intended for safety measures.

3. THE SALMON BAY BRIDGE

3.1 Background

The Jim Hills Seattle & Montana Railroad used a large wooden trestle in the early 1890's that crossed from Interbay into Ballard (Pierce, 2013; Dorpat, 2012). The bridge was known at the time as Bridge No. 4, and was later replaced with a swing span installation. When the Army Corps of Engineers began construction of the Chittenden Locks due to Seattle's flooding problems, the Great Northern Railroad re-located their railroad line over the Salmon Bay, near the Lake Washington Ship Canal. The Salmon Bay Bridge was designed by the Strauss Bascule Bridge Co. of Chicago, Illinois in 1913 as a Strauss Heel-trunnion Bascule Bridge type (Pierce, 2013). The leaf is balanced by a 1500 ton reinforced concrete counterweight that rotates about the main trunnion when the bridge opens (Story et al., 2010). It is a two-track moveable bridge. It was later bought by the Burlington Northern Santa Fe (BNSF) Railroad, and now lies on the major rail route from Vancouver to Seattle. The national register of historic places lists the Ballard Bridge, which is also on the canal, and the Chittenden Locks and Lake Washington Ship Canal (National Register of Historic Places, 2013). Although the Salmon Bay Bridge is not specifically on the Register, it is still part of the related features of the lake and has become a landmark for the community in Seattle (Dorpat, 2012). The bridge is shown in Figure 2.1.

In 1948 the counterweight truss fractured due to fatigue and detailing of one of the steel counterweight truss members near the counterweight connection point (Story, 2012; Pierce, 2013). The counterweight and several of its members were taken out and replaced. Six months after the accident the bridge opened again for service. The failure was caused by stress reversal and fatigue within the counterweight truss (Story, 2012). BNSF made technical updates in 1992, including the re-location of the gear house above the tracks

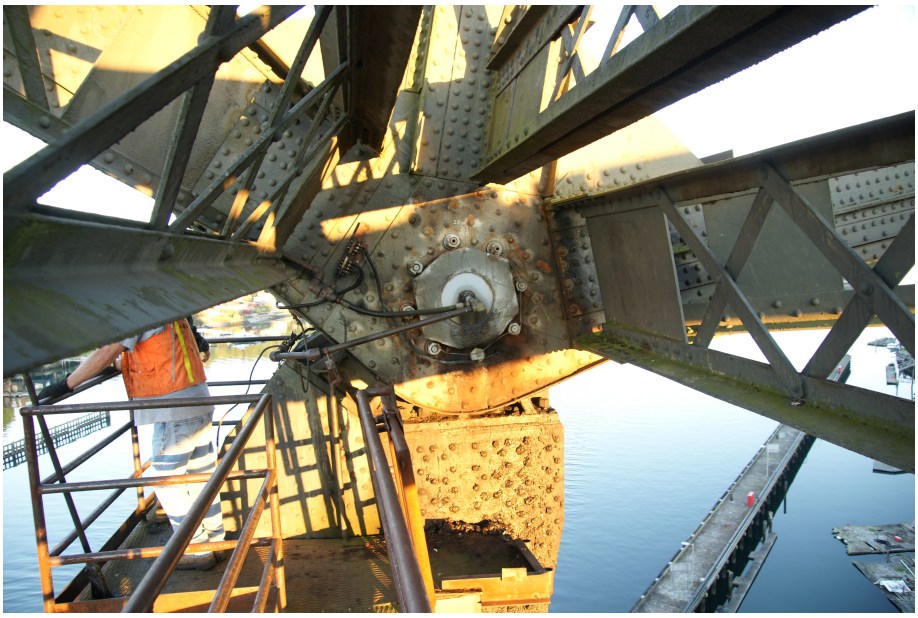

Figure 3.1: The trunnion bearing pin within the Salmon Bay Bridge. (Photo taken by Dr. Fry.)

and replacement of the original hand controlled levers of the signal system (Pierce, 2013).

3.2 Trunnion Bearing

As shown in Figure 2.2 and 3.1, the trunnion bearing pin is a problematical part to inspect because the pin is covered by other steel members, thus the inspection is constrained to the center hole passage of the pin and the top exterior of the pin.

The counterweight trunnion bearing pin of the Salmon Bay Bridge was taken out of service during one of the technical updates by BNSF. Parts of the original bearing pin is now located at the Riverside Campus. A mock-up trunnion pin was re-created for the conventional ultrasonic testing in Story et al. (2010). For this research, the laboratory testing is conducted on a mock-up bearing pin and the field testing is conducted on the original parts of the bearing pin.

It is important to note that for the field testing not all of the original pin is available for the inspection. As shown in Figure 3.2, only parts of the whole pin are at the Riverside campus. It is uncertain which side Part I and Part II were originally from on the Salmon

Bay Bridge, i.e. the West or East pin side.

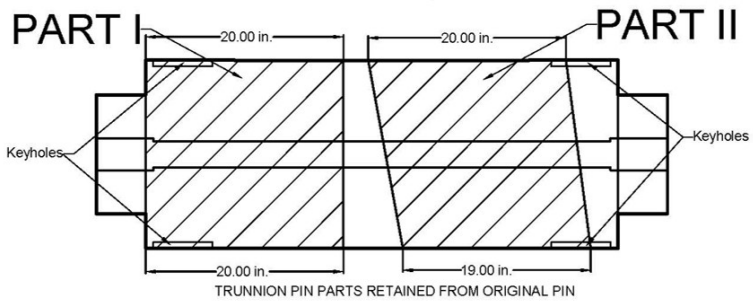

Figure 3.2: The two original pin parts available for inspection with respect to the entire trunnion bearing pin from the bridge. See the drawings in Appendix A.

The mock-up pin has three visible circular layers. The most outer circle has a diameter of 18-1/2 in., the middle circle with threads measures 12 in., and the inner top opening is approximately 3.45 in. For the out-of-service pin, the diameters measure 19 in., 12 in., and 4-1/4 in., respectively. The original pin was taken out with part of the sleeve which has a diameter of 31 in., but the sleeve is not taken into account for the inspection. This is because the sleeve is not connected to the pin and the various gaps between the two limits the sound wave from penetrating into the sleeve. Both pins have a through-hole where the original shaft went through. The inner hole of the mock-up pin measures 2-3/4 in., and the out-of-service inner hole measures 2-5/8 in. Because of the difference in the through-hole diameter, two different PMMA diameter cases were used. See the Appendix drawings for the original and the mock-up trunnion pin dimensions. The original drawings for the bascule bridge are also given.

3.2.1 Mock-up Pin Visual Details

The mock-up trunnion bearing pin has two key holes on opposite sides, and three grease holes that span from the exterior of the second level of the pin to the interior of the first level. There are two keyholes shown in Figure 3.3, one which has a grease hole

Figure 3.3: Mock-up Pin details: (Left) Keyhole #1 with grease holes, and (right) Keyhole #2.

on each side and the other with no grease holes on its sides. For classifying purposes the latter keyhole is named Keyhole #1 and the former is named Keyhole #2. The grease holes, beginning clockwise from Keyhole #2 shown in Figure 3.4, are labeled Hole #1, Hole #2, and Hole #3.

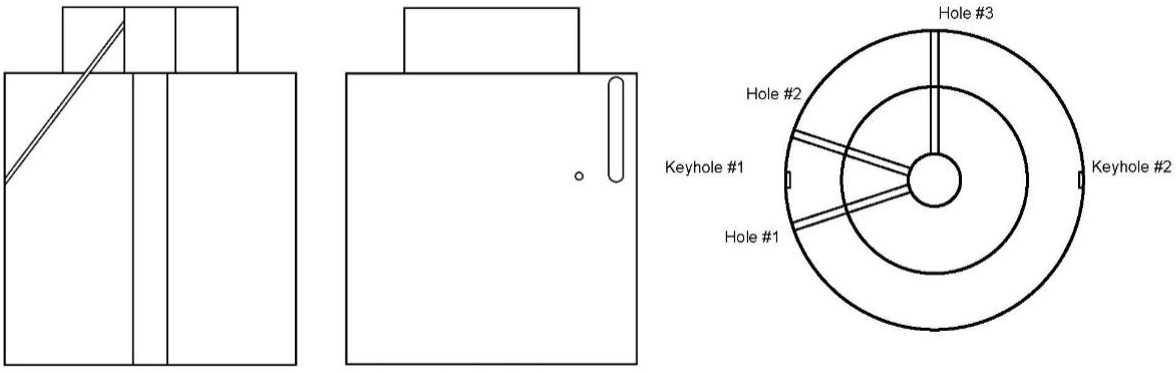

Figure 3.4: Mock-up Pin details CAD drawings showing the grease hole directions.

The three diagonal grease holes have an 8 in. rise with an 8.5 in. run, making a 47°

from a horizontal plane. A top view of the pin with the three grease hole directions are shown in Figure 3.4.

The diameter of the grease hole is 5/8 in., with a length of about 11.7 in. from the exterior bottom level to the interior top level of the pin.

3.2.2 Original Pin Visual Details

The Salmon Bay Bridge trunnion bearing pin was taken out of service in two parts, labeled Pin Part I and Pin Part II. The exterior circle layer with the large screw holes is called the sleeve, but this is not taken into account for the pin inspection. For recording purposes the exterior surface of the sleeve of Pin Part I is shown in Figure 3.5. This part has many exterior defects, including a large diagonal openings, interior holes, and keyholes.

Figure 3.5: Exterior surface of Pin Part I.

On the sleeve are eight 2-1/2 in. holes arrayed around the exterior circular layer, where massive bolts were locked in place. The bolts are shown in Figure 3.1. The middle circle, or the body of the pin, is a separate entity from the sleeve, and in many parts there are 1 to 1-1/2 in. gaps. Figure 3.6 shows the top side of Pin Part I and the angle references for the Omniscan inspection. There are two side keyholes that come out of the circumference of Pin Part I. These are shown in Figure 3.7. Pin Part II with the sleeve is shown in Figure 3.8.

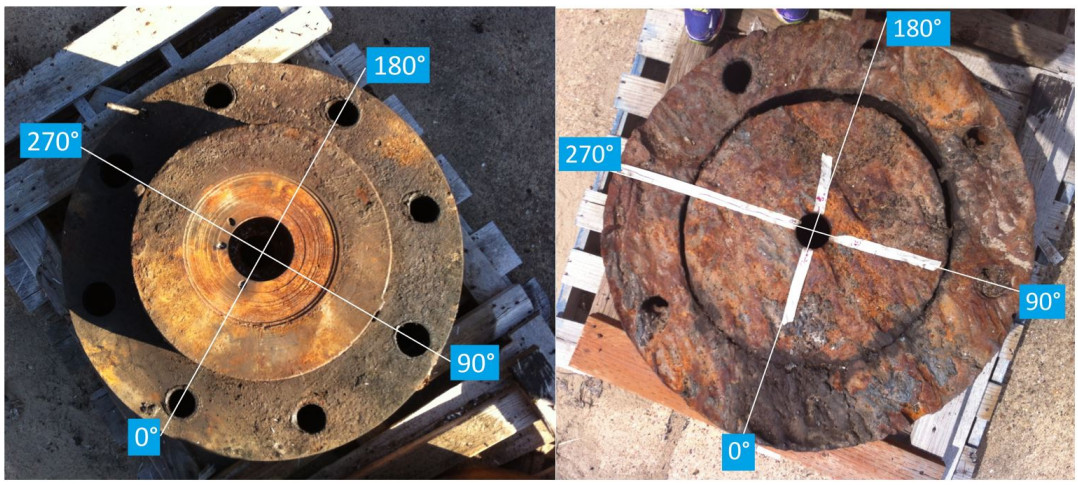

Figure 3.6: Top view of the out-of-service pins. (Left) Pin Part I, and (right) Pin Part II. The angle references were taken from the bolt hole at 0°.

Because of the uneven cut between the two parts, the heights around the pin parts varied. After the removal of the sleeve, Pin Part I was roughly 20 in. in height near the keyholes, but it still had some variation. For Pin Part II, the height changed from 19 in. to 20 in. near the keyholes.

Figure 3.7: The two keyholes on Pin Part I. (Left) Keyhole #2, (Right) Keyhole #1.

On the top surface of Pin Part I are three grease holes that run down like the grease holes shown in Figure 3.4. These holes also have a 47° angle from the horizontal plane.

Figure 3.8: Top and side views of Pin Part II with the sleeve.

After the removal of the sleeve, Pin Part I was placed upside down and Pin Part II stayed in the same direction. Figure 3.9 shows the pin parts without the sleeves. Both pin parts have keyholes, meaning that they are near one of the East or West side of the original whole trunnion bearing pin, as shown in Figure 3.2.

Figure 3.9: Pin parts without the sleeves.

4. EXPERIMENTAL PROGRAM

Ultrasonic testing is based on acoustics, or vibrations in the material. Sound waves can propagate in four principal modes: longitudinal waves, shear waves, surface waves, and plate waves. Longitudinal and shear waves are the most widely used modes in ultrasonic testing, displayed in Figure 4.1. Longitudinal waves are wave oscillations that occur in the direction of the wave propagation. Shear waves oscillate at right angles to the direction of energy transfer.

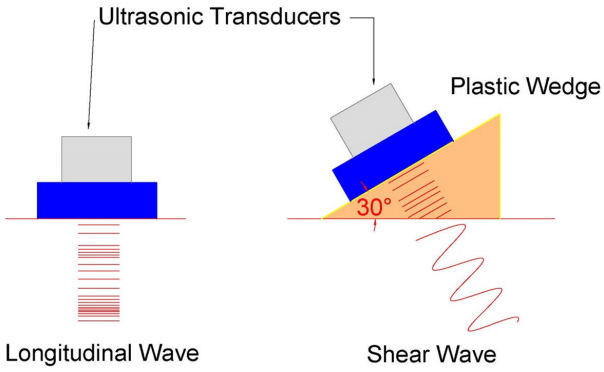

Figure 4.1: Conventional ultrasonic usage of longitudinal and shear waves.

Conventional transducers use one element to send a sound wave through the wedge. Depending on the shape of the wedge, the wave impacts in different points on the wedge and the material that allows the wavefront to experience small delay intervals. Ultrasonic Phased Array transducers use various individual elements, each with its individual pulser and receiver. All of the elements are controlled by a focus law, which controls the timing or phasing of the individual element pulse to create various types of wavefronts. Using different phase patterns results in different wavefronts. Unlike the conventional transducer, the UPA transducer can steer the ultrasonic beam.

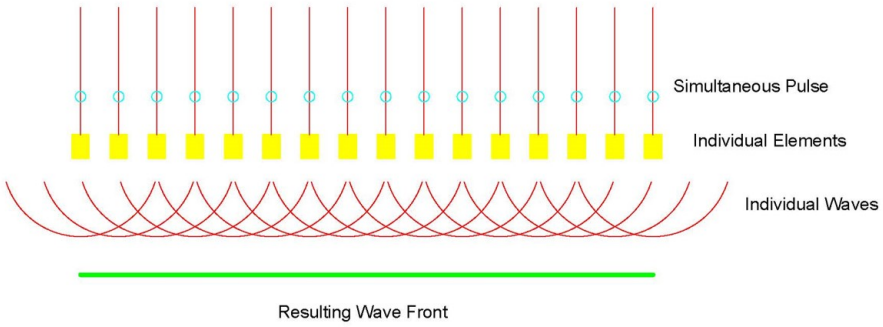

Figure 4.2: A linear wavefront resulting from a simultaneous timing of the 16 elements in a phased array. Recreated from Olympus (2013).

Figure 4.2 shows 16 elements that are each sent a simultaneous pulse to create a linear wavefront.

4.1 Experimental Set-up

Figure 4.3 shows a simple overview of the UPA system used to inspect the trunnion bearing pins. The system consists of three parts: sensors, data acquisition, and data analysis.

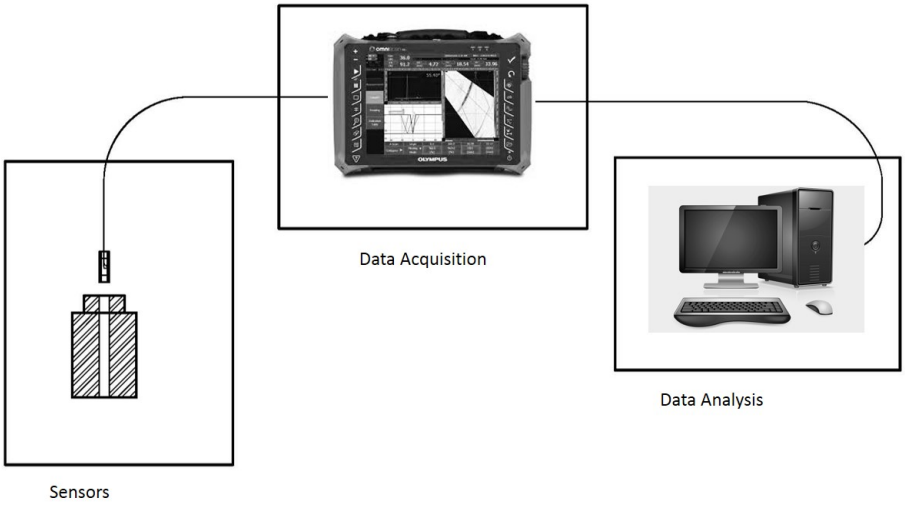

Figure 4.3: Ultrasonic Phased Array system.

4.1.1 Sensors

Two different sensors are used for interior and exterior inspection. This section will describe each sensor with their corresponding wedge.

4.1.1.1 16-element Probe and Wedge

For the internal inspection, a 2.25L16-A1 probe is used, which is a 12x12 mm phased array transducer that houses 16-elements, shown in Figure 4.4. The transducer characteristics are shown in Table A.2. Using the PMMA case as its wedge, the 16-element probe provides sectorial scanning at the angles between $-30°$ and $30°$.

A proper transducer size had to be chosen in order to fit into a modified PMMA case. The PMMA case consists of a steel rod used to control the navigation of the probe, and inner cap with a hole slider for the transducer, a half curved wedge with two holes for the screw rods to hold the case together, a second half curved wedge with a modified interior to fit the transducer, an outer cap, two screw rods that are secured with a nut and washer on each side, four springs, and the UPA transducer. A viscous ultrasonic

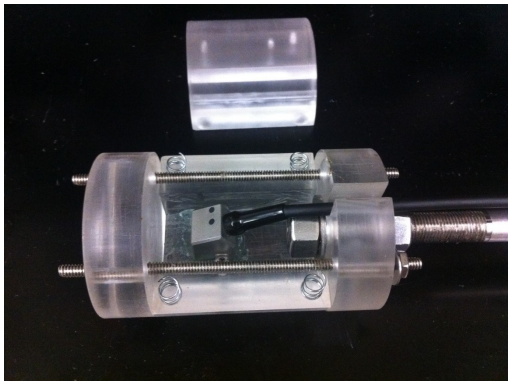

Figure 4.4: PMMA case with UPA probe.

couplant is applied between the transducer and the interior of the wedge, as well as the exterior of the PMMA case and the interior surface of the trunnion bearing pin in order to reduce acoustic impedance mismatch. The design drawings for the PMMA case are shown in Appendix A.

The PMMA wedge was calibrated within the OMNISCAN MX2 system by inputing the ultrasonic velocity. The PMMA material's ultrasonic velocity was calculated using a pulser-receiver technique. The experimental set-up, procedure, and results of the sound velocity is detailed in Appendix A.

Due to the difference in diameters for the internal hole between the mock-up and the original pin, a smaller PMMA diameter case is also applied with the 16-element sensor. The large-diameter case is referred to as PMMA Case I, and the smaller-diameter case is referred to as PMMA Case II.

4.1.1.2 32-element Probe and Wedge

For the external inspection, a SA5-N60S 5L32 wedge and probe was used, shown in Figure 4.5, which reads between 25° to 75°. This probe has an active area of 19.2x20 mm that contains 32 elements. The transducer characteristics are shown in Table A.3.

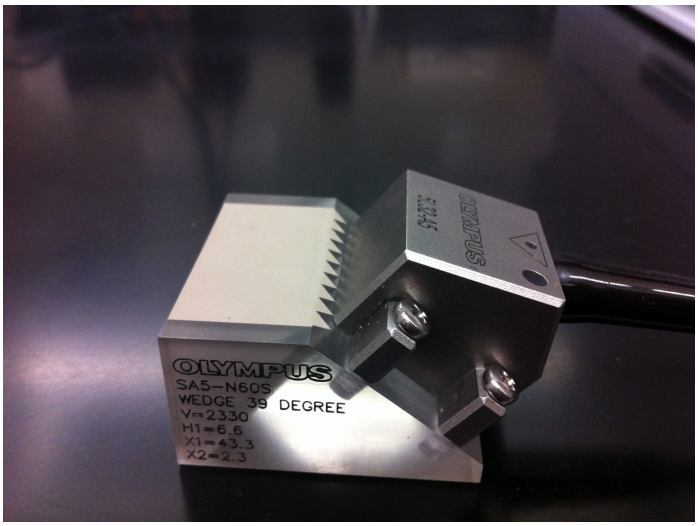

Figure 4.5: SA5-N60S 5L32 wedge and probe used for the exterior inspection of the grease hole.

4.1.2 Data Acquisition

The data acquisition system is accomplished through the flaw detector system made by Olympus and called Omniscan MX2, which the UPA sensor is connected to. This device, shown in Figure 4.6, sends time-delay pulses and receives the data from the phased array transducer by the use of focal laws. It provides a touch screen interface that allows the user to save scan data onto an SD card for easy file transfer. Different parameters were established within the system in order to allow for correct readings. The wedge information seen in Table A.4, including the PMMA ultrasonic velocity and distance from the phased array transducer to the edge of the curved wedge, was added to the Omniscan MX2 to create a customized wedge file. Gates were created to specify the depths of interest. For instance, a gate was made between 8.0 in. to 8.4 in. to read the keyhole scan for the mock-up pin, since the measurements indicated that the reading should appear around 8.2 in.

The Omniscan screen is able to produce A-scan, B-scan, S-scan, and C-scan imaging. The two scans mainly used for this research are the A-scan and the S-scan. The A-

Figure 4.6: The Omniscan MX2 used for Data Acquisition (Olympus 2013).

scan shows a rectified waveform presentation related by the time and amplitude of an ultrasonic signal (Olympus, 2013). The amplitude relies on the waveform thickness gages, which is controlled with the Omniscan MX2.

The A-scan graph represents the average reflections for one specific sound beam position. The Omniscan takes different A-scan readings to average the ultrasonic signal for each sound beam position. As the sound beam is rotated through the available angles the A-scan changes to that specific beam. The S-scan is a sectorial scan of the phased array that uses fixed apertures and can steer through a sequence of angles. It is composed of average A-scans from each angle with a 1° increment. Using this sectorial scan the user can go through different beam angles and see the specific amplitude and location from the A-scan. The B-scan is simply the A-scans plotted with respect to time and/or distance for a specified beam angle. The C-scan is not used for this research because the inspection does not depend on a constant time inspection. The advantages of UPA technology are the S-scan outputs rather than the accuracy of the A-scan.

4.1.3 Data Analysis

The data analysis section uses a computer-based system through the software TomoViewer. This software is downloaded from the Olympus website. As shown in Figure 4.7 the TomoViewer screen may show an A-scan, S-scan, and C-scan used to inspect the material though a certain angle section.

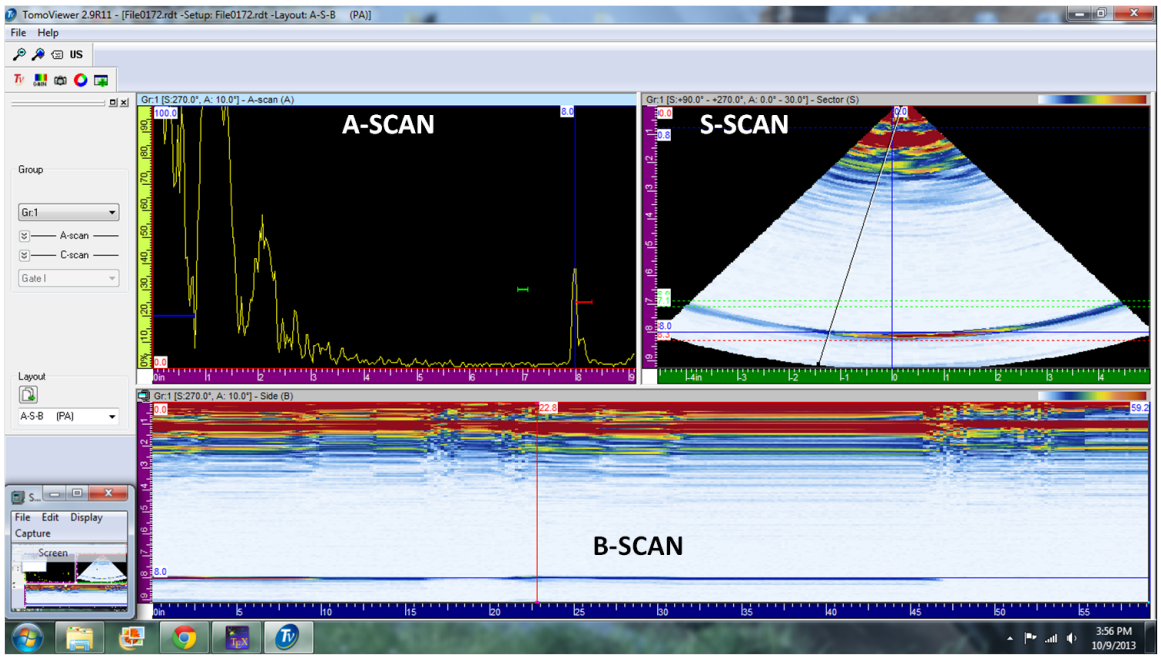

Figure 4.7: Tomoviewer Screen Sample

The phased array has the ability to scan through different sectorial angles. As introduced in the data acquisition section, the A-scan, shown on the top left of Figure 4.7, demonstrates the waveform amplitudes of the beam angle line from the S-scan, shown on the top right window. The B-scan, shown on the bottom left, displays this specific angle during some specified length of time.

The Tomoviewer program is also able to adjust the gain measured in decibels (dB), and allows the exportation of figures.

4.2 Experimental Procedure

In order to apply the UPA system properly to the pin specimens, a laboratory and field testing were assessed. The UPA system, shown in Figure 4.3, was applied first in a laboratory setting to the mock-up trunnion bearing pin and then in a field settng to the original pin parts. This section describes the various testing with respect to the set-up.

4.2.1 External Inspection of Pin

The inspection of the diagonal grease holes on the mock-up pin was difficult because the vertical beam scan of the interior pin were not able to identify the wave reflections from the grease hole within the limited beam spread of $-30°$ to $30°$. This was explained through a geometrical approach. The plane of the direction of the diagonal grease hole must be perpendicular to the plane of the wave reflection for the probe in order to pick up the grease hole location. The direction of the grease hole has a $47°$ angle from the ground plane. In order for this line to be perpendicular to the probe it requires the probe to read at a $-44°$ angle, as seen in Figure 4.8. Since the probe only reads to $-30°$, the diagonal grease hole cannot be inspected unless a built-in wedge was added inside the PMMA probe case to adjust the angle of inspection.

The inspection of the diagonal grease holes on the original pin was also difficult because the grease holes were similar to the mock-up pin, rising 11.5 in. and running 12.5 in. Using the same principle as mentioned for the mock-up pin, the required angle for inspecting the grease holes is $47.39°$,

$$\gamma = 90° - \arctan(\frac{11.5}{12.5}) = 47.39° \tag{4.1}$$

Because the grease holes are undetectable by internal inspection with the designed PMMA case for this research, an external inspection is required to identify the inclined grease holes in order to prove that the grease holes can be inspected with phased array technology if the built-in wedge was applied. This inspection requires the use of the

32-element sensor with the wedge that provides a 25° to 75° view.

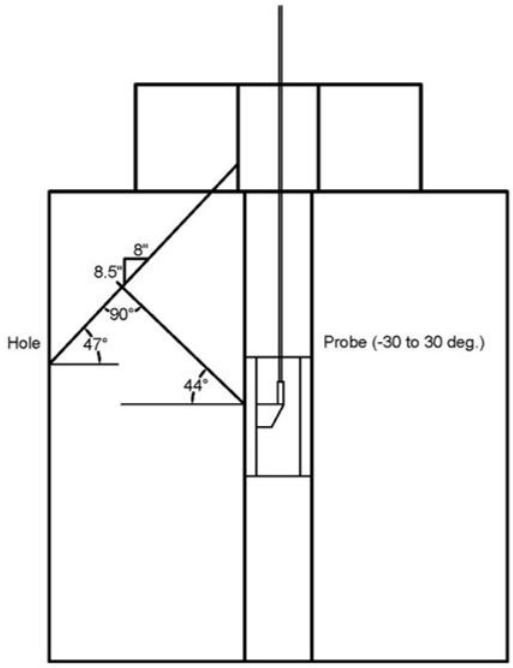

Figure 4.8: Diagonal grease hole inspection with required angle using the mock-up pin dimensions.

This would not be allowed when inspecting the trunnion bearing pin on a real bascule bridge because of the pin's limited accessibility, but it still allows for a way to prove that the grease holes can be inspected if an angled wedge would be built-in within the PMMA case. It also provides an understanding of phased array technology used as inspection on removed bridge parts.

This inspection allows for the inspection of the grease holes is explained with the law of perpendicular angles. Since the probe was directed at a perpendicular angle to the plane of the grease hole, then the angle from the sound wave of the probe also made a perpendicular angle with the grease hole.

The transducer was placed in two ways, as shown in Figure 4.9, which provides two different tests, shown in Table 4.1. The first external inspection test looks for the grease

Table 4.1: External Inspection Testing.

Testing	Inspecting Part	Testing Type
E.1	Inclined grease holes	Probe placed on top flat surface
E.2	Inclined grease holes	Probe placed on curved exterior

holes with the probe being placed on the top surface of the pin. The second test places the probe on the curved surface of the second level of the pin. Both of these testing are applied to locate the three diagonal grease holes from the pin. All of the scan readings using a SA5-N60S 5L32 wedge and probe for the holes were taken at a gain of 69dB.

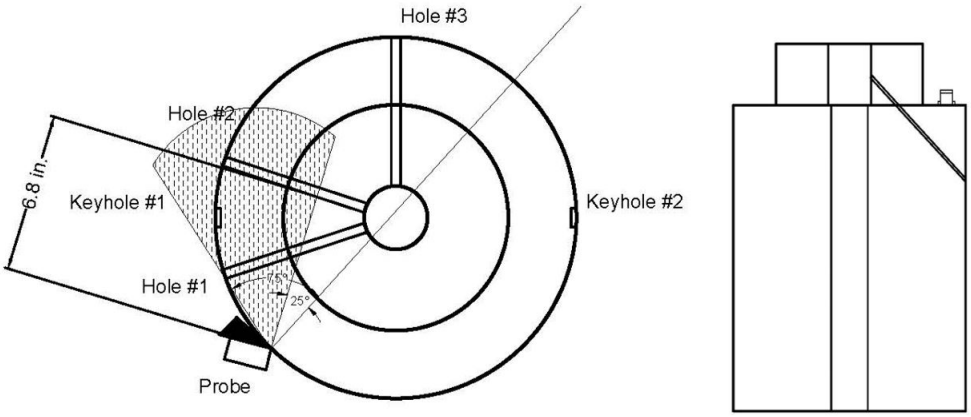

Figure 4.9: Exterior inspections using a SA5-N60S 5L32 probe and wedge. (Left) Probe used on exterior side on the second level of the pin, and (right) Probe used on the top side of the second level.

A Matlab program was written to provide a visual understanding of the reading in 3D. It is written for the Testing E.2 set-up, and it is also tested using one of the E.2 results. The program takes the starting point of the hole from the interior of the pin as the reference point of all the calculations. Using the dimensions of the mock-up pin, and the rise and run distances of its grease holes, a relationship was found to locate inspection point,

$$f(z) = (-\tan\theta)z + b \tag{4.2}$$

A function provides the slope and z-intersection of the linear relationship of the beam line at a certain angle, using Equation 4.2.

$$z = \frac{8.5}{8\,x} \tag{4.3}$$

In order to plot the line of the grease hole, a linear equation using the endpoints resulted in Equation 4.3.

4.2.2 Internal Inspection of Pin Parts

The internal inspection of the pins requires the 16-element sensor with the PMMA case to be inserted into the through-hole of the pin, as shown in Figure 4.10. The probe

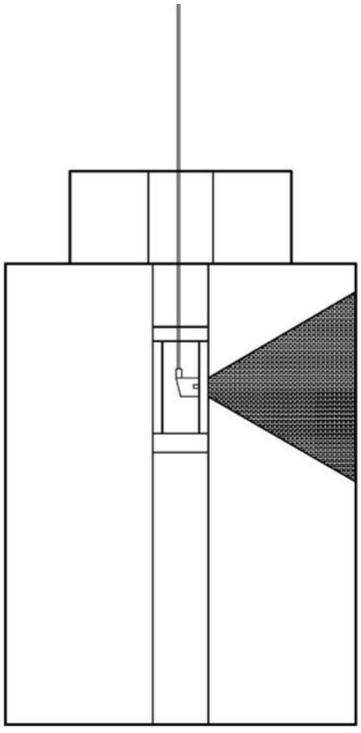

Figure 4.10: Beam angle spread of the UPA probe within the trunnion bearing pin.

encased in the PMMA case is lowered into the trunnion bearing pin. The PMMA case expands to an appropriate diameter size by the use of four springs in order to fit into the trunnion pin for a complete 360° inspection. Figure 4.10 shows the inspection of the trunnion bearing pin using the PMMA case with the 16-element transducer to read a vertical cross-section.

Using this type of inspection, four different tests are convenient, and listed in Table 4.2.

Table 4.2: Internal Inspection Testing.

Testing	Inspecting Part	Testing Type
I.1	The pin's outer edge	Known distance and compare with Omniscan reading
I.2	The pin's keyholes	Known distance and compare with Omniscan reading
I.3	The pin's keyhole height	-6dB Method
I.4	The entire pin	A 360° inspection scan of the pin

The inspection of the pin's outer edge and the keyholes were performed by inserting the PMMA case and probe to a certain height into the pin, at a recorded angle. The readings from the A-scans and S-scans from the Omniscan screen were recorded to check with the calculated measurement from the pin dimensions. The data was also saved for further analysis.

Testing I.1 and I.2 were applied to both PMMA Case I and Case II for the laboratory setting. Thus, this provides four testing results. For the field setting only Case II is used, providing two more testing results. The testing numbering as well as the targeted distance for each testing with respect to the PMMA case type is shown in Table 4.3. The calculation of these readings is shown in Appendix A.

Two different calibration approaches for the PMMA curved wedge is used. They are both tested in the laboratory testing on the PMMA Case I (Testing I.1.1 and I.2.1) and Case II (Testing I.1.2 and I.2.2). The first calibration approach considers the wedge

Table 4.3: Target Reading for the Internal Inspection of the PIn.

PMMA Case	Testing Setting	Testing No.	Target Reading (in.)
I	Lab	I.1.1	8.665
I	Lab	I.2.1	8.29
II	Lab	I.1.2	8.125
II	Lab	I.2.2	7.75
II	Field	I.1.3	8.125
II	Field	I.2.3	6.935

height within the target reading. To do this, the user makes a new wedge identity in the Omniscan MX2 and inputs the wedge height. For example, the exterior edge target reading of the mock-up pin with the first calibration approach is calculated as follows,

$$\frac{19\,\text{in.} - 2.75\,\text{in.}}{2} + 0.54\,\text{in.} = 8.125\,\text{in.} + 0.54\,\text{in.} = 8.665\,\text{in.} \tag{4.4}$$

The second calibration approach considers adjusting the wedge height that is inputted into the Omniscan MX2 so that it takes into account the curved edges. Because the PMMA wedge is curved, the wedge height is not uniform for all of the sound waves, as shown in Figure 4.11. And, the custom wedge option within Omniscan assumes that this PMMA wedge is rectangular because of the other inputs shown in Table A.3. Thus, it is appropriate to adjust the built-in wedge height for accuracy.

This allows the target reading calculations to disregard the wedge height. For example, the exterior edge target reading of the mock-up pin with the second calibration approach is calculated as follows,

$$\frac{19\,\text{in.} - 2.75\,\text{in.}}{2} = 8.125\,\text{in.} \tag{4.5}$$

The inspection of the pin's keyhole height, Testing I.3, for the lab testing on the mock-up pin required the usage of the -6dB method. The Gain (dB) measurement was adjusted so that the highest reading for the keyhole was set to 80 % in the A-scan. For each side

of this line the 40 % reading was recorded. The steel rod connected to the PMMA case also acted as a measuring device to calculate the distance between the extremes on each side of the 80 % reading for the 40 %. This distance would be an estimate of the keyhole height. It is not applied to the field testing because the keyhole locations interfere with a change in the internal through-hole size, and the sensor cannot be moved vertically to identify the entire keyhole.

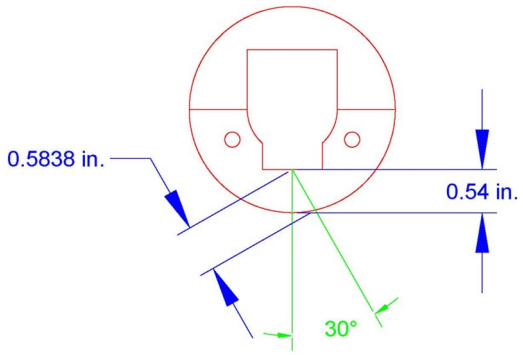

Figure 4.11: PMMA wedge height differences.

The last inspection testing using the PMMA case, Testing I.4, wraps up all of the scanning testing by providing a one-line 360° scan of the entire pin parts. The PMMA case is lowered at a certain height within the pin and rotated completely around the pin, while viewing a -30° to 30° window in one document by taking advantage of the B-scan. Therefore, the UPA sensor can cover a large area of the pin within seconds. This provides a fast defect detection application. If a defect is found, then it is readily located with respect to the pin angle for further study. This scan is possible by setting a constant scanning velocity of the inspection within the Omniscan MX2. For this research, the 360° scanning ability is used merely for fast defect detection manually. Because the inspection was done manually the speed was not constant.

4.2.3 Visual Inspection

In order to provide a complete inspection of the pins, a visual inspection is also given for the field testing. During the process of this research, the sleeves were taken off from the pin parts at Riverside Campus. This allowed for a clear visual inspection of the pin part's exterior surface. The important parts of investigation were the identification of the keyholes, and any other exterior surface defects.

4.3 Laboratory Testing: Mock-up Pin

4.3.1 External Testing

The exterior inspection used a SA5-N60S 5L32 wedge and probe, which has a beam window between 25° and 75°. Since the probe was directed at a perpendicular angle to the plane of the grease hole, the angle from the sound wave of the probe also made a perpendicular angle with the grease hole due to the law of perpendicular planes. The measurements shown were used to manually provide the location of the probe with respect to the grease hole, and to check with the Omniscan lengths. All of the exterior scan readings were taken at a gain of 69dB.

4.3.1.1 Testing E.1 Results

The Omniscan readings were used to identify the location of the grease hole, shown in Figure 4.12 and Figure 4.13.

Figure 4.13 shows a dark blue curved line that represents the grease hole being inspected. The A-scan file in Figure 4.12 shows a peak at 5.65 in. The noise from 0 in. to 3.5 in. can be ignored because it does not contribute to the inspection. Holes 2 and 3 are also identified through the same exterior inspection, shown in Figures B.3 through Figure B.6.

Using the Matlab program described in the Experimental Procedure section and the data from File0001, it was further developed to display the probe scanning window with respect to the grease hole. The location of the probe was set at (-5.5, -5.5, -2.25) with

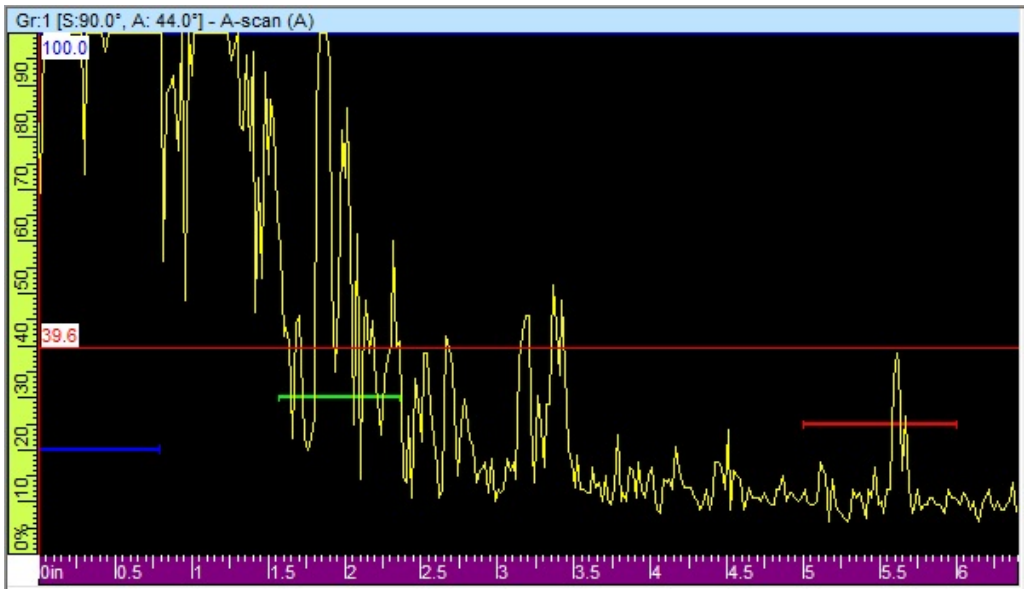

Figure 4.12: File0001 A-Scan of exterior top scan for Hole 1 (Testing E.1).

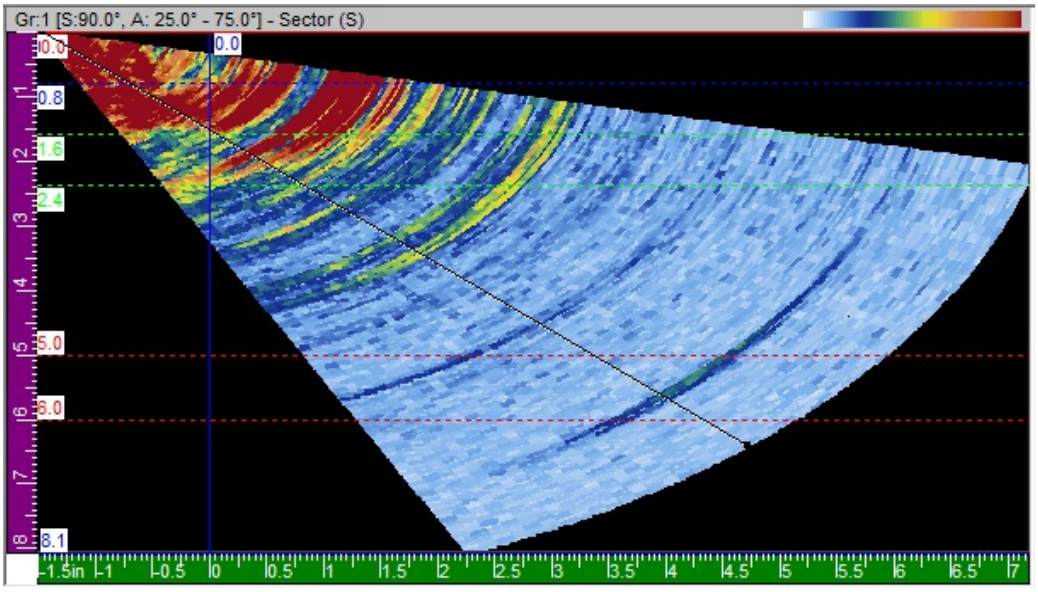

Figure 4.13: File0001 S-Scan of exterior top scan for Hole 1 (Testing E.1).

respect to the internal grease hole location. In other words, the probe was 5.5 inches away from the hole in the x- and y-direction, and 2.25 inches below the hole in the z-direction. The parameters used for Figure 4.14 are listed in Table D.1. This representation of the

pin and the probe shows the probe sound beam at 45° with the blue line, the hole in red, and the beam boundaries of the probe in green.

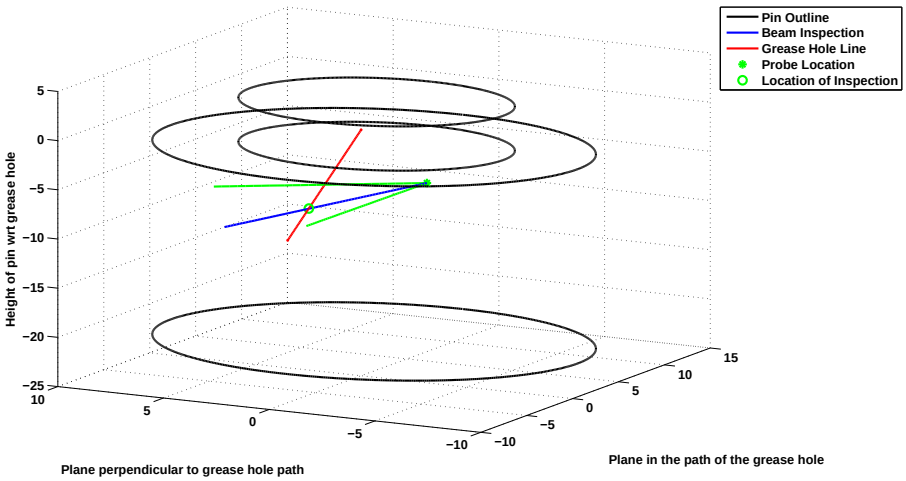

Figure 4.14: Matlab recreation of probe and wedge reading.

This Matlab program could be modified to receive the A-scans from the Omniscan inspection and to plot the whole S-scan with respect to the pin for a 3D visualization inspection technique. Since this research is focused on the internal inspection of the pin, this development is not needed at this time.

4.3.1.2 Testing E.2 Results

Other exterior scans of the holes were taken from the curved exterior surface of the pin rather than from the top surface. Figure B.2 shows the inspection of Hole 2 being inspected from the left side. Because only part of the wedge made contact with the pin, the S-scan was only used to inspect angles between 25° and about 45°, as an estimated cut-off point. See Figure 4.9 for a depiction of the probe inspection from the exterior curved surface. Figure 4.15 and 4.16 shows the A-scan and S-scan of Hole 1, respectively.

The red marking clearly indicates the grease hole between 6 and 7.5 in. inside of the

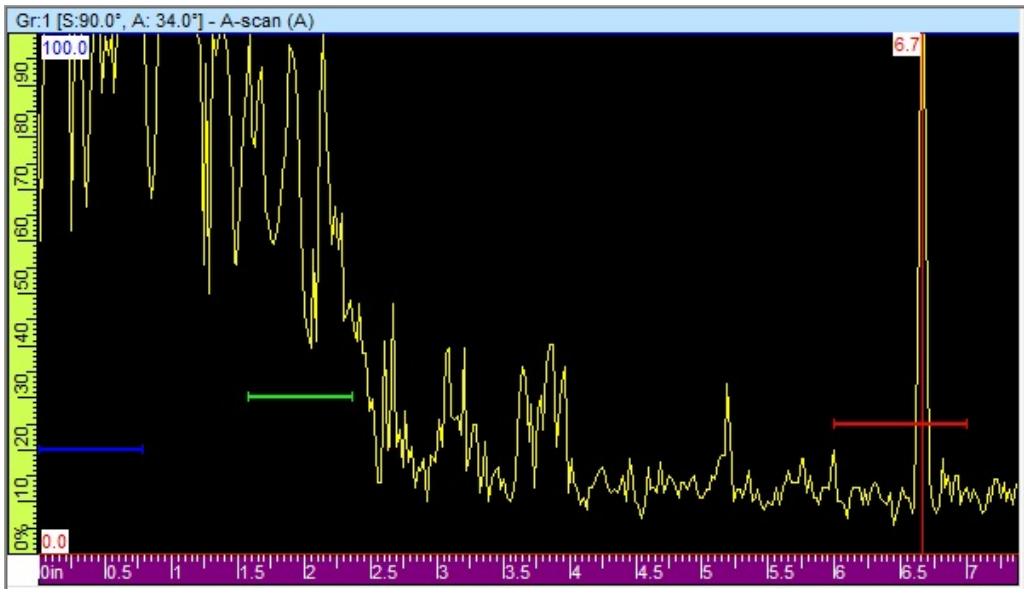

Figure 4.15: File0005 A-Scan of exterior side inspection for Hole 1 (Testing E.2).

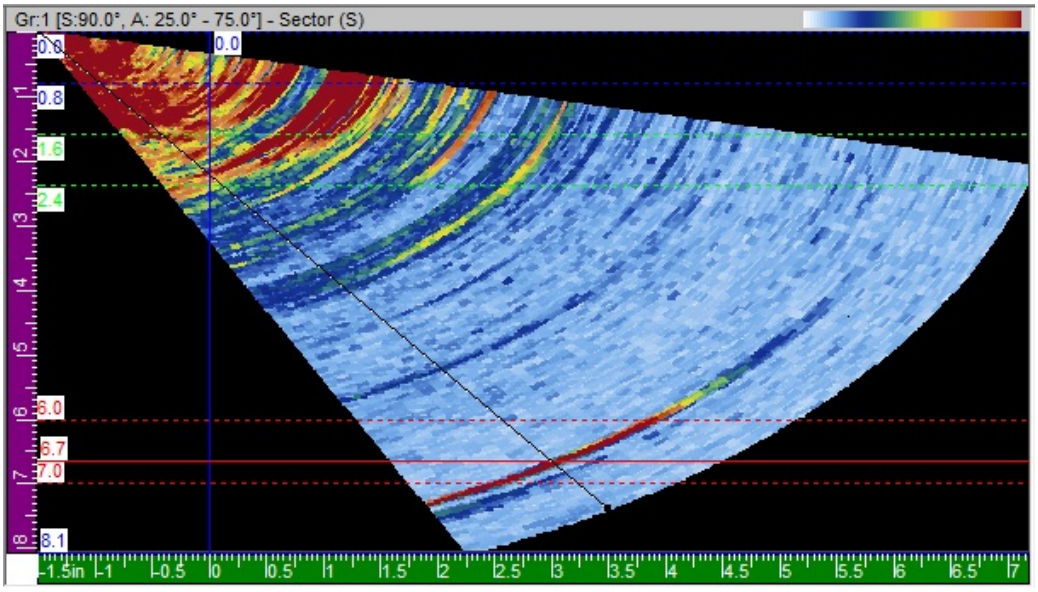

Figure 4.16: File0005 S-Scan of exterior side inspection for Hole 1 (Testing E.2).

pin, which corresponds to the distance from the probe and the angled hole at the time of this specific measurement. The measurements for Hole 2 and 3 are shown in Figures B.7 through B.10.

4.3.2 Internal Testing

The two PMMA cases, Case I and Case II, are tested on the mock-up pin to provide an accurate calibration method in order to use them properly to the original pin for the field testing.

4.3.2.1 Testing I.1.1 Results

The inspection of the mock-up pins outer edge using Case I takes into account the wedge height, 0.54 in., as shown in the calculations in the Experimental Procedure section. The target reading is 8.665 in. As shown in Figures 4.17 and 4.18, the sensor picks up a strong reading at 8.6 in., which is a correct measurement to the outer edge.

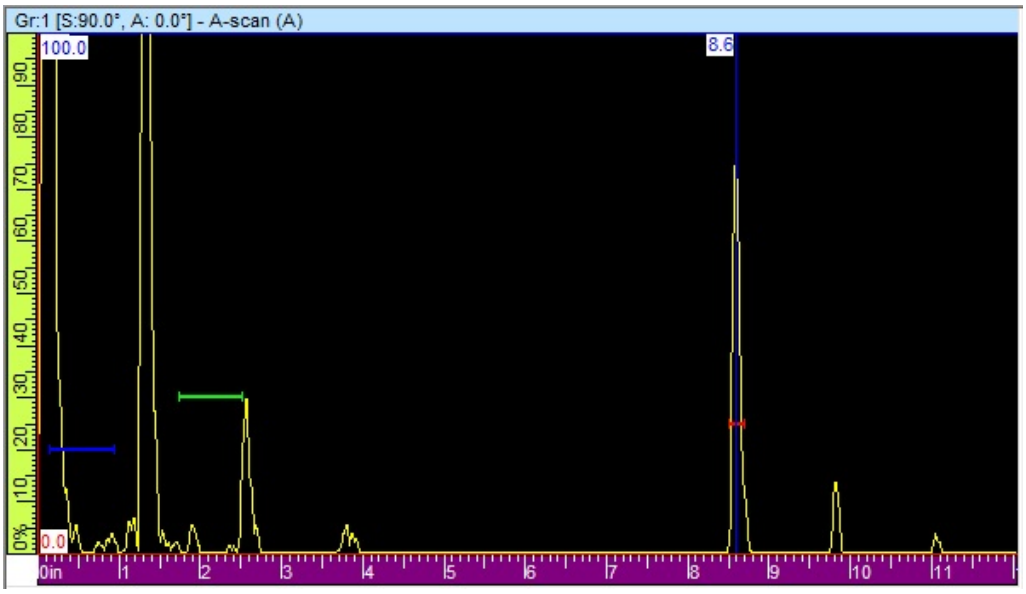

Figure 4.17: File106 A-scan showing the outer edge of the mock-up pin, using a 30dB gain (Testing I.1.1).

Ten samples measuring the readings of the exterior edge from different parts of the mock-up pin were taken directly from the Omniscan MX2 screen. The gate was set between 8.5 in. and 8.8 in. Table B.1 shows the average to be 8.599 in. Using this

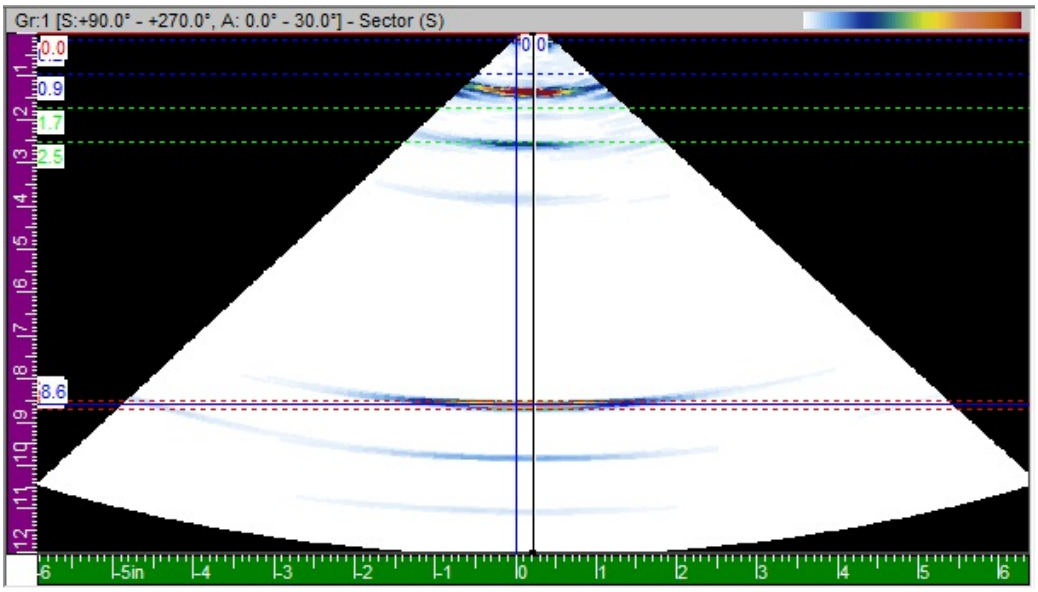

Figure 4.18: File106 S-scan showing the outer edge of the mock-up pin, using a 30dB gain (Testing I.1.1).

on-site average (8.599 in.), there is a 0.7 % error in the measurement.

4.3.2.2 Testing I.2.1 Results

The keyhole inspection of the mock-up pin using Case I also takes into account the wedge height. The keyhole depth is assumed to be 0.375 in., providing a target reading of 8.29 in. Figure 4.20 and Figure 4.19 show the A-scan and S-scan readings, respectively, for Keyhole #1.

These readings almost match the hand measurements taken from the mock-up pin. The figure states a distance of 8.2 in. from the interior to the exterior surface of the pin. Ten samples were also taken, switching between Keyhole #1 and #2, directly from the Omniscan MX2 screen. A gate was set between 8.1 in. and 8.3 in. Table B.2 shows the average of the ten samples to be 8.196 in. File107 and File109 were the first two readings from the ten trials. Using this on-site average (8.196 in.), there is a 1.13 % error in the measurement.

The scans for Keyhole #2, shown in Figures B.11 and B.12, also contribute to the

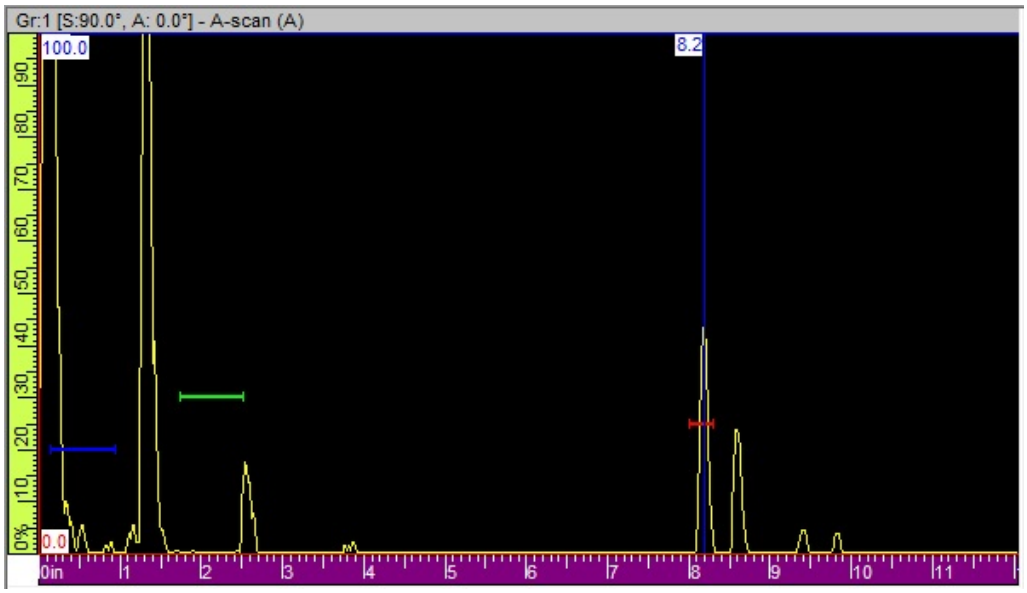

Figure 4.19: File0107 A-scan showing Keyhole #1 at 8.2 in., using a 40dB gain (Testing I.2.1).

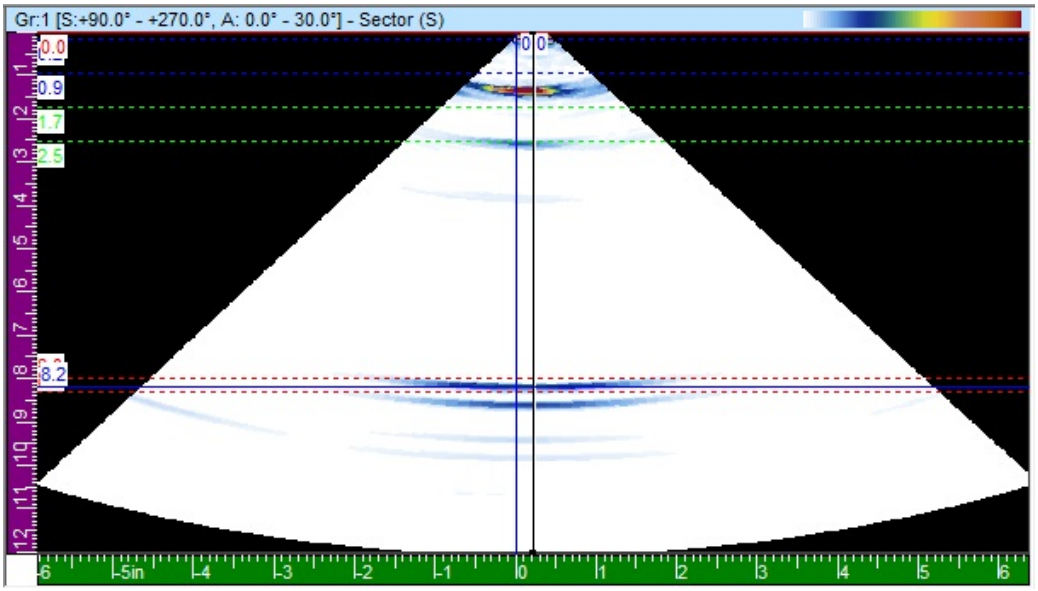

Figure 4.20: File0107 S-scan showing Keyhole #1 at 8.2 in., using a 40dB gain (Testing I.2.1).

same conclusion.

4.3.2.3 Testing I.3 Results

The inspection of the keyhole height is the last lab testing for Case I. Figure 4.21 and B.13, respectively, show the results for Keyhole #1 and Keyhole #2. The table that lists the different measurements shown from these figures are seen in Table B.3 and B.4.

Figure 4.21: Sample readings for Keyhole #1 using the -6dB method (Testing I.3.1).

The readings taken from these measurements indicate the distance from the transducer to the top of the pin. For Keyhole #1, the bottom 40% reading was 11.125 in. from the top of the pin, and the top 40% reading was 7 in. from the top. For Keyhole #2, they measured 11.375 in. and 7.25 in., respectively. These measurements were then placed on the pin to verify, and it became evident that the PMMA case was limited when reading the top 3 in. of the keyholes, as shown in Figure B.14. This is a limiting factor that has to be considered when examining the real trunnion bearing pin.

4.3.2.4 PMMA Case I Analysis

The wave detections shown in both the S-scan and the A-scan for the exterior edge detection and the keyhole detection from 0 to 0.5 in., or the first peak readings, are identified as noise from the pulse. This is normal for all UPA readings. The peaks

between 1 in. to 4 in. are noise from the contact intersection between the probe and the wedge, and the wedge and the interior pin surface. Both noises, shown as two peaks at 1.4 in. and 1.9 in. in Figure 4.19. A small peak at 3.8 in. can be contributed to possible noise. This data can be ignored as it does not provide insight on real defects. For the keyhole inspection, the sound reading at 8.2 in. is followed by a 8.6 in. reading. This is concluded to be the reading from the exterior surface of the pin. Up to this point all of the readings are found in the first leg. The second leg, which is a mirror version of the A-scan readings shown, begins with the peaks at 9.4 in. and 9.9 in. This is also common in UPA readings.

Because the Omniscan screen does not actually give the distance to the highest peak, but rather the concentrated measurement closest to the probe, it provides a quick and fast inspection on the field. For example, File107, seen in Figure 4.19, shows a peak at 8.2 in. but the on-site Omniscan reading, shown in Table B.2, provided 8.18 in. The entire reading varies between 8.1 in. and 8.3 in., which includes the actual dimension of 8.29 in. This reasoning can also be applied to the exterior surface reading. The peak for Figure 4.17 is seen at 8.6 in., but the reading begins at 8.6 and ends at 8.8 in., which includes the calculated 8.665 in. dimension.

From the A-scan, two peak readings are seen at 8.2 in. and 8.6 in. It has been already stated that the former reading measures to the exterior of the keyhole. The latter reading could be a skewed reading of the exterior pin surface since it adds 0.2 in. to the distance calculated in Equation 4.4. The A-scan also shows their reflection at 9.4 in. and 9.8 in. These are ignored because they are part of the second leg.

4.3.2.5 PMMA Case I Summary

A summary of the results and the errors for the mock-up pin readings are shown in Table 4.4 and 4.5. The UPA readings for the keyhole and the exterior surface have a very low % error. This result provides confidence that defects will be easily found due to the characteristic of the S-scan for the UPA system.

As for the inspection of the keyhole height, the measurements are not available for the top 3 in. of the pin. This is probably because as the probe is taken out at the top, the springs at the top part of the case stretch and might cause the PMMA surface to lose contact with the interior surface of the pin. This is a problem that needs to be considered for this particular PMMA case.

Table 4.4: Errors of Mock up Pin Results for PMMA Case I

Type	Real (in.)	Reading (in.)	% Error	Δ Tolerable (in.)
Exterior surface	8.665	8.599	0.7	$\pm$ 0.06
Keyhole	8.29	8.196	1.13	$\pm$ 0.09

Table 4.5: Errors of -6dB Method for Keyhole Heights, for PMMA Case I

Type	Real (in.)	Reading (in.)	Δ (in.)
Keyhole 1	7.16	4.125	3.035
Keyhole 2	7.16	3.875	3.285

The inspection of the interior diagonal grease hole in the pin could not be found using this PMMA case. Instead, it is recommended that an angled wedge be inserted or built-in to the inside of the PMMA case so that the probe might have a different angle sweep. The exterior inspections, albeit not possible at a real bridge site, provide the assurance that the hole can be inspected with UPA.

4.3.2.6 Second Calibration Method Results

A second calibration approach that allows the Omniscan inspection to disregard the wedge height into the target calculations was performed by calculating a proper wedge height input for more accurate results.

The readings of different wedge heights were observed, shown in Table B.7. A linear relationship between them was found when graphed in Figure B.21. The relationship is expressed as,

$$\text{Wedge Height} = -0.5036 \times (\text{Reading to Exterior Surface of Pin}) + 4.657 \tag{4.6}$$

In order to eliminate the wedge height value from the target readings, like in Equation 4.4, the reading to the exterior pin would need to be 8.125 in. Therefore, the wedge height input required would need to be 0.565 in. This result is basically the average of the direct wedge height between the probe and the exterior surface of the PMMA (0.54 in.), and the wedge height at a 30° angle (0.5838 in.), as seen in Figure 4.11.

4.3.2.7 Testing I.1.2 Results

The inspection of the mock-up pin's outer edge using Case II considered both of the calibration approach mentioned. Using the first calibration approach for Testing I.1.2 provided a 2.68 % error. See Table B.5 for the readings.

Using the second calibration approach, the percent error decreased to 0.27 %. Figures B.15 through B.16 show results of the A-scan and S-scan using Case II.

Table 4.6: Errors of Mock up Pin Results with PMMA Case II

Testing	Real (in.)	Reading (in.)	% Error	Δ Tolerable (in.)
I.1.2	8.125	8.103	0.27	± 0.022
I.2.2	7.75	7.7039	0.59	± 0.046

4.3.2.8 Testing I.2.2 Results

The inspection of the mock-up pin's outer edge using Case II considered both calibration approach mentioned. Using the first calibration approach for Testing I.2.2 provided

a 3.01 % error. See Table B.6 for the readings.

Using the second calibration approach, the percent error decreased to 0.59 %. Figures B.17 through B.20 show the results of the A-scan and S-scan for Keyhole #1 and #2.

Table 4.7 shows the results of the adjusted wedge height when inspecting the exterior edge and the keyhole. Both percent errors, 0.27 % for the exterior edge and 0.59 % for the keyhole, are very low compared to the errors found using the first calibration approach.

Table 4.7: PMMA Case II testing with Calibrated Wedge Height, using a 40 dB Gain.

Trial	Exterior Edge Reading (in.)	Keyhole Reading (in.)
1	8.128	7.710
2	8.127	7.705
3	8.067	7.677
4	8.185	7.663
5	8.081	7.698
6	8.026	7.775
7	8.08	7.710
8	8.069	7.686
9	8.108	7.680
10	8.103	7.735
Average	8.103	7.704
Target	8.125	7.750
% Error	0.24 %	0.59%

4.4 Field Testing: Original Pin Parts

This section presents the field testing of the original trunnion pin at Riverside Campus. As noted in Chapter 3, the pin parts at Riverside are only part of the original pin. Thus, only part of the whole trunnion pin can be inspected. The through-hole of the pin from the original drawings is said to measure 2-5/8 in., but it actually measures between 2-5/8 in. and 2-1/2 in. The calculations use a 2-1/2 in. PMMA diameter for the through-hole

to be consistent with the pin in the field. Because this through-hole diameter is smaller than the mock-up pin, the PMMA Case II is used. The second calibration approach providing a wedge height of 0.565 in. is used with the PMMA Case II.

4.4.1 Testing I.1.3 Results

The inspection of the pin parts were done while the sleeve was still attached to the pin parts, thus the body of the pin could not be visually inspected. For clarification purposes, see Figure 3.2 to identify the location of Pin Parts I and II with respect to the original whole trunnion bearing pin. The pins were inspected at different polar locations and heights from the 2-1/2 in. diameter through-hole. Ten samples with readings directly from Omniscan for both pins were averaged to calculate the percentage error. The target reading for the exterior edge measurement from the interior of the through-hole for both pin parts is 8.125 in, as shown in Table 4.3.

A compilation of the exterior edge measurements for the entire pin is shown in Figure 4.22. This figure shows the distance from the center of the pin, with the angles being referenced as shown in Figure 3.6. The data taken from the Omniscan is found in Tables C.1 and C.2.

The percent errors shown in Table 4.8 are very low and provide assurance of positive results. The data points from the polar display in Figure 4.22 also create a perfect circle aligned with the circumference of the exterior pin. These points show the distance from the center of the pin to the measured exterior edge. The target distance for this case would be equal to the radius of the pin, or 9.375 in.

Table 4.8: Exterior Edge Reading Summary.

Pin	Real (in.)	Avg. Reading (in.)	% Error	Δ Tolerable (in.)
I	8.125	8.123	0.02	0.0016
II	8.125	8.1027	0.27	0.022

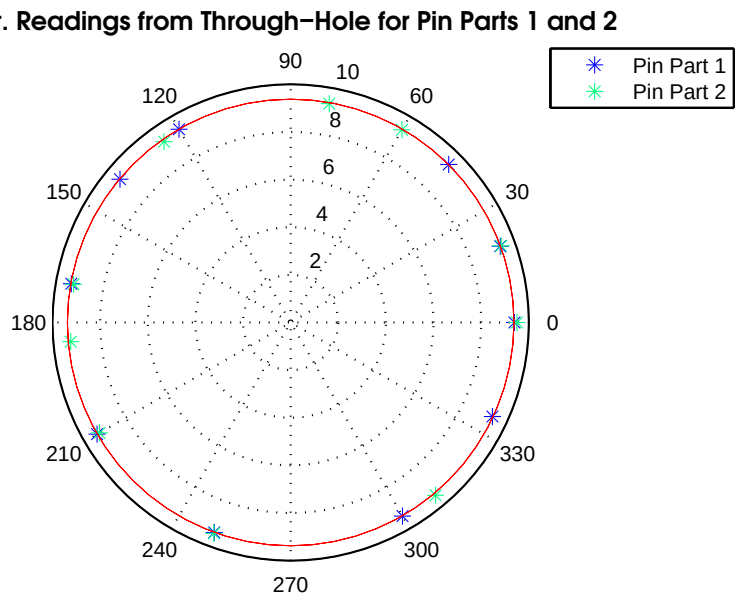

Figure 4.22: Combined data points of Pin Parts I and II showing the location for the Exterior Edge readings at Riverside (Testing I.1.3).

4.4.2 Testing I.2.3 Results

The two keyholes initially on the Pin Part I were each covered with a steel key. No keyholes were visually seen on the Pin Part II, so the keyhole testing was not applicable for the Pin Part II. The inspection of the two keyholes was then performed by comparing the keyhole readings to the exterior edges of the pin because the keyhole depth was unknown. This inspection, though, was performed on the top 3.5 in. of the pin, which has a 4.88 in. diameter. The target reading for the exterior edge measurement of the top 3.5 in. from the interior of the through-hole for both pin parts, as shown in Table 4.3, is 6.935 in.

While inspecting the exterior edge, the UPA probe picked up readings in the direction of the keyholes in Pin Part I that are shown in Figure 3.7. The compiled data for the exterior edge and the keyhole readings are shown in Figure 4.23.

As noted, the keyholes visually are not set back, like in the mock-up pins, but rather come out of the circular layer. Yet, the scans for the keyholes, shown in Table 4.9, come

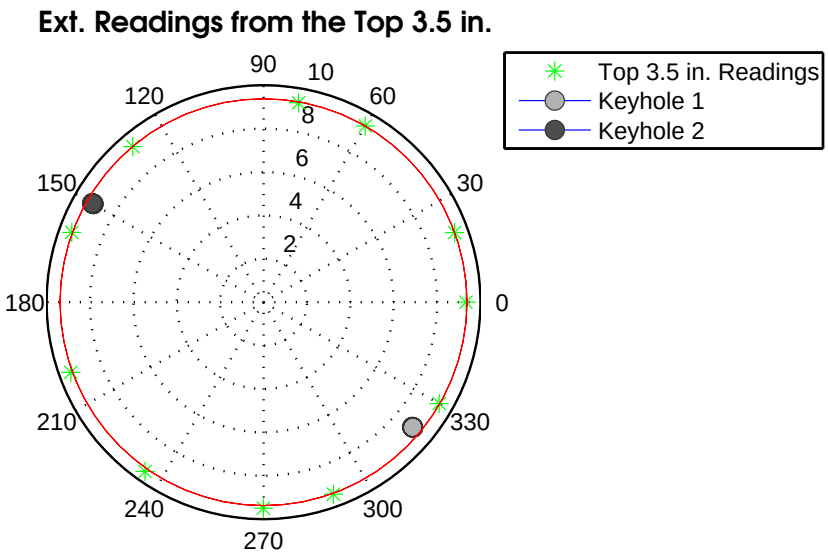

Figure 4.23: The two keyhole readings with respect to the exterior edge readings for the top 3.5 in. of Pin Part I (Testing I.2.3).

in by half an inch. After the removal of the sleeves from the pin it was understood that the keyholes do actually come into the pin.

The measurement for the exterior edge results in a 0.34 % error. The pin does have threads on the exterior which disrupts the measurement averages.

Table 4.9: Exterior Edge Reading of the top 3.5 in. with Keyholes Summary.

Type	Avg. Reading (in.)	Target Reading (in.)	Error (%)	Δ Tolerable (in.)
Top 3.5 in.	6.959	6.935	0.34	0.02
Keyhole 1	6.531	-	-	-
Keyhole 2	6.642	-	-	-

4.4.3 Comments on Resolution

During the inspection of the pin some scans picked up streaks, like the ones shown in Figure 4.24. Initially this was assumed to be a resolution problem, so the focal law angle increment was changed from 1° to 0.5° and 0.3°. These streaks were still spotted

even after the resolution adjustment, but it became evident that the readings were noise disturbance due to the connection instability between the probe and the Omniscanner.

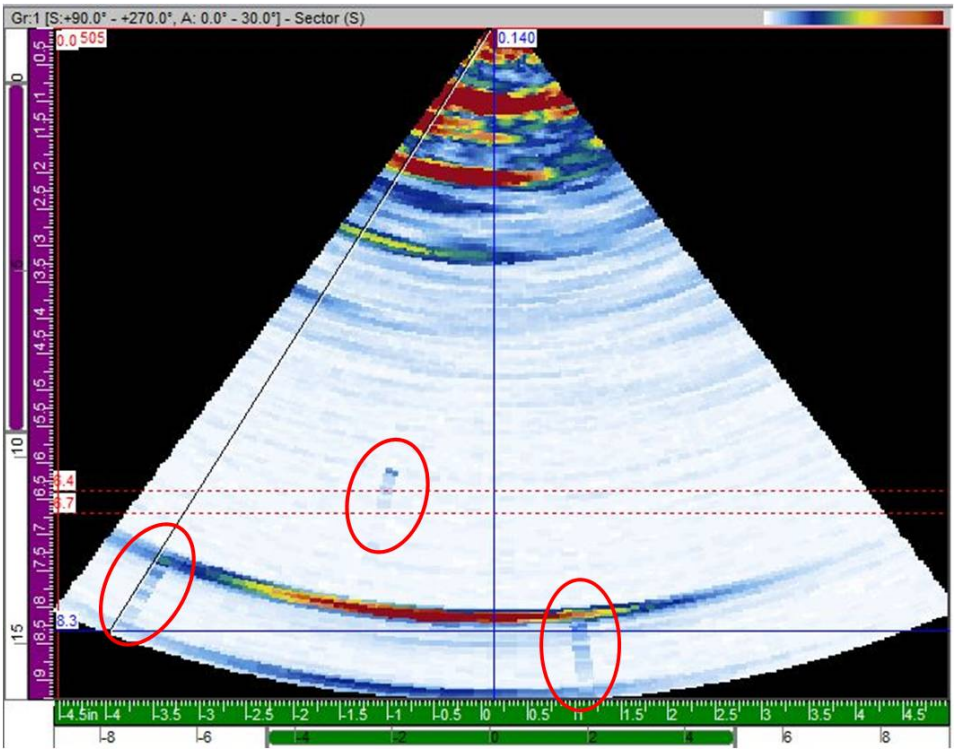

Figure 4.24: File167 S-scan showing error streaks.

4.4.4 Testing I.4 Results

The one-line scan was performed in Pin Parts I and II. Figure 4.25 shows the B-scan of Pin Parts I taken at 10 in. below the pin. As shown, the contact between the probe and surface was not perfect throughout the scan. The exterior pin surface can be identified by the sound near 8.1 in. The scan does not show any readings within the pin, besides the initial noise. This conclusion was also found for Pin Part II.

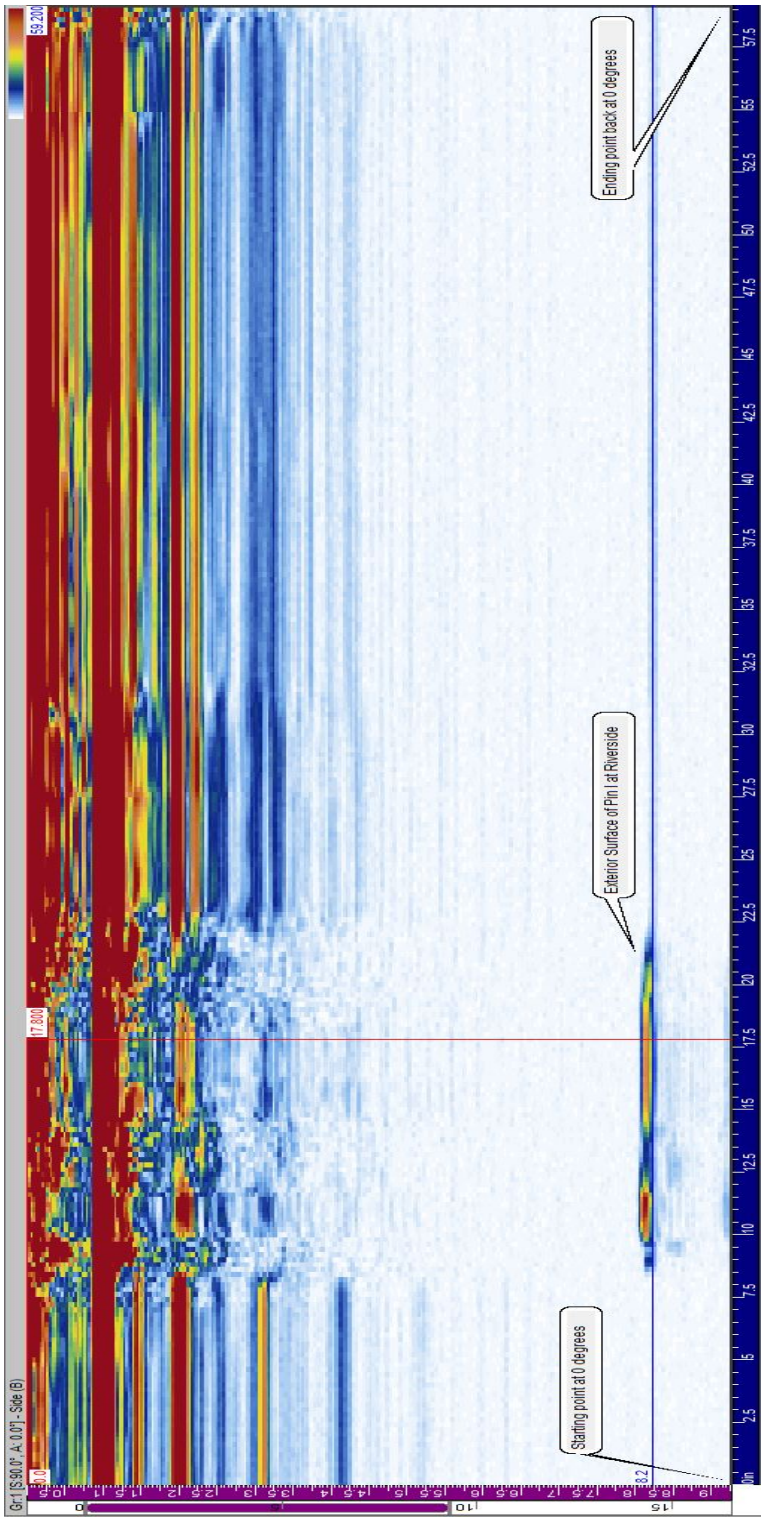

Figure 4.25: File170 showing the 360 degree of Pin Part I at 10 in. below the top of pin.

4.4.5 Visual Inspection

The sleeve was removed from the pin after the UPA testing in order to provide a visual inspection on the current state of the pin. As shown in Figure 4.26, the keyholes come inside of the pin, which verified the keyhole readings from the top 3.5 in. of Pin Part I. Also noted from the provided figure, after the keyhole there is a large section that steps into the pin, but it returns back out. This inconsistency does not continue throughout the entire surface of the pin. It is also similar to the surface above Keyhole #1 from Pin Part II, shown in Figure 4.27. The original drawings of the pin, shown in the Appendix, shows that the pin steps in between the keyholes by 15/32 in. on each side. An "4" detail was found above the Keyhole #2 of Pin Part II, shown in Figure 4.27.

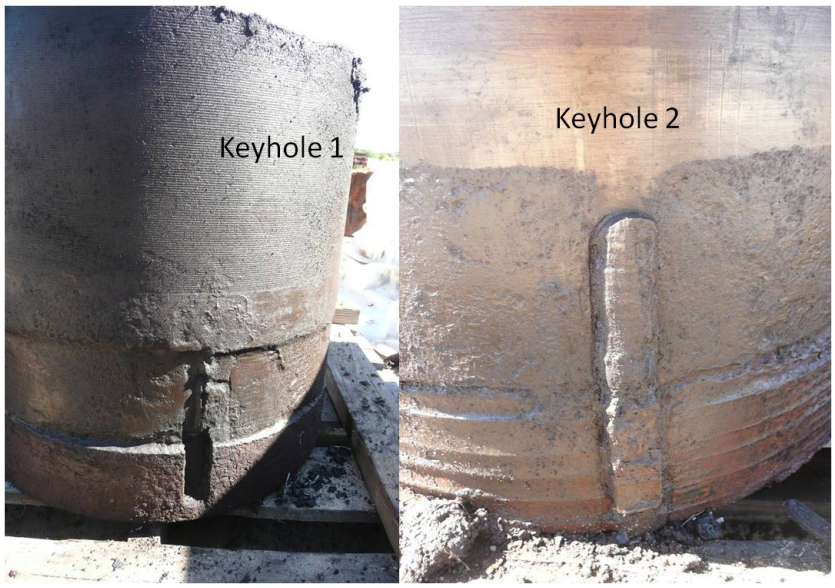

Figure 4.26: Keyholes of Pin Part I.

It was also found that for Pin Part II the UPA system is only able to inspect 12 in. from the top.

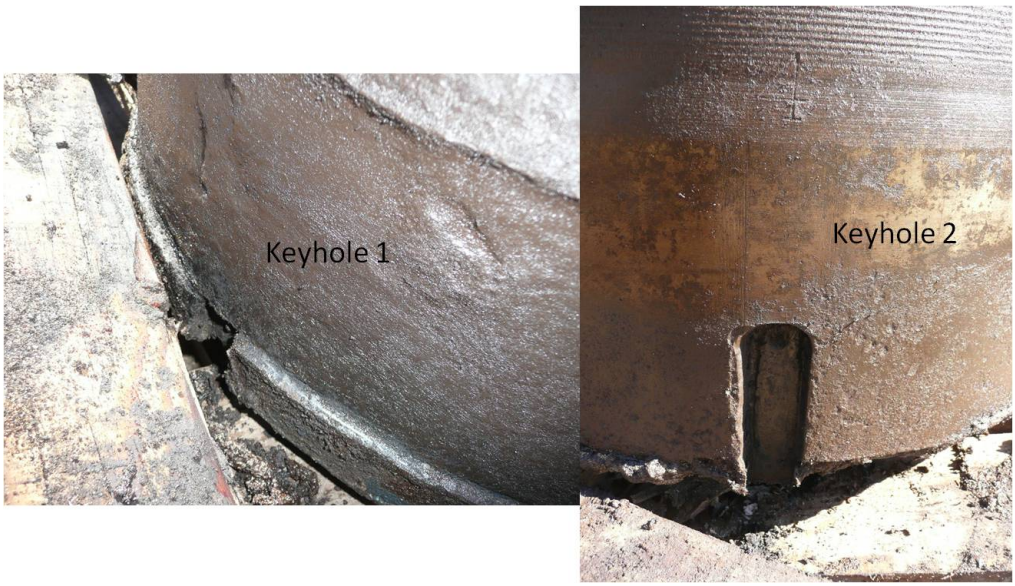

Figure 4.27: Keyholes of Pin Part II. A "4" detail is shown above Keyhole 2.

4.4.6 Comments on the Field Inspection

The inspection of the original trunnion pin parts at Riverside Campus with the PMMA Case II resulted in different advantages and limitations of the case. The PMMA case was freely able to be rotated within the through-hole for a 360° scan, using a one-line scan type. It also provided accurate results for the exterior edges beginning from two different through-hole diameter surfaces. The probe also provided easy scanning access through the use of sectorial scanning, allowing the inspector to visualize the interior pin using various angles. The UPA technology provided correct readings for the keyholes from the top part of Pin Part I available without the possibility of visual inspection. These results were verified by the visual inspection after the removal of the sleeves.

Although these points provide a strong argument for the use of UPA system for this inspection, some constraints encourage future research development. The through-hole from the trunnion pin at Riverside had sinuous surfaces throughout. There were also some depths where the pin sides came inward. Even though the couplant used between the wedge and the surface provided access despite of the varying area, there were still

many parts where the probe had difficult scanning due to the inability to be in contact with the surface.

5. CONCLUSION

The long term goals of the project were to develop a transportable UPA system to inspect a 100-year old trunnion bearing pin that would make it possible to identify unknown defects within the pin. This project would also contribute to the on-going technological research for nondestructive testing in historic structures and their members. To ensure a thorough investigation, the UPA system was tested in a laboratory setting on a mock-up pin model, and in a field setting on the original parts of the counterweight trunnion bearing pin taken out of service from the Salmon Bay Bridge. The testing done in the mock-up pin provided a way to calibrate the PMMA case in order to provide accurate readings in the authentic pin.

The UPA system was developed by designing and fabricating a PMMA case to house the designated probe. The material sound velocity was found by testing the TOF of sound from one side transducer to the other. This result was entered into the Omniscanner and the probe was calibrated by providing an adjusted wedge height. Two PMMA cases with different diameters were tested with the mock-up pin. The calibration method for the PMMA Case II proved to be more accurate, and the exterior edge and the keyholes were identified with a 0.27 % and 0.59 % error, respectively. Its limitations included finding the accurate height of the keyholes, and identifying the diagonal grease holes.

The same case was used to test the two parts of the original trunnion pin at Riverside campus. The exterior edges were found for both pin parts and from the top 3.5 in. of Pin Part I. A reading near the top keyholes on Pin Part I indicated that the keyholes also came into the pin even though they were covered by the keys. This was verified by the visual inspection done on the pin parts. A one-line scan was also used to inspect both pin parts at Riverside, but no interior defects were found. This UPA calibrated system provided accurate results during inspection, even though the pin's interior surface was rough and denied perfect contact with the PMMA case.

In the future this technology should be combined with an automatic system that allows the PMMA case to be rotated at a constant speed for accurate one-time scans. This reduces human interaction errors with the inspection. A membrane-like surface adaptable to rough faces, along with a constant flow of water between the wedge and surface, would facilitate the need to remove the PMMA case out of the pin to re-apply couplant for inspections. A modified angled wedge could also be applied within the PMMA case to search for diagonal cracking.

REFERENCES

AASHTO (1994). *Manual for Condition Evaluation of Bridges*. American Association of State Highway and Transportation Officials, Washington, D.C., 2nd edition.

AASHTO (1998). *Movable Bridge Inspection, Evaluation, and Maintenance Manual*. American Association of State Highway and Transportation Officials, Washington, D.C., 1st edition.

Anon (1908). "Doubletrack Trunnion Bascule Bridge over Bodine Creek, Staten Island Rapid Transit Railway," *Engineering News*, 3, 57–59.

ASCE (2009). "2009 Report Card for America's Infrastructure," American Society of Civil Engineers, <https://apps.asce.org/reportcard/2009/grades.cfm>.

ASCE (2013). "2013 Report Card for America's Infrastructure," American Society of Civil Engineers, <http://www.infrastructurereportcard.org/bridges/> (March).

ASM International (2005). "Industry Updates: Ultrasonic Inspection Technology in Development for Queensboro Bridge," *Journal of Failure Analysis and Prevention*, 5(3), 38.

Bastianini, F., Ceriolo, L., Tommaso, A. D., and Zaffaroni, G. (2004). "Mechanical and Nondestructive Testing to Verify the Effectiveness of Composite Strengthening on Historical Cast Iron Bridge in Venice, Italy," *Journal of Materials in Civil Engineering*, American Society of Civil Engineers, 16, 407–413.

Brown, D. (1993). *Bridges*. Macmillan Maxwell Macmillan International, New York, NY.

Catbas, F., Gul, M., Zaurin, R., Terrell, T., Dere, Y., Ansley, M., Frangopol, D., and Grimmelsman, K. (2009). "Structural Health Monitoring of Bridges: Fundamentals, Application Case Study and Organizational Considerations," *Structures Congress 2009*, Vol. 1, American Society of Civil Engineers, 1–11 (April).

DeLony, E. and Klein, T. (2005). "Rehabilitation of Historic Bridges," Vol. 131, American Society of Civil Engineers, 178–186 (July).

Dorpat, P. (2012). "Seattle Now and Then: Ballard's Bascule Bridge," Seattle Now and Then, <pauldorpat.com/seattle-now-and-then/seattle-now-then-ballards-bascule-bridge>.

Ginzel, E. and Thompson, R. (2013). "Errors Resulting From Curved Phased-Array Wedges," NDT.net, <http://www.ndt.net/article/ndtnet/2011/22_Ginzel.pdf> (Feb).

Griggs, F. (2006). "Development of the Vertical Lift Bridge: Squire Whipple to J.A.L. Waddell, 1872–1917," *Journal of Bridge Engineering*, American Society of Civil Engineers, 11(5), 642–654.

Hool, G. and Kinne, W. (1923). *Moveable and Long-Span Steel Bridges.* McGraw-Hill Book Company, New York, NY.

Hovey, O. (1927). *Movable Bridges*, Vol. 2. John Wiley & Sons, Brooklyn, NY.

Isohata, H. (2005). "A Study on Repair and Strengthening of Historic Steel Bridges," *ICE Current and Future Trends in Bridge Design, Construction and Maintenance*, 4, 249–259.

Jemec, V., Jurman, J., and Grum, J. (2007). "Evaluation of Defects and Cracks in Carriage Axles Using Non-Destructive Testing," *NDT for Safety*, NDT.net, 107–118.

JFE Group (2012). "Nondestructive Inspection by Phased Array Ultrasonic Method for Steel Structures," *Report No. 17*, New Products & Technologies: JFE Technical Report (April).

Johnson, J. (1991). "The Design of a Trunnion Bascule Bridge," B.S. Thesis, Armour Institute of Technology, Chicago, IL.

Kappes, W., Rockstroh, B., Barh, W., Kroning, M., Rodner, C., Goetzer, J., and Nemec, D. (2006). "Application of New Front-end Electronics for Non-destructive Testing of Railroad Wheel Sets," ECNDT, 1–12.

Koglin, T. (2003). *Movable Bridge Engineering.* John Wiley & Sons, Hoboken, NJ.

Lacroix, B., Lupien, V., Duffy, T., Kinney, A., Khandelwal, P., and Wasan, H. (2002). "Phased-Array Ultrasonic System for the Inspection of Titanium Billets," *American*

Institute of Physics Conference Proceedings, 615(1), 861–868.

Lichtenstein Consulting Engineers, Inc. (2002). "Delaware's Historic Bridges: Survey and Evaluation of Historic Bridges with Historic Context for Highways and Railroads," DelDOT Archeaology Series No. 170.

Long, R. and Cawley, P. (2007). "Phased Array Inspection of Irregular Surfaces," *American Institute of Physics Conference Proceedings*, 894(1), 814–821.

Malvern, L., Lu, S., and Jenkins, D. (1985). "Balancing of Trunnion-Type Bascule Bridges," *Report No. 40*, Dept. Engineering Services, University of Florida, Gainesville, FL.

Melewski, P., Brizzell, J., and Cooper, M. (2009). "Conversion of the 1.25 Mile Long Poughkeepsie-Highland Railroad Bridge into a Multi-Use State Park using the Public-Private Partnership Process," *Structures Congress 2009: Don't Mess with Structural Engineering*, American Society of Civil Engineers, 34, 1–9.

National Register of Historic Places (2013). "State Listings: Washington, King County," <http://www.nationalregisterofhistoricplaces.com/wa/king/state.html> (March).

Olympus (2013). "Phased Array Tutorial," <http://www.olympus-ims.com/en/ndt-tutorials/phased-array> (March).

Paine, C. (1929). "Analysis of Dynamic Stresses in Hackensack Bascule," *Engineering News Record*, 103(9), 340–344.

Pierce, G. (2013). "GN's Bridge 4: The Great Northern's Bridge at the Locks," <http://www.gngoat.org/index.htm> (March).

Pospisil, K., Stryk, J., Korenska, M., and Pazdera, L. (2005). "Acoustic Emission as a Tool for Non-Destructive Diagnostics of Bridges," *Proceedings ICE Current and Future Trends in Bridge Design, Construction and Maintenance*, 323–332.

Quaegebeur, N. and Masson, P. (2012). "Correlation-Based Imaging Technique Using Ultrasonic Transmit-Receive Array for Non-Destructive Evaluation," *Elsevier: Ultrasonics*, 52, 1056–1064.

Reichmann, A. (1924). "American Bridge Type Bascule Bridge," *Journal of the Western Society of Engineers*, 29(4), 177–181.

Rens, K. and Kim, T. (2006). "Quebec Bridge Inspection Using Common Nondestructive and Destructive Testing Techniques," *Structures Congress 2006*, American Society of Civil Engineers, 1, 1–16.

Rudlin, J., Raude, A., Volz, U., and Lo Conte, A. (2012). "New Methods of Rail Axle Inspection and Assessment," *18th World Conference on Nondestructive Testing*, 16–20.

Saldibar III, J. (1997). "Rehabilitating a Historic Iron Bridge: The Stillwater Road (SHEA) Bridge," Heritage Preservation Services (April).

Shan, B. and Ou, J. (2005). "An Ultrasonic Phased Array System for NDT of Steel Structures," *Proceedings SPIE The International Society for Optical Engineering*, 273–277.

Song, S. and Kim, C. (2002). "Simulation of 3-D Radiation Beam Patterns Propagated Through a Planar Interface from Ultrasonic Phased Array Transducers," *Elsevier Science: Ultrasonics*, 40, 519–524.

Song, S., Shin, H., and Jang, Y. (2000). "Ultrasonic Phased Array Transducers for Nondestructive Evaluation of Steel Structures," *American Institute of Physics Conference Proceedings*, 509(1), 1079–1086.

Sparks, S. (2008). "Evaluation of Iron and Steel in Historic Bridges," *Structural Analysis of Historic Construction: Preserving Safety and Significance: Proceedings of the VI International Conference on Structural Analysis of Historic Construction*, 451–458 (July).

Story, B. (2012). "Structural Impairment Detection Using Arrays of Competitive Artificial Neural Networks," Ph.D. thesis, Texas A&M University, College Station, TX.

Story, B., Hurlebaus, S., and Fry, G. (2010). "Nondestructive Evaluation of Trunnion Bearing Pins," *American Institute of Physics Conference Proceedings*, Vol. 1211, 1733–1740.

Sugiyama, H., Tabata, A., Nakajima, H., Yamagami, T., Tsukamoto, S., Uchima, M., Okuno, M., and Kohno, Y. (2010). "Development of a Compound Inspection Method to Detect Fatigue Damages on Orthotropic Steel Deck," *Bridge Maintenance, Safety, Management and Life-Cycle Optimization: Frangopol, Sause & Kusko*, Taylor & Francis Group, 393.

Tilly, G. and Gifford and Partners (2002). *Conservation of Bridges*. Spoon Press, New York, NY.

Walle, G. and Netzelmann, U. (2006). "Thermographic Crack Detection in Ferretic Steel Components Using Inductive Heating," ECNDT, 1–10.

Wallner, M. and Pircher, M. (2007). "Kinematics of Movable Bridges," *Journal of Bridge Engineering*, 10(1), 43–48.

Weingardt, R. (2010). "Leonardo da Vinci," *Leadership and Management in Engineering*, American Society of Civil Engineers, 10(1), 43–48.

Wood, J. and Rens, K. (2006). "Nondestructive Testing of the Lawrence Street Bridge," *Structures Congress 2006*, American Society of Civil Engineers, 1, 1–15.

Zhang, K., Lin, J., Lin, F., and Yu, X. (2012). "Development of Ultrasonic Testing System for Large Diameter Hollow Shaft," *18th World Conference on Nondestructive Testing*, 16–20.

Zimmer, A., Vrana, J., Meiser, J., Maximini, W., and Blaes, N. (2010). "Evolution of the Ultrasonic Inspection of Heavy Rotor Forgings over the Last Decades," *American Institute of Physics Conference Proceedings*, 1211(1), 1631–1638.

APPENDIX A

SET-UP PROPERTIES

A.1 Ultrasonic Velocity of PMMA

This section explains the nondestructive testing (NDT) method to determine the ultrasonic velocity of the PMMA material. This information was added to the new wedge information within the Omniscanner.

A.1.1 Experimental Set-up

The experimental set-up includes two parts: the Signal Generator and the Oscilloscope, as shown in Figure A.1.

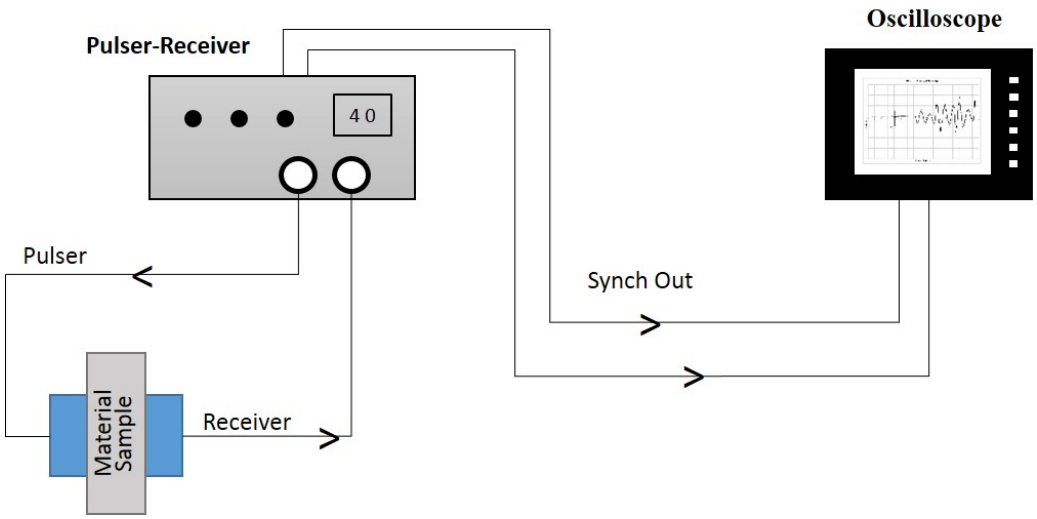

Figure A.1: Experimental Set-up for PMMA material sound velocity.

A.1.2 Experimental Procedure

The Pulser-Receiver consisted of a manually controlled ultrasonic pulser-receiver system that sends the voltage signals, two ultrasonic transducers, and a material testing

sample. The pulser channel produces an electrical pulse that excites one transducer. The transducer then converts the electrical pulse into mechanical energy to create an ultrasonic wave into the material sample. The exiting wave is received by a second transducer, which reconverts the mechanical energy to an electrical pulse. This pulse continues into the receiver channel of the Pulser-Receiver system. The Pulser-Receiver system used was a Model 5072PR, two 50 MHz transducers, and the outer PMMA cap, shown in Figure A.2.

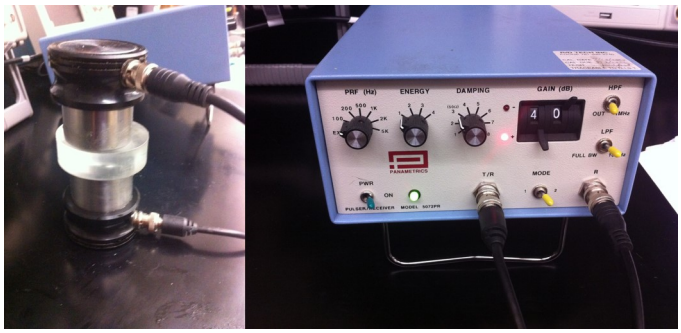

Figure A.2: The Pulser-Receiver system.

The Pulser-Receiver system sends the feedback data to the Digital Phosphor Oscilloscope (DPO), which provides a graphical output of the received signals. The DPO scans for the Time Of Flight (TOF) to provide the measurements of voltage (mV) and time (μs). The time it took for the pulse to travel through the entire testing sample thickness is taken when the volt reading becomes greater than or less than zero on the TOF graph. The DPO used, shown in Figure A.3, was a TDS 3034C model with 300 MHz and 2.5 GS/s.

With the known traveled time and the measured sample thickness, the longitudinal wave speed v was calculated using the equation relating length L (in. or mm), and TOF t (μs).

Figure A.3: The Digital Phosphor Oscilloscope.

$$v = \frac{L}{t} \tag{A.1}$$

To obtain an accurate ultrasonic velocity of the PMMA sample, ten testing trials were used to calculate the average time delay between the pulser-receiver transducers for the PMMA material.

A.1.3 Experimental Results

The outer PMMA cap was measured with a caliper to be 0.897 in. (22.8 mm). A DPO graphic output is shown in Figure A.4.

The ten trial results are shown in Table A.1. The average time delaying calculated to be 8.144 μs.

Using Equation A.1 and the time delay average, the ultrasonic velocity of the PMMA sample is 0.1101 in/μs (2799.61 m/s).

$$v_{\text{metric}} = \frac{0.0228\,\text{m}}{8.141\,\mu\text{s}} = 2799.61\,\text{m/s} \tag{A.2}$$

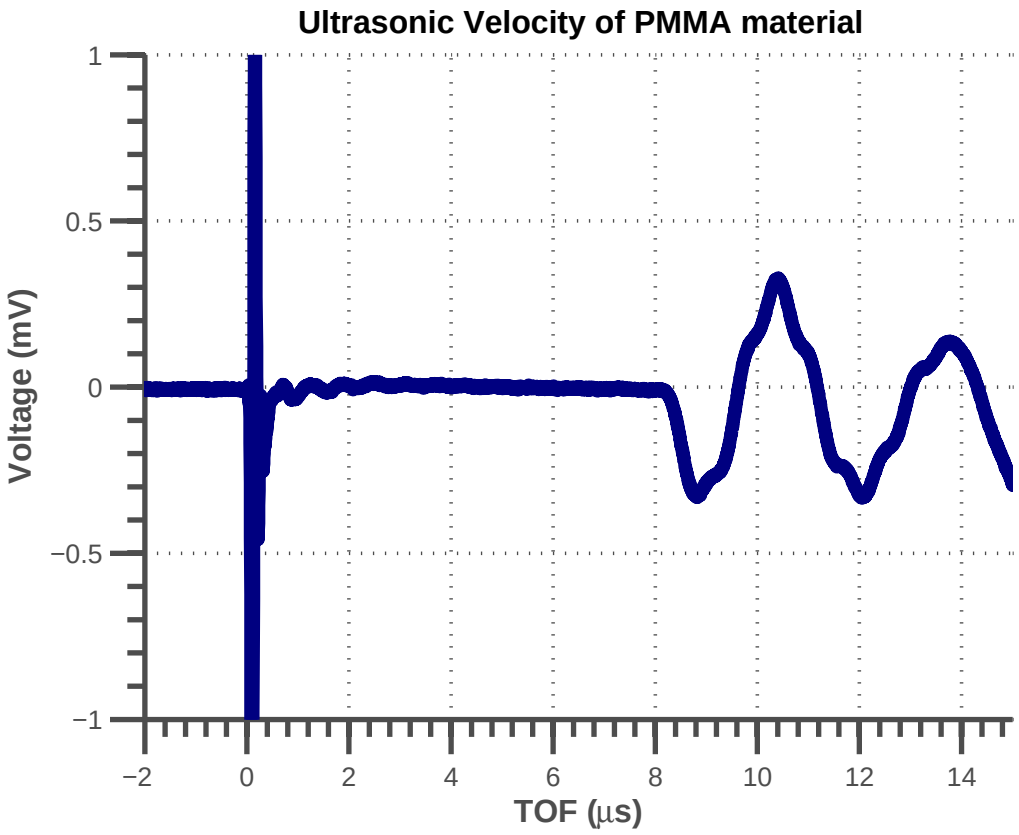

Figure A.4: Oscilloscope TOF signal: The received pulse of the transducer.

$$v_{\mathrm{USC}} = \frac{0.897\,\mathrm{in.}}{8.144\,\mu\mathrm{s}} = 0.1101\,\mathrm{in}/\mu\mathrm{s} \tag{A.3}$$

A.2 Ultrasonic Phased Array Transducer

Table A.1: Ten Trials for Time Delay Average.

Trial	$\Delta(\mu s)$
1	8.08
2	8.16
3	8.24
4	8.24
5	8.16
6	8.08
7	8.16
8	8.16
9	8.08
10	8.08
Average	8.144

Table A.2: UPA Transducer Characteristics for 2.25L16-A1 probe.

Frequency	2.25	MHz
Probe Type	Linear Array	
Element Count	16	
Active Area Dimension	12x12	mm
Pitch	0.75	mm
Housing	Angle Beam	
Cable Jacket	PVC	
Cable Length	2.5	m
Case Type	A1	

Table A.3: UPA Transducer Characteristics for SA5-N60S 5L32 probe.

Frequency	5.0	MHz
Probe Type	Linear Array	
Element Count	32	
Active Area Dimension	19.2 x 20	mm
Pitch	0.60	mm
Housing	Angle Beam	
Cable Jacket	PVC	
Cable Length	2.5	m
Case Type	A5	

Table A.4: PMMA Case I Wedge Information for Omniscan MX2.

Wedge Angle	0	Deg.
Probe Type	Linear Array	
Orientation	Normal	
Velocity	0.1101	in/μs
Pri. offset	0	in.
Sec. offset	0	in.
Height	0.563	in.

Table A.5: PMMA Case II Wedge Information for Omniscan MX2.

Wedge Angle	0	Deg.
Probe Type	Linear Array	
Orientation	Normal	
Velocity	0.1101	in/μs
Pri. offset	0	in.
Sec. offset	0	in.
Height	0.440	in.

A.3 Equations for Target Measurements

A.3.1 Testing I.1.1 Calculation

$$ExteriorEdge_{\text{PMMA Case I}} = \frac{19\,\text{in.} - 2.75\,\text{in.}}{2} + 0.54\,\text{in.} = 8.665\,\text{in.} \tag{A.4}$$

A.3.2 Testing I.2.1 Calculation

$$KeyholeDistance_{\text{PMMA Case I}} = 8.665\,\text{in.} - 0.375\,\text{in.} = 8.29\,\text{in.} \tag{A.5}$$

A.3.3 Testing I.1.2 Calculation

$$ExteriorEdge_{\text{PMMA Case II}} = \frac{19\,\text{in.} - 2.75\,\text{in.}}{2} = 8.125\,\text{in.} \tag{A.6}$$

A.3.4 Testing I.2.2 Calculation

$$KeyholeDistance_{\text{PMMA Case II}} = 8.125\,\text{in.} - 0.375\,\text{in.} \tag{A.7}$$

A.3.5 Testing I.1.3 Calculation

$$ExteriorEdge_{\text{PMMA Case II}} = \frac{18.75\,\text{in.} - 2.5\,\text{in.}}{2} = 8.125\,\text{in.} \tag{A.8}$$

A.3.6 Testing I.2.3 Calculation

$$KeyholeDistance_{\text{PMMA Case II}} = \frac{18.75\,\text{in.} - 4.88\,\text{in.}}{2} = 6.935\,\text{in.} \tag{A.9}$$

A.4 Pin Dimensions

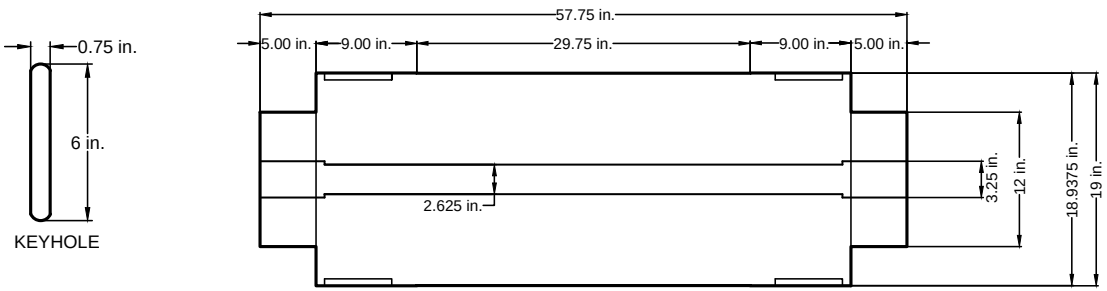

COUNTERWEIGHT TRUNNION PIN
FORGED STEEL - 2 REQ'D

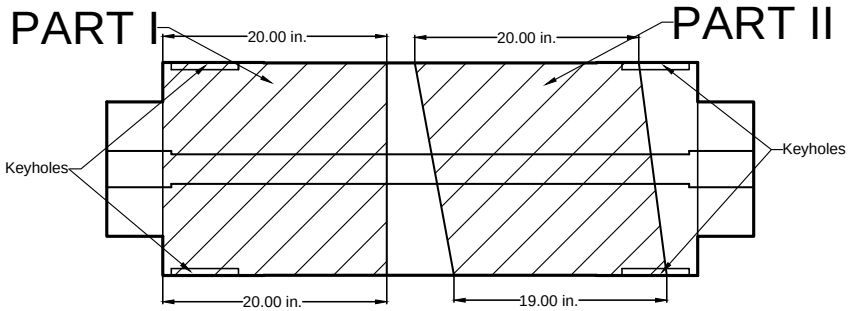

TRUNNION PIN PARTS RETAINED FROM ORIGINAL PIN

DIMENSIONS ARE IN INCHES
TOLERANCES:
FRACTIONAL ±
ANGULAR: MACH ± BEND ±
TWO PLACE DECIMAL ±
THREE PLACE DECIMAL ±

MATERIAL ---

FINISH ---

DO NOT SCALE DRAWING

	NAME	DATE
DRAWN		
CHECKED		
ENGAPPR.		
MFGAPPR.		
Q.A.		

COMMENTS:

TAMU NDT Project

Trunnion pins taken out-of-service

SIZE	DWG. NO.	REV.
A		

SCALE 1:2 | WEIGHT: | SHEET 1 OF 1

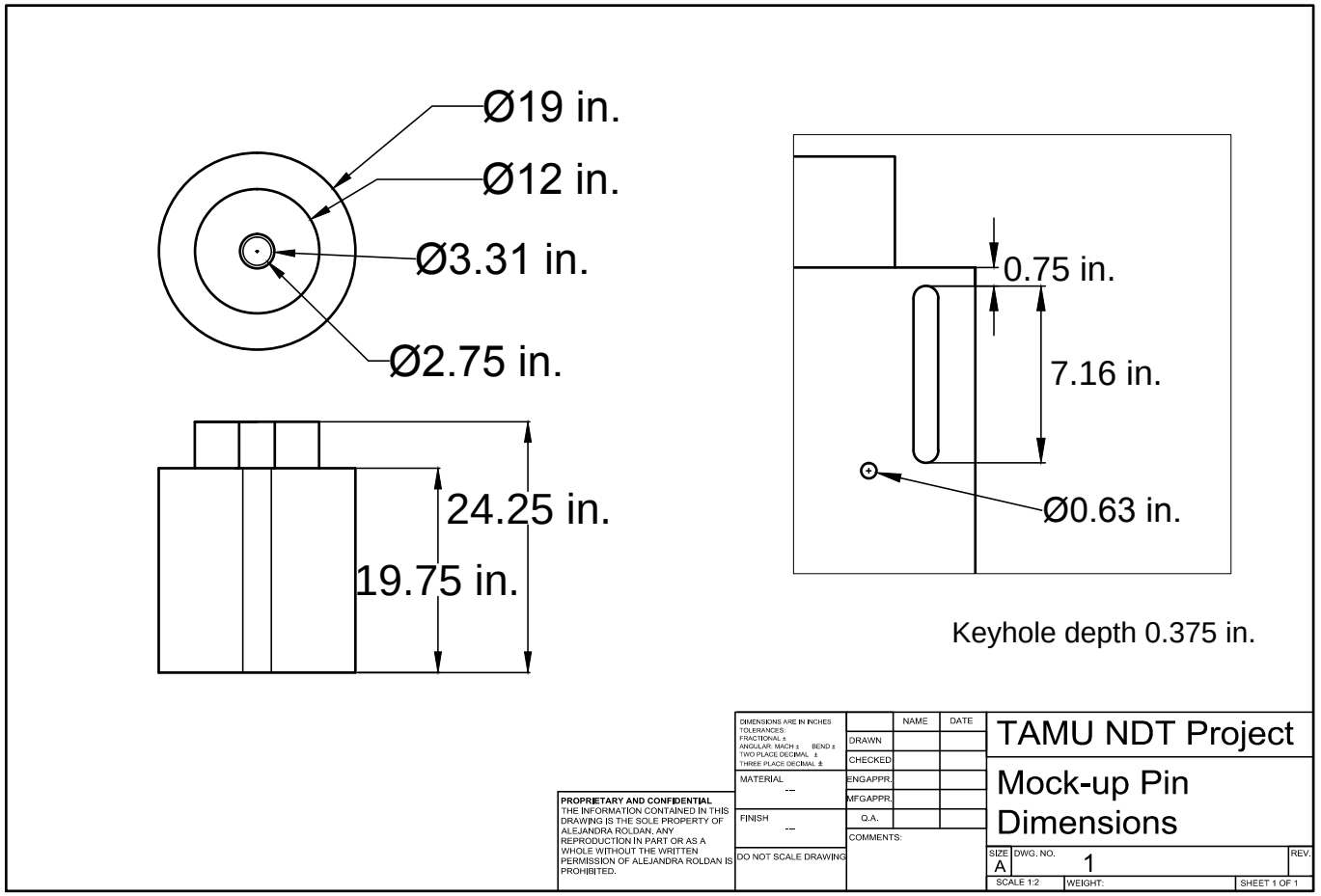
Ø19 in.
Ø12 in.
Ø3.31 in.
Ø2.75 in.
24.25 in.
19.75 in.
0.75 in.
7.16 in.
Ø0.63 in.
Keyhole depth 0.375 in.
DIMENSIONS ARE IN INCHES
TOLERANCES:
FRACTIONAL ±
ANGULAR: MACH ± BEND ±
TWO PLACE DECIMAL ±
THREE PLACE DECIMAL ±
MATERIAL ---
FINISH ---
DO NOT SCALE DRAWING
NAME
DATE
DRAWN
CHECKED
ENGAPPR.
MFGAPPR.
Q.A.
COMMENTS:
PROPRIETARY AND CONFIDENTIAL
THE INFORMATION CONTAINED IN THIS DRAWING IS THE SOLE PROPERTY OF ALEJANDRA ROLDAN. ANY REPRODUCTION IN PART OR AS A WHOLE WITHOUT THE WRITTEN PERMISSION OF ALEJANDRA ROLDAN IS PROHIBITED.
TAMU NDT Project
Mock-up Pin Dimensions
SIZE A
DWG. NO. 1
REV.
SCALE 1:2
WEIGHT:
SHEET 1 OF 1

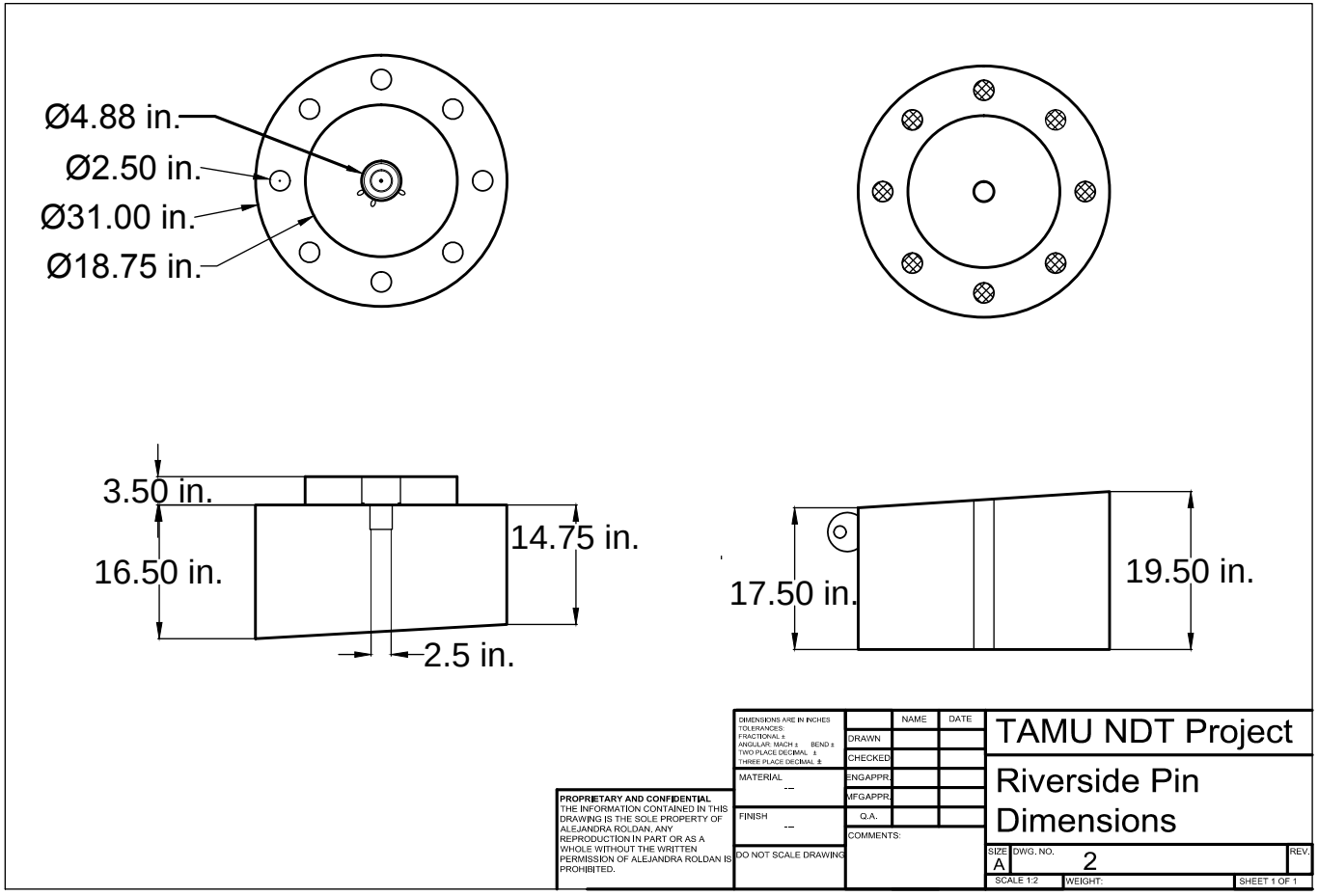
Ø4.88 in.
Ø2.50 in.
Ø31.00 in.
Ø18.75 in.
3.50 in.
16.50 in.
14.75 in.
2.5 in.
17.50 in.
19.50 in.
DIMENSIONS ARE IN INCHES
TOLERANCES:
FRACTIONAL ±
ANGULAR: MACH ± BEND ±
TWO PLACE DECIMAL ±
THREE PLACE DECIMAL ±
MATERIAL

FINISH

DO NOT SCALE DRAWING
NAME
DATE
DRAWN
CHECKED
ENGAPPR.
MFGAPPR.
Q.A.
COMMENTS:
PROPRIETARY AND CONFIDENTIAL
THE INFORMATION CONTAINED IN THIS DRAWING IS THE SOLE PROPERTY OF ALEJANDRA ROLDAN. ANY REPRODUCTION IN PART OR AS A WHOLE WITHOUT THE WRITTEN PERMISSION OF ALEJANDRA ROLDAN IS PROHIBITED.
TAMU NDT Project
Riverside Pin Dimensions
SIZE A
DWG. NO. 2
REV.
SCALE 1:2
WEIGHT:
SHEET 1 OF 1

A.5 Bridge Drawings

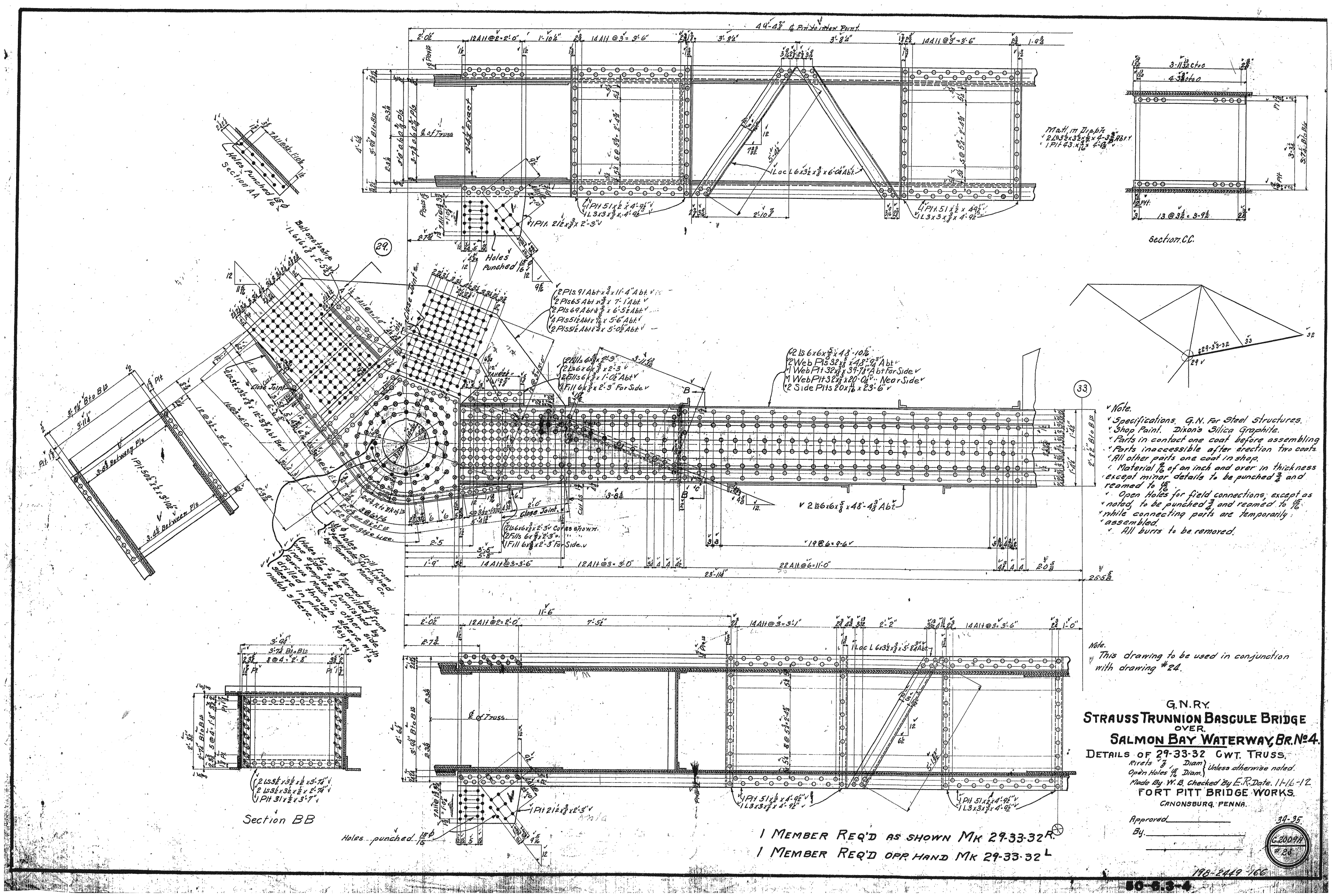
Section AA
Section CC
Section BB
Holes punched
Note.
Specifications. G.N. For Steel Structures.
Shop Paint. Dixon's Silica Graphite.
Parts in contact one coat before assembling
Parts inaccessible after erection two coats.
All other parts one coat in shop.
Material 9/16 of an inch and over in thickness except minor details to be punched 3/4 and reamed to 15/16.
Open Holes for field connections, except as noted, to be punched 3/4 and reamed to 15/16 while connecting parts are temporarily assembled.
All burrs to be removed.
Note.
This drawing to be used in conjunction with drawing #24.
1 Member Req'd as shown Mk 29-33-32 R.
1 Member Req'd opp. hand Mk 29-33-32 L
G.N.RY.
Strauss Trunnion Bascule Bridge
over
Salmon Bay Waterway, Br. No 4.
Details of 29-33-32 Cwt. Truss.
Rivets 7/8 Diam
Open Holes 15/16 Diam.
Unless otherwise noted.
Made By W.B. Checked By E.R. Date. 11-16-12
Fort Pitt Bridge Works.
Canonsburg, Penna.
Approved
By.
34-35.
C.2009R
#25
198-2449-166
50-6.3-4

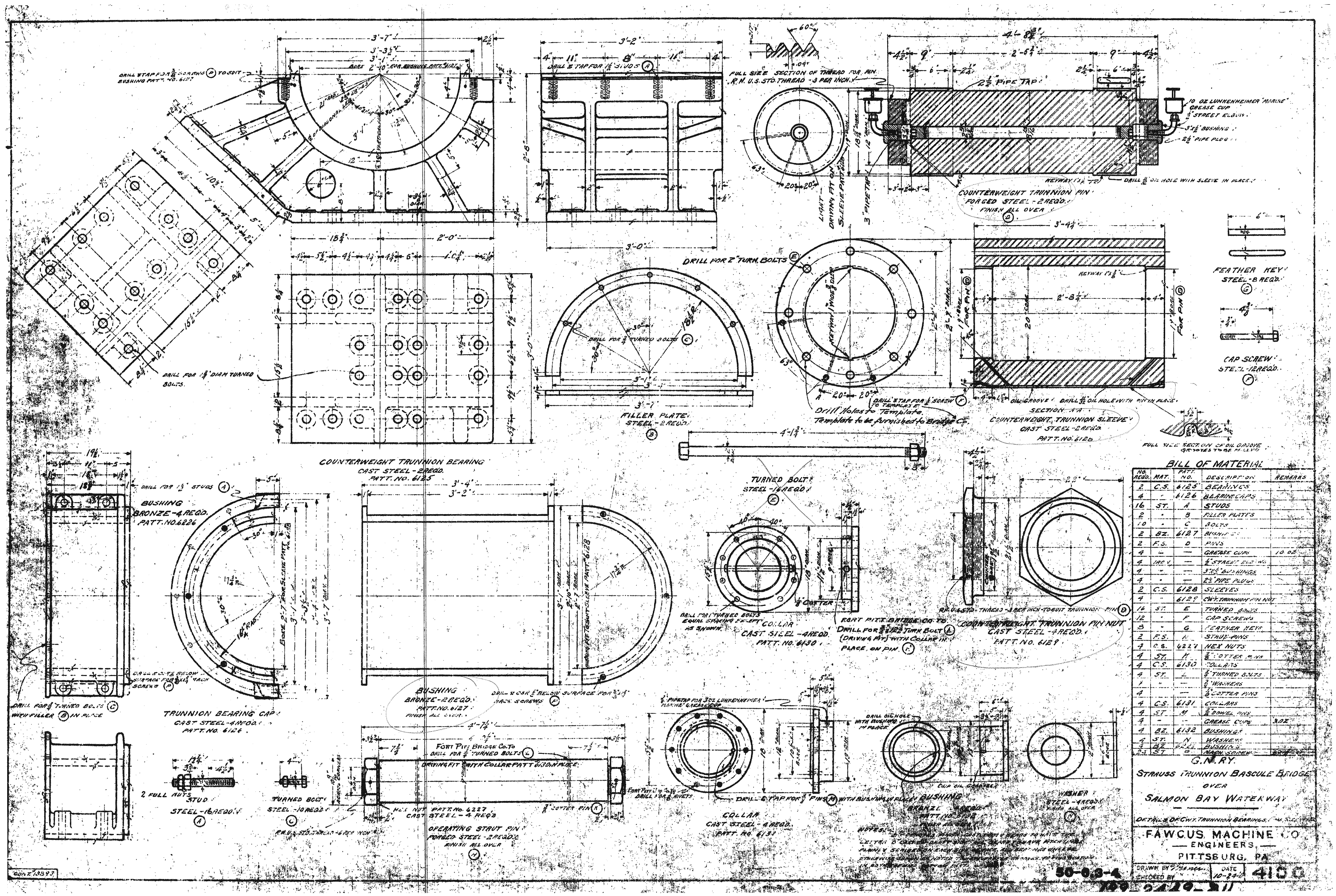
COUNTERWEIGHT TRUNNION BEARING
CAST STEEL - 2 REQD.
PATT. NO. 6125
FILLER PLATE
STEEL - 2 REQD.
COUNTERWEIGHT TRUNNION PIN
FORGED STEEL - 2 REQD.
FINISH ALL OVER
FULL SIZE SECTION OF THREAD FOR PIN
R.H. U.S. STD. THREAD - 3 PER INCH
COUNTERWEIGHT TRUNNION SLEEVE
CAST STEEL - 2 REQD.
PATT. NO. 6128
FEATHER KEY
STEEL - 8 REQD.
CAP SCREW
STEEL - 12 REQD.
FULL SIZE SECTION OF OIL GROOVE
BUSHING
BRONZE - 4 REQD.
PATT. NO. 6226
TRUNNION BEARING CAP
CAST STEEL - 4 REQD.
PATT. NO. 6126
BUSHING
BRONZE - 2 REQD.
PATT. NO. 6127
FINISH ALL OVER
TURNED BOLT
STEEL - 16 REQD.
COLLAR
CAST STEEL - 4 REQD.
PATT. NO. 6130
COUNTERWEIGHT TRUNNION PIN NUT
CAST STEEL - 4 REQD.
PATT. NO. 6129
STUD
STEEL - 16 REQD.
TURNED BOLT
STEEL - 10 REQD.
OPERATING STRUT PIN
FORGED STEEL - 2 REQD.
FINISH ALL OVER
HEX NUT PATT. No. 6227
CAST STEEL - 4 REQD.
COLLAR
CAST STEEL - 4 REQD.
PATT. No. 6131
BUSHING
WASHER
BILL OF MATERIAL
NO. REQD. | MAT. | PATT. NO. | DESCRIPTION | REMARKS
2 | C.S. | 6125 | BEARINGS
4 | " | 6126 | BEARING CAPS
16 | ST. | A | STUDS
2 | " | B | FILLER PLATES
10 | " | C | BOLTS
2 | BZ. | 6127 | BUSHINGS
2 | F.S. | D | PINS
4 | — | — | GREASE CUPS | 10 OZ
4 | — | — | 3"x½" BUSHINGS
4 | " | — | 2½" PIPE PLUGS
2 | C.S. | 6128 | SLEEVES
4 | " | 6129 | CWT. TRUNNION PIN NUT
16 | ST. | E | TURNED BOLTS
12 | " | F | CAP SCREWS
8 | " | G | FEATHER KEYS
2 | F.S. | H | STRUT-PINS
4 | C.S. | 6227 | HEX NUTS
4 | ST. | K | ⅜" COTTER PINS
4 | C.S. | 6130 | COLLARS
4 | ST. | L | ¾" TURNED BOLTS
4 | — | — | GREASE CUPS | 3 OZ
4 | C.S. | 6131 | COLLARS
4 | ST. | M | ⅜" DOWEL PINS
4 | BZ. | 6132 | BUSHINGS
4 | ST. | N | WASHERS
G.N.RY.
STRAUSS TRUNNION BASCULE BRIDGE
OVER
SALMON BAY WATERWAY
DETAILS OF CWT. TRUNNION BEARINGS
FAWCUS MACHINE CO.
— ENGINEERS —
PITTSBURG, PA.
DRAWN BY
CHECKED BY
DATE
4100

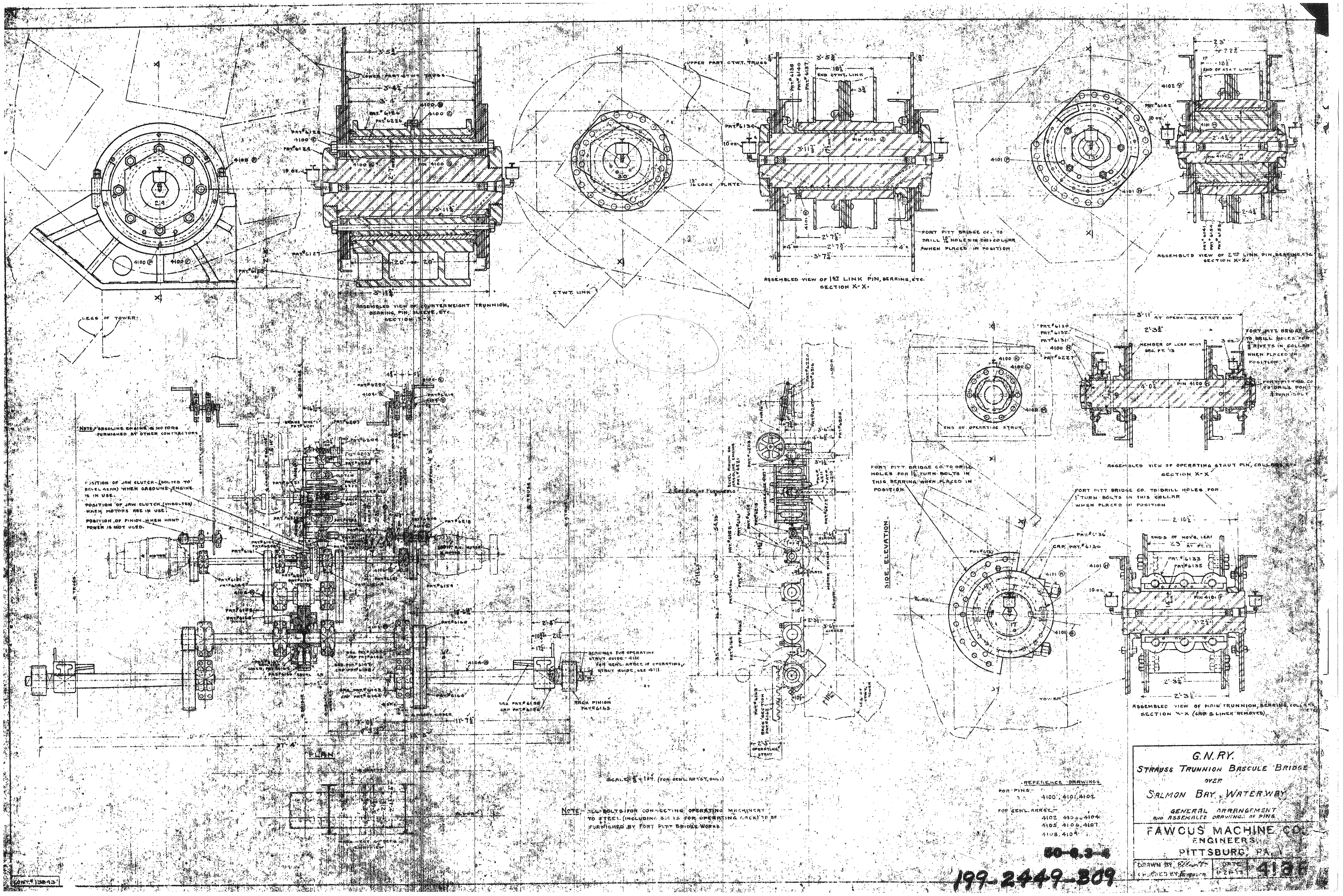
ASSEMBLED VIEW OF 1ST LINK PIN, BEARING, ETC.
SECTION X-X.
ASSEMBLED VIEW OF 2ND LINK PIN, BEARING, ETC.
SECTION X-X.
ASSEMBLED VIEW OF OPERATING STRUT PIN, COLLARS
SECTION X-X
END OF OPERATING STRUT
SIDE ELEVATION
ASSEMBLED VIEW OF MAIN TRUNNION, BEARING, COLLARS, ETC.
SECTION X-X (CAP & LINER REMOVED)
G.N.RY.
STRAUSS TRUNNION BASCULE BRIDGE
OVER
SALMON BAY WATERWAY
GENERAL ARRANGEMENT
AND ASSEMBLED DRAWINGS OF PINS
FAWCUS MACHINE CO.
ENGINEERS
PITTSBURG, PA.
DRAWN BY
CHECKED BY
DATE
199-2449-309

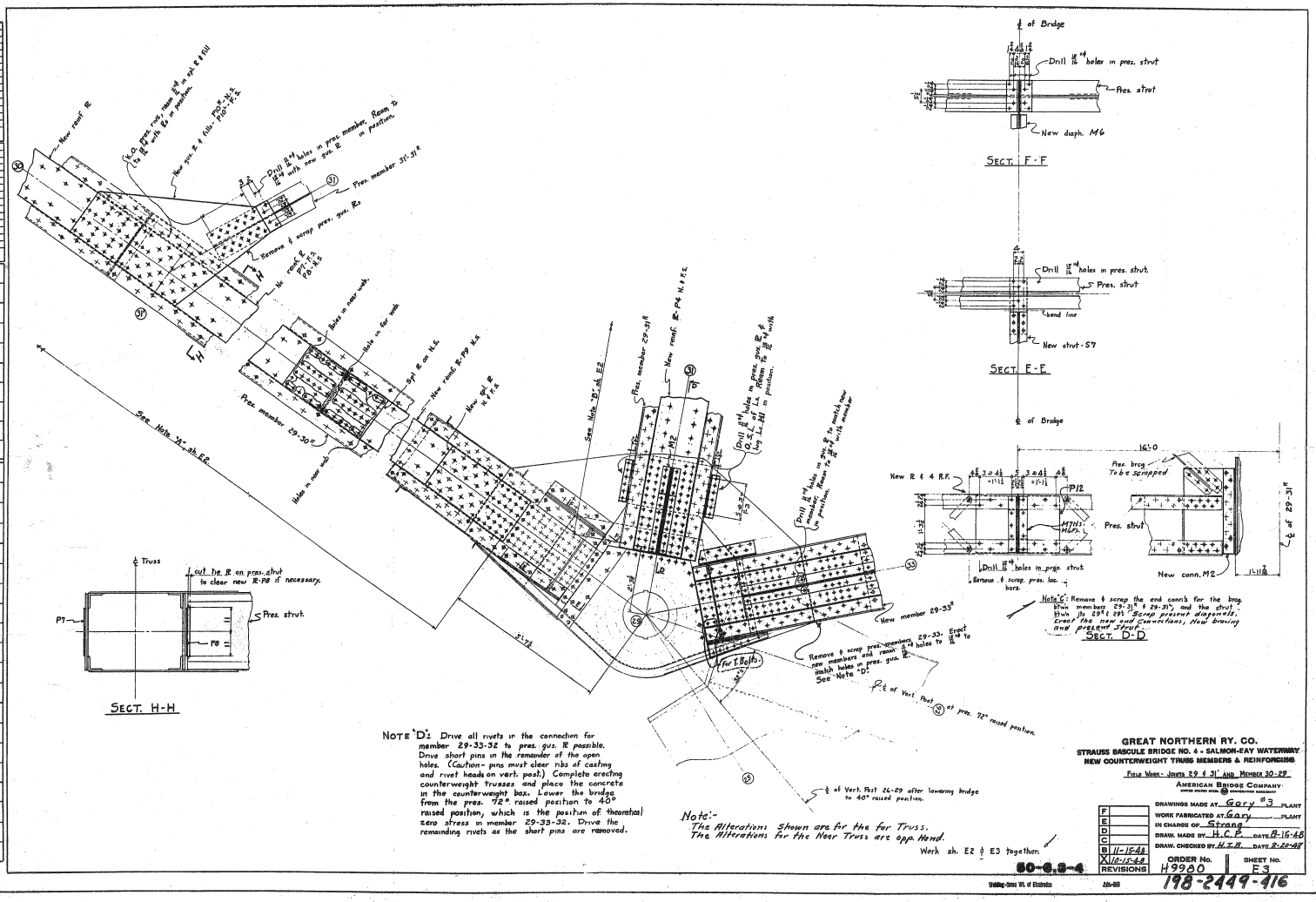

NOTE 'D': Drive all rivets in the connection for member 29-33-32 to pres. gus. R possible. Drive short pins in the remainder of the open holes. (Caution- pins must clear ribs of casting and rivet heads on vert. post.) Complete erecting counterweight trusses and place the concrete in the counterweight box. Lower the bridge from the pres. 72° raised position to 40° raised position, which is the position of theoretical zero stress in member 29-33-32. Drive the remaining rivets as the short pins are removed.

Note:- The Alterations shown are for the far Truss. The Alterations for the Near Truss are opp. Hand.

GREAT NORTHERN RY. CO.
STRAUSS BASCULE BRIDGE NO. 6 - SALMON-BAY WATERWAY
NEW COUNTERWEIGHT TRUSS MEMBERS & REINFORCING
Field Work - Joints 29 & 31' and Member 30-29
AMERICAN BRIDGE COMPANY

F	
E	
D	
C	
B	11-15-48
X	10-15-48
REVISIONS	

DRAWINGS MADE AT Gary 3 PLANT
WORK FABRICATED AT Gary PLANT
IN CHARGE OF Strang
DRAW. MADE BY H.C.P. DATE 8-16-48
DRAW. CHECKED BY H.T.R. DATE 8-20-48
ORDER No. H9980 | SHEET No. E3

80-6.3-4

198-2449-416

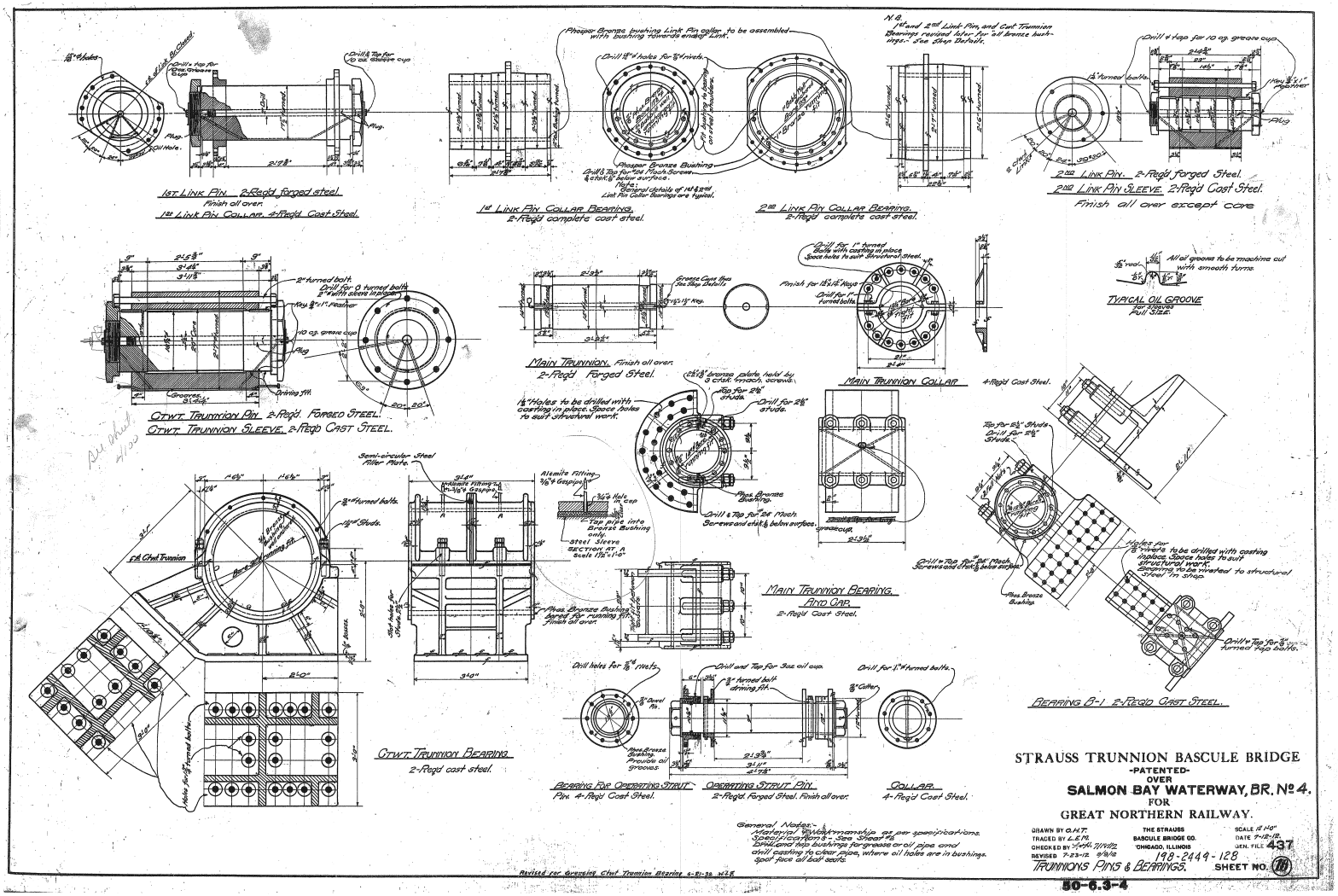

STRAUSS TRUNNION BASCULE BRIDGE
-PATENTED-
OVER
SALMON BAY WATERWAY, BR. No 4.
FOR
GREAT NORTHERN RAILWAY.

DRAWN BY C.H.T.
TRACED BY L.E.N.
CHECKED BY T-H-H. 11-1-12.
REVISED 7-23-12. 9-9-12

THE STRAUSS BASCULE BRIDGE CO. CHICAGO, ILLINOIS

SCALE 1" = 1'-0"
DATE 7-12-12.
GEN. FILE 437
198-2449-128
SHEET NO. 18

TRUNNIONS PINS & BEARINGS.

50-6.3-4

A.6 Drawings of Ultrasonic PMMA Probe

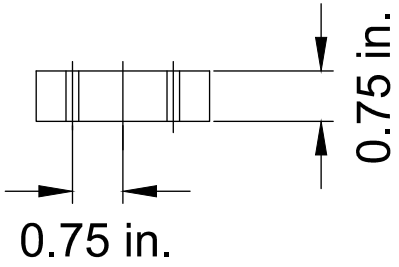

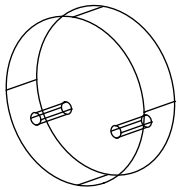

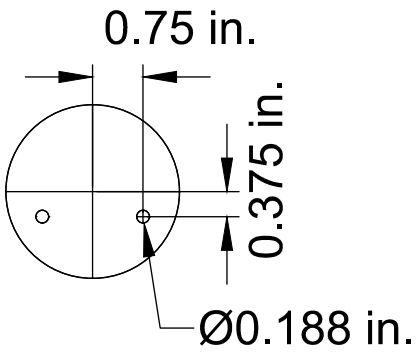

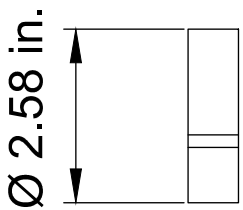

DIMENSIONS ARE IN INCHES TOLERANCES: FRACTIONAL ± ANGULAR: MACH ± BEND ± TWO PLACE DECIMAL ± THREE PLACE DECIMAL ±		NAME	DATE
	DRAWN		
	CHECKED		
MATERIAL ---	ENGAPPR.		
	MFGAPPR.		
FINISH ---	Q.A.		
	COMMENTS:		
DO NOT SCALE DRAWING			

TAMU NDT Project

Outer PMMA Cap

SIZE	DWG. NO.	REV.
A	4	
SCALE 1:2	WEIGHT:	SHEET 1 OF 1

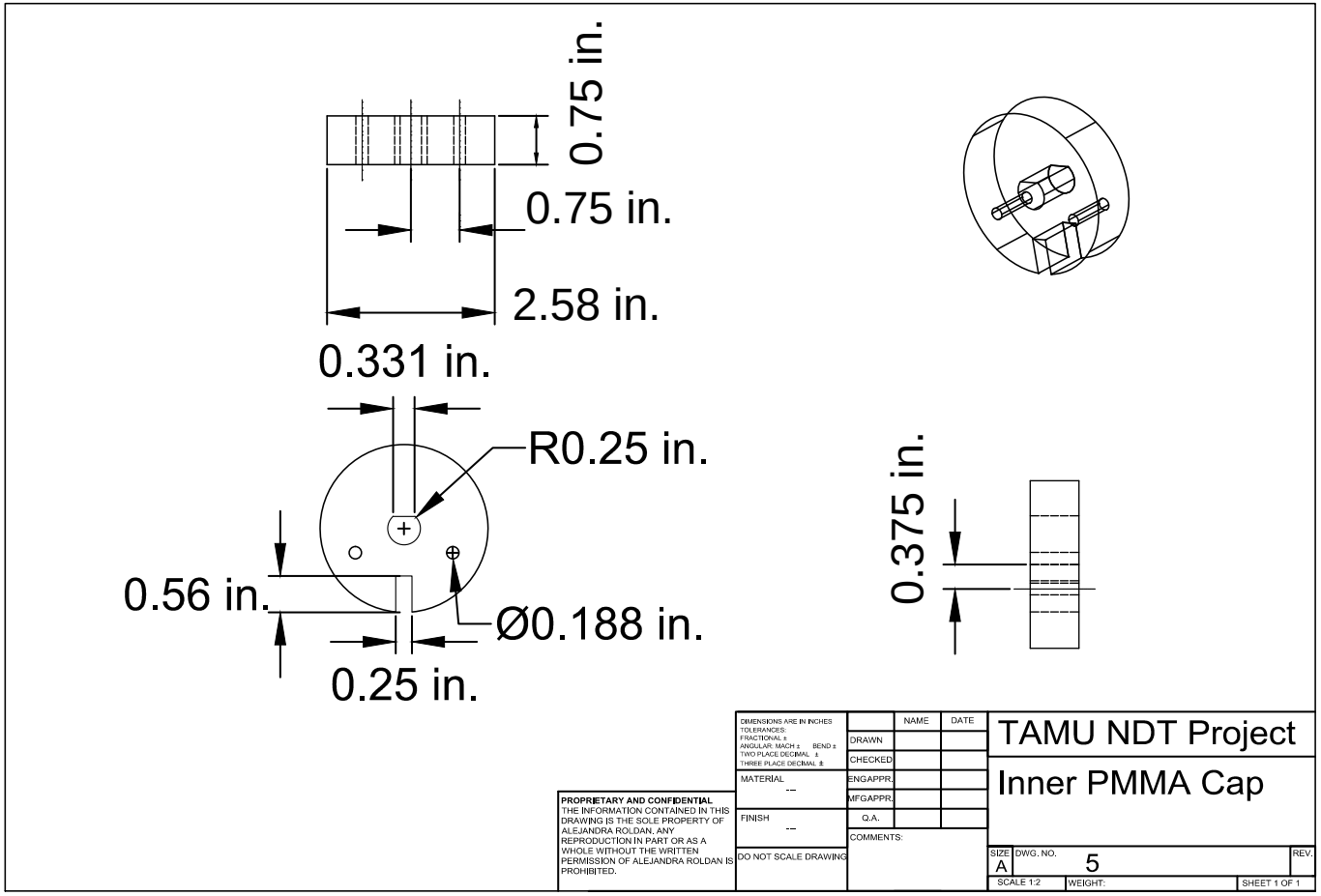

DIMENSIONS ARE IN INCHES TOLERANCES: FRACTIONAL ± ANGULAR: MACH ± BEND ± TWO PLACE DECIMAL ± THREE PLACE DECIMAL ±		NAME / DATE
	DRAWN	
	CHECKED	
MATERIAL ---	ENGAPPR.	
	MFGAPPR.	
FINISH ---	Q.A.	
	COMMENTS:	
DO NOT SCALE DRAWING		

TAMU NDT Project

Inner PMMA Cap

SIZE	DWG. NO.	REV.
A	5	
SCALE 1:2	WEIGHT:	SHEET 1 OF 1

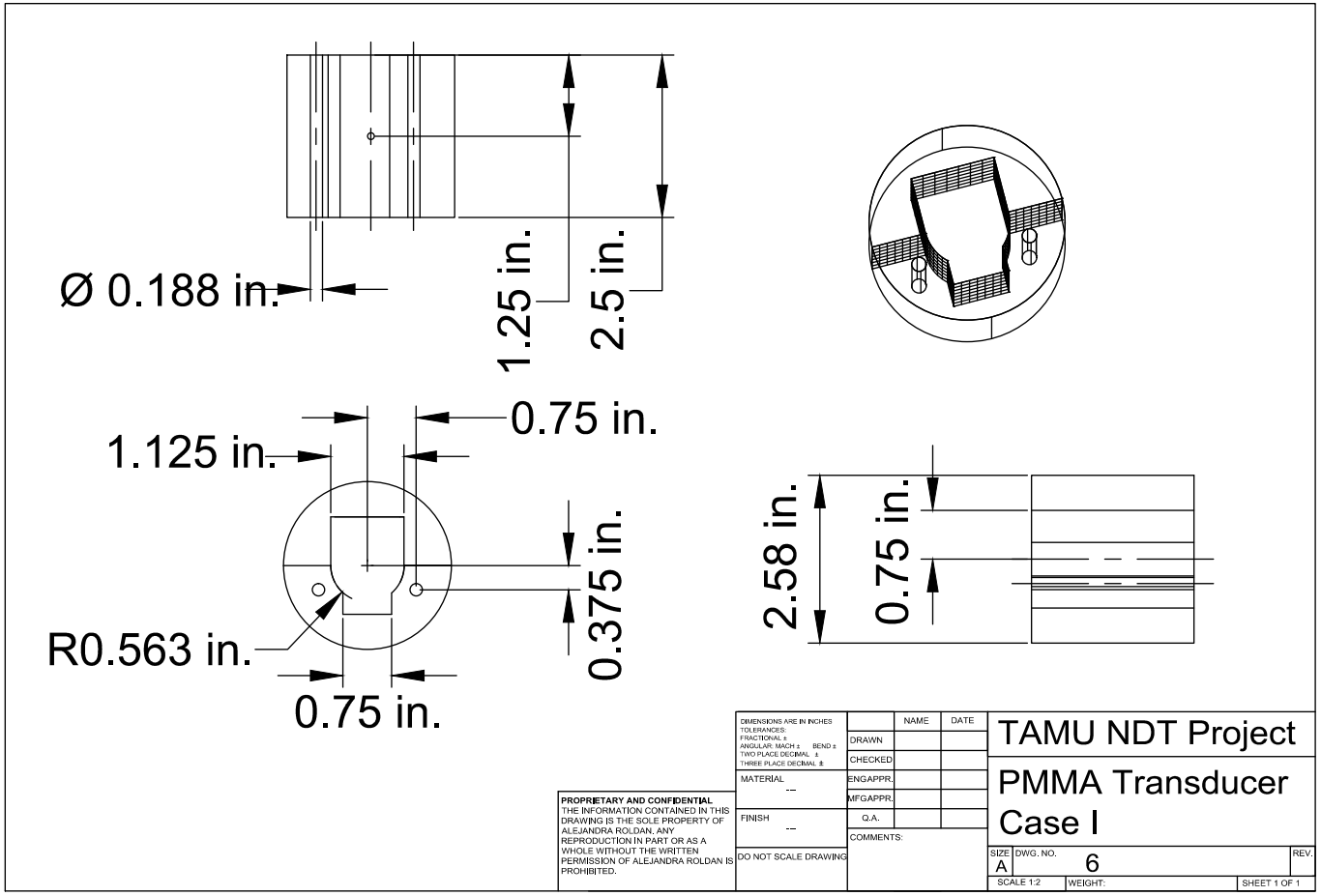
Ø 0.188 in.
1.25 in.
2.5 in.
1.125 in.
0.75 in.
R0.563 in.
0.375 in.
0.75 in.
2.58 in.
0.75 in.
DIMENSIONS ARE IN INCHES
TOLERANCES:
FRACTIONAL ±
ANGULAR: MACH ± BEND ±
TWO PLACE DECIMAL ±
THREE PLACE DECIMAL ±
MATERIAL --
FINISH --
DO NOT SCALE DRAWING
NAME
DATE
DRAWN
CHECKED
ENGAPPR.
MFGAPPR.
Q.A.
COMMENTS:
PROPRIETARY AND CONFIDENTIAL
THE INFORMATION CONTAINED IN THIS DRAWING IS THE SOLE PROPERTY OF ALEJANDRA ROLDAN. ANY REPRODUCTION IN PART OR AS A WHOLE WITHOUT THE WRITTEN PERMISSION OF ALEJANDRA ROLDAN IS PROHIBITED.
TAMU NDT Project
PMMA Transducer Case I
SIZE A
DWG. NO. 6
REV.
SCALE 1:2
WEIGHT:
SHEET 1 OF 1

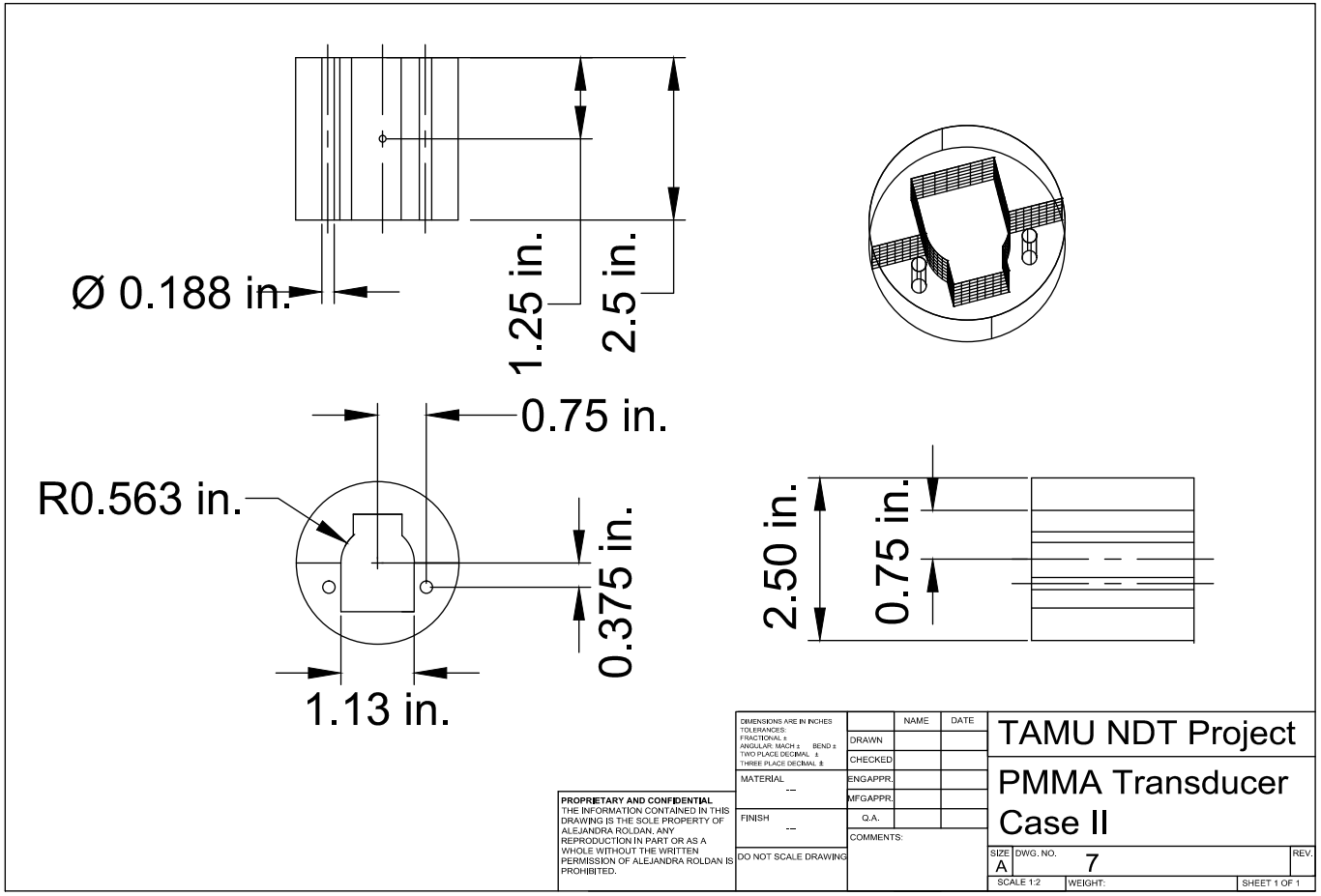
Ø 0.188 in.
1.25 in.
2.5 in.
0.75 in.
R0.563 in.
0.375 in.
1.13 in.
2.50 in.
0.75 in.
DIMENSIONS ARE IN INCHES
TOLERANCES:
FRACTIONAL ±
ANGULAR: MACH ± BEND ±
TWO PLACE DECIMAL ±
THREE PLACE DECIMAL ±
MATERIAL

FINISH

DO NOT SCALE DRAWING
NAME
DATE
DRAWN
CHECKED
ENGAPPR.
MFGAPPR.
Q.A.
COMMENTS:
PROPRIETARY AND CONFIDENTIAL
THE INFORMATION CONTAINED IN THIS DRAWING IS THE SOLE PROPERTY OF ALEJANDRA ROLDAN. ANY REPRODUCTION IN PART OR AS A WHOLE WITHOUT THE WRITTEN PERMISSION OF ALEJANDRA ROLDAN IS PROHIBITED.
TAMU NDT Project
PMMA Transducer Case II
SIZE A
DWG. NO. 7
REV.
SCALE 1:2
WEIGHT:
SHEET 1 OF 1

One end to be threaded for a length of 3"

Thread: 1/2-20

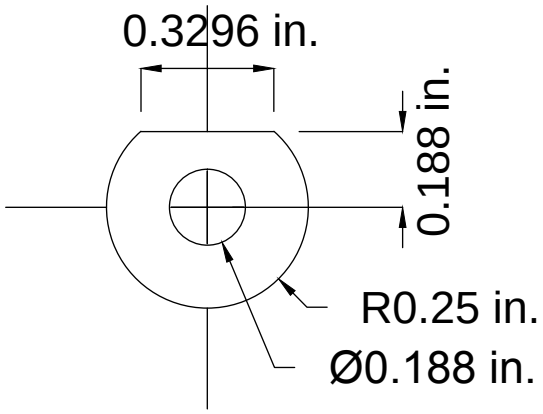

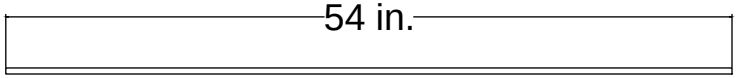

Note: Scale is 1:10

Note: Cross-Section
Scale is 3:1

DIMENSIONS ARE IN INCHES TOLERANCES: FRACTIONAL ± ANGULAR: MACH ± BEND ± TWO PLACE DECIMAL ± THREE PLACE DECIMAL ±		NAME	DATE
	DRAWN		
	CHECKED		
MATERIAL ---	ENGAPPR.		
	MFGAPPR.		
FINISH ---	Q.A.		
	COMMENTS:		
DO NOT SCALE DRAWING			

TAMU NDT Project

1/2" Steel Pipe

SIZE	DWG. NO.	REV.
A	8	
SCALE 1:2	WEIGHT:	SHEET 1 OF 1

Both ends to be threaded for a length of 1" each end.

Thread: No. 10-24

0.188 in.

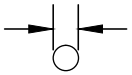

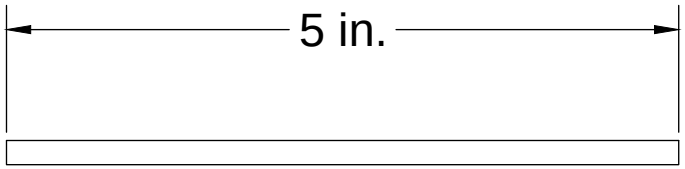

DIMENSIONS ARE IN INCHES TOLERANCES: FRACTIONAL ± ANGULAR: MACH ± BEND ± TWO PLACE DECIMAL ± THREE PLACE DECIMAL ±		NAME	DATE
	DRAWN		
	CHECKED		
MATERIAL ---	ENGAPPR.		
	MFGAPPR.		
FINISH ---	Q.A.		
	COMMENTS:		
DO NOT SCALE DRAWING			

TAMU NDT Project

Steel Bolt

SIZE	DWG. NO.	REV.
A	9	
SCALE 1:2	WEIGHT:	SHEET 1 OF 1

1-Single Plexiglass Case to be Divided Horizontally into 2 Pieces as Shown

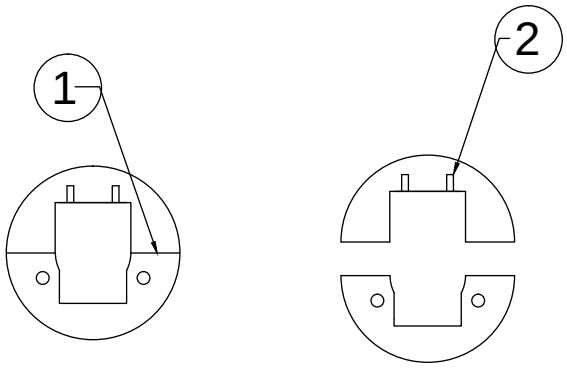

2-Vertical holes are to be Threaded with a M6x1.0 flute to Receive Transducer Screws

DIMENSIONS ARE IN INCHES TOLERANCES: FRACTIONAL ± ANGULAR: MACH ± BEND ± TWO PLACE DECIMAL ± THREE PLACE DECIMAL ±		NAME	DATE
	DRAWN		
	CHECKED		
MATERIAL ---	ENGAPPR.		
	MFGAPPR.		
FINISH ---	Q.A.		
DO NOT SCALE DRAWING	COMMENTS:		

TAMU NDT Project

PMMA Case Fabrication

SIZE	DWG. NO.	REV.
A	10	
SCALE 1:2	WEIGHT:	SHEET 1 OF 1

APPENDIX B

LABORATORY TESTING

B.1 Exterior Inspection

Figure B.1: Exterior scan of the grease hole from the top of the second level of the pin (Testing E.1).

Figure B.2: Grease hole inspection of Hole #2 from the exterior curved surface (Testing E.2).

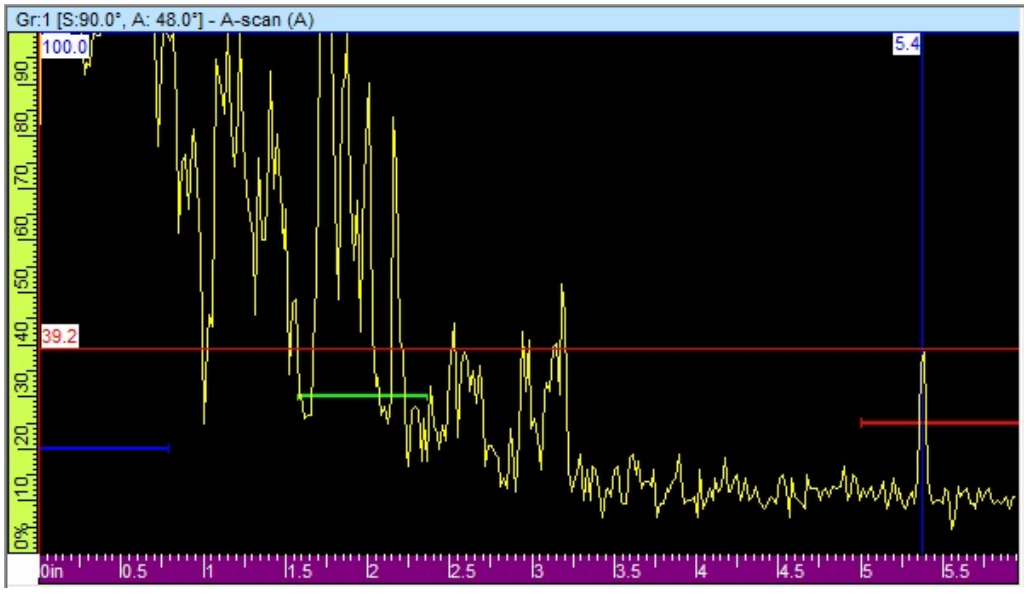

Figure B.3: File0002 A-scan of exterior top scan for Hole 2 (Testing E.1).

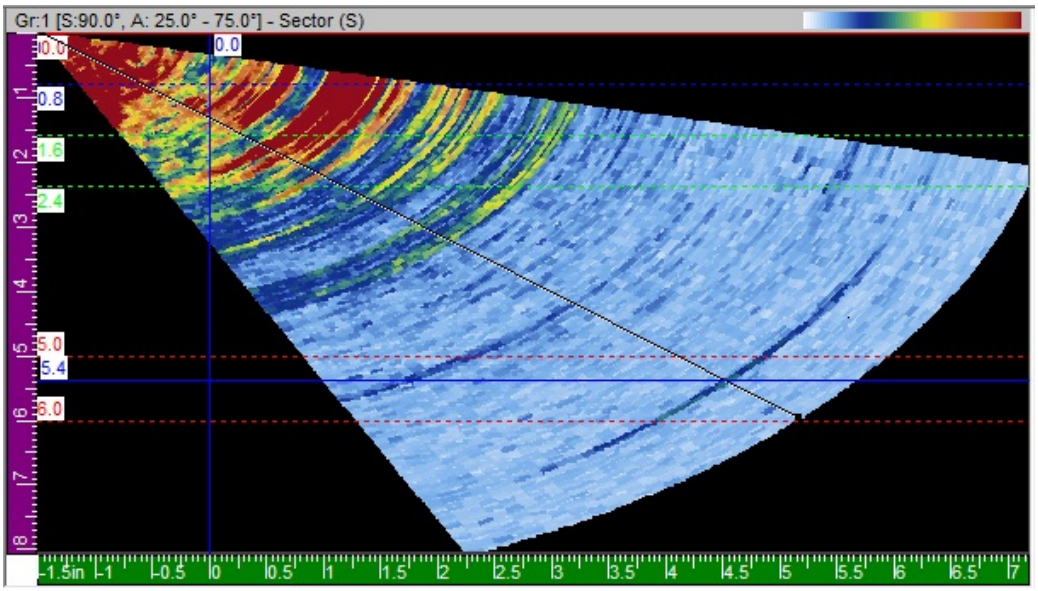

Figure B.4: File0002 S-scan of exterior top scan for Hole 2 (Testing E.1).

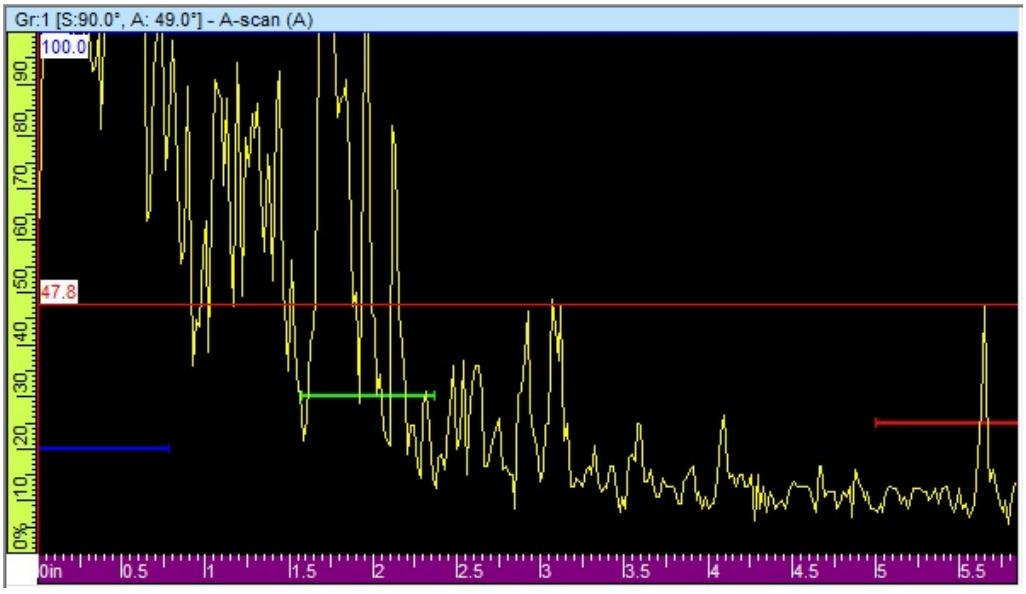

Figure B.5: File0003 A-scan of exterior top scan for Hole 3 (Testing E.1).

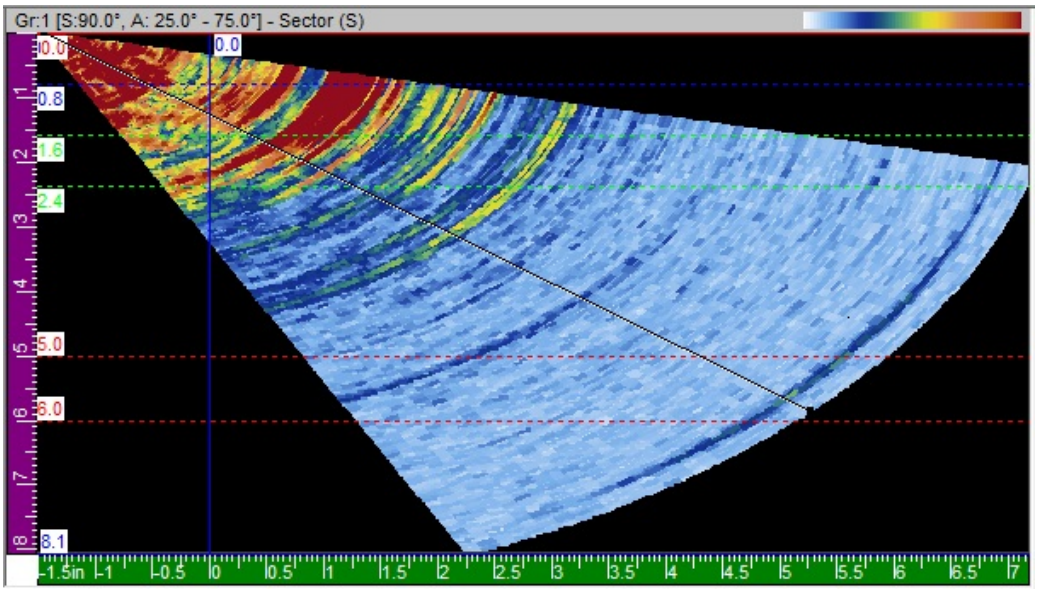

Figure B.6: File0003 S-scan of exterior top scan for Hole 3 (Testing E.1).

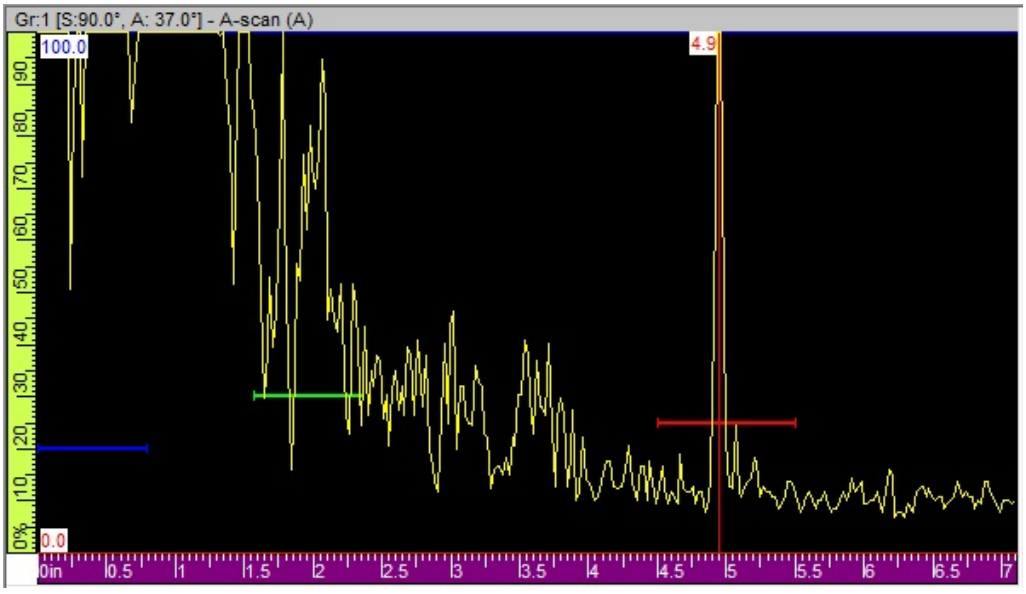

Figure B.7: File0006 A-scan of exterior curved side scan for Hole 2 (Testing E.2).

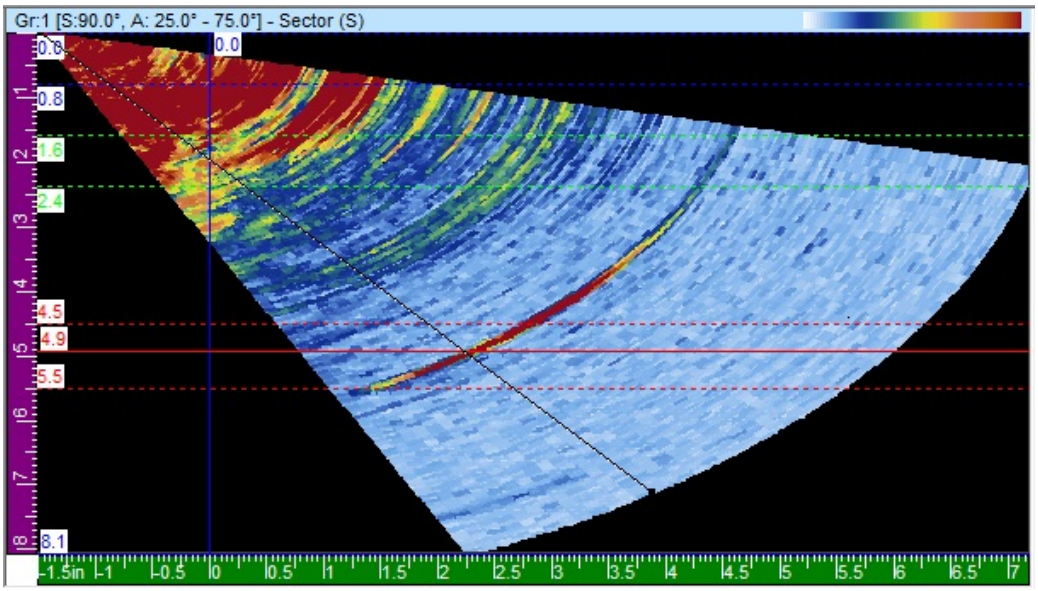

Figure B.8: File0006 S-scan of exterior curved side scan for Hole 2 (Testing E.2).

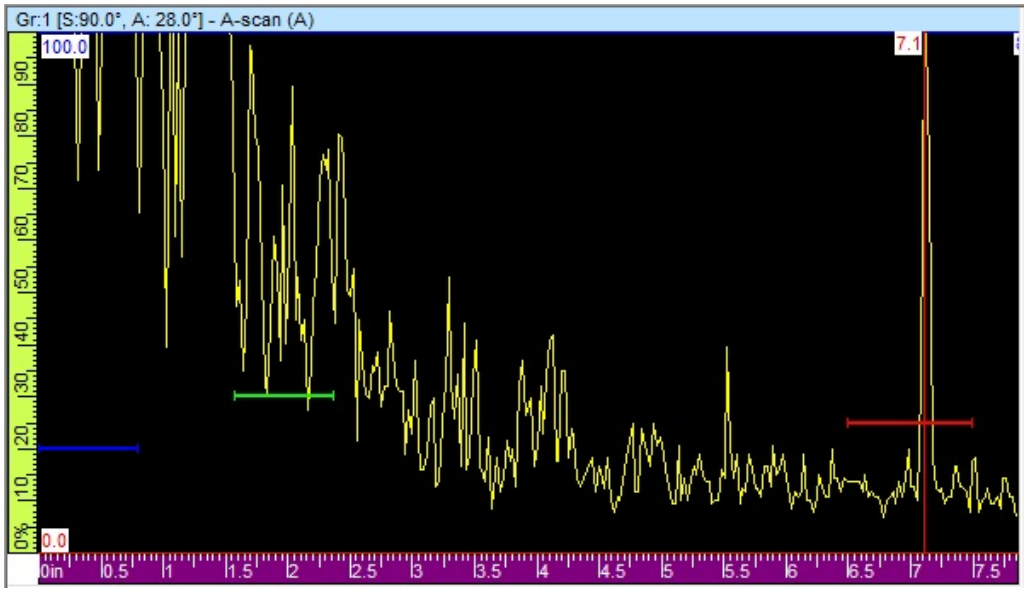

Figure B.9: File0007 A-scan of exterior curved side scan for Hole 3 (Testing E.2).

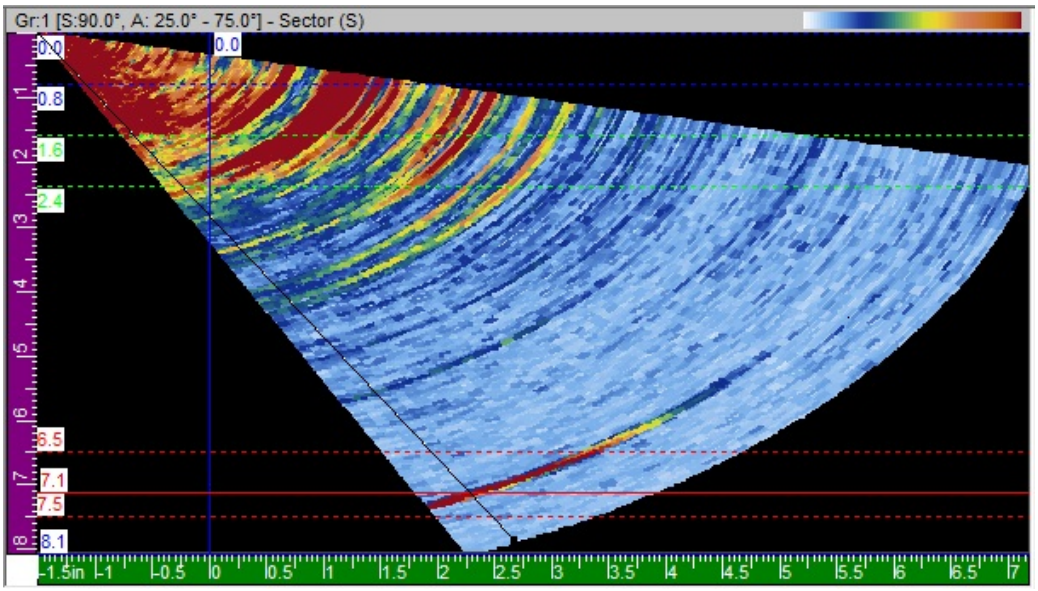

Figure B.10: File0007 S-scan of exterior curved side scan for Hole 3 (Testing E.2).

B.2 Interior Inspection

Table B.1: Testing I.1.1 using UPA system

Trial	Reading (in.)	dB
1	8.596	30
2	8.595	30
3	8.597	30
4	8.593	30
5	8.597	30
6	8.599	30
7	8.600	30
8	8.611	30
9	8.609	30
10	8.593	30
Average	8.599	in.

Table B.2: Testing I.2.1 using UPA system

Trial	Reading (in.)	KH	dB
1	8.180	1	30
2	8.183	2	30
3	8.194	1	30
4	8.193	2	30
5	8.194	1	30
6	8.210	2	30
7	8.187	1	30
8	8.185	2	30
9	8.202	1	30
10	8.202	2	30
Average	8.193	in.	

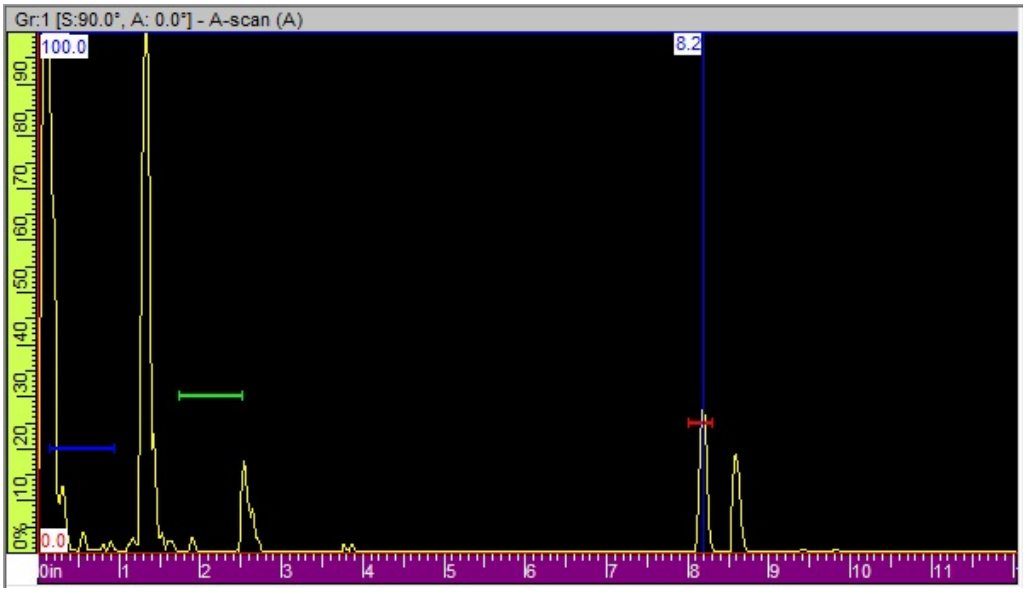

Figure B.11: File109 A-scan showing Keyhole #2 at 8.2 in. (Testing I.2.1).

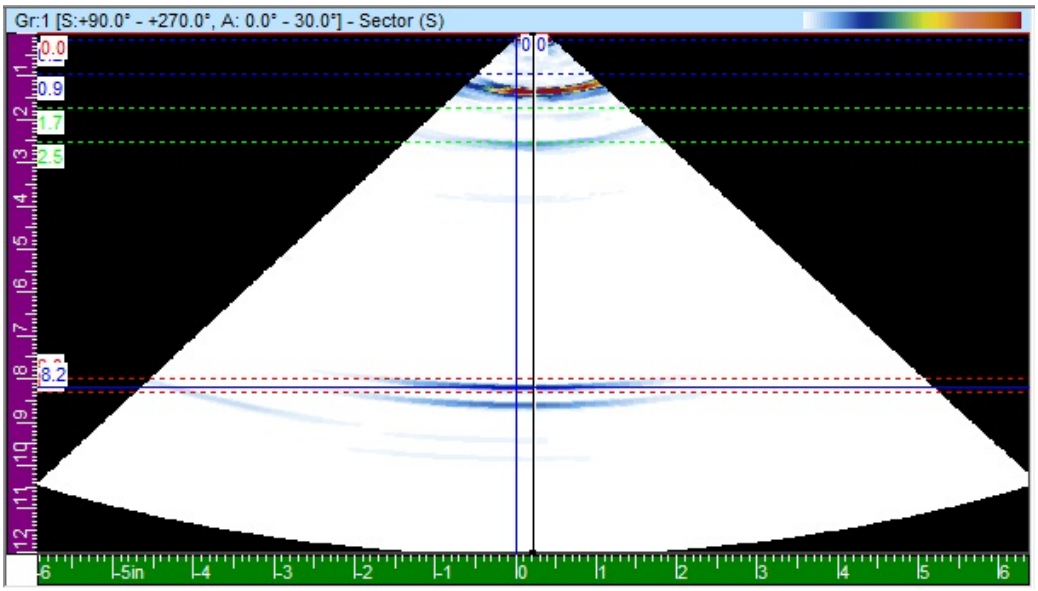

Figure B.12: File109 S-scan showing Keyhole #2 at 8.2 in. (Testing I.2.1).

Figure B.13: Readings for Keyhole #2 using -6dB method (Testing I.3).

Figure B.14: Measurements of the keyholes used to verify with the -6dB method measurements (Testing I.3).

Table B.3: Keyhole #1 Readings from -6dB Method, using a Gain of 32dB (Testing I.3).

Gain(%)	Keyhole #	Δ (in.)	Δ+6 (in.)
40	1	1.25	7.25
40	1	1.75	7.75
40	1	1.875	7.875
40	1	2	8
40	1	2.25	8.25
40	1	2.4375	8.4375
40	1	2.875	8.875
40	1	3.25	9.25
40	1	4.125	10.125
40	1	4.75	10.75
40	1	5.125	11.125
40	1	5.25	11.25
40	1	5.375	11.375

Table B.4: Keyhole #2 Readings from -6dB Method, using a Gain of 32dB (Testing I.3).

Gain(%)	Keyhole #	Δ (in.)	Δ+5 (in.)
40	2	2	7
40	2	2.125	7.125
40	2	2.25	7.25
40	2	2.3125	7.3125
40	2	2.4375	7.4375
40	2	2.5	7.5
40	2	2.75	7.75
40	2	3.25	8.25
40	2	3.4375	8.4375
40	2	4.25	9.25
40	2	4.375	9.375
40	2	5.5	10.5
40	2	5.75	10.75
40	2	5.875	10.875
40	2	5.9375	10.9375
40	2	6.125	11.125

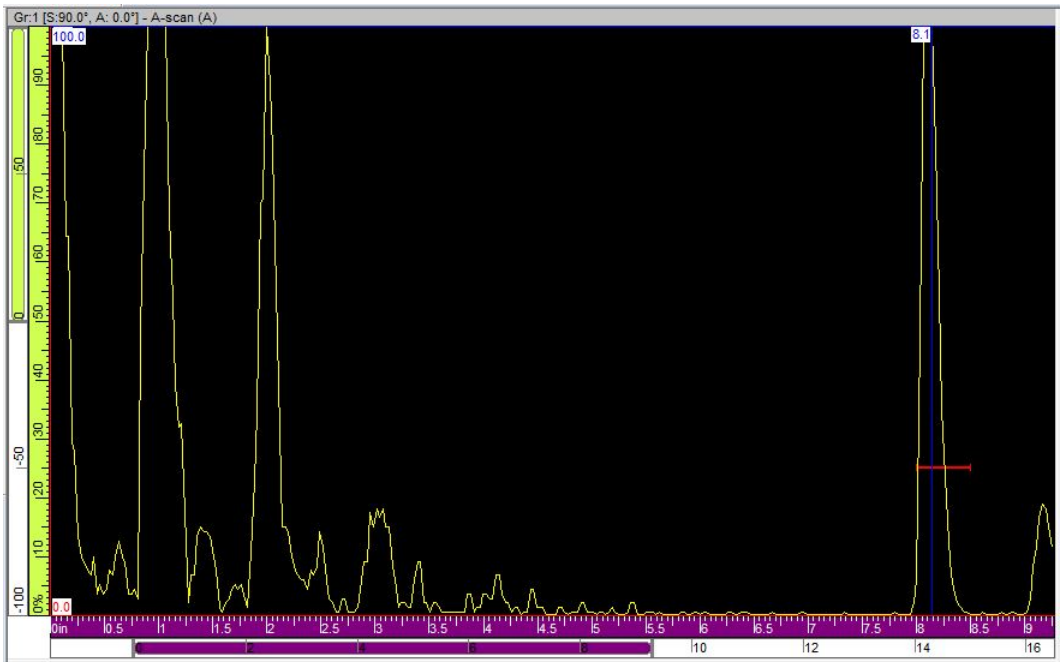

Figure B.15: File0145 A-scan of Exterior Edge with calibrated PMMA Case II (Testing I.1.2).

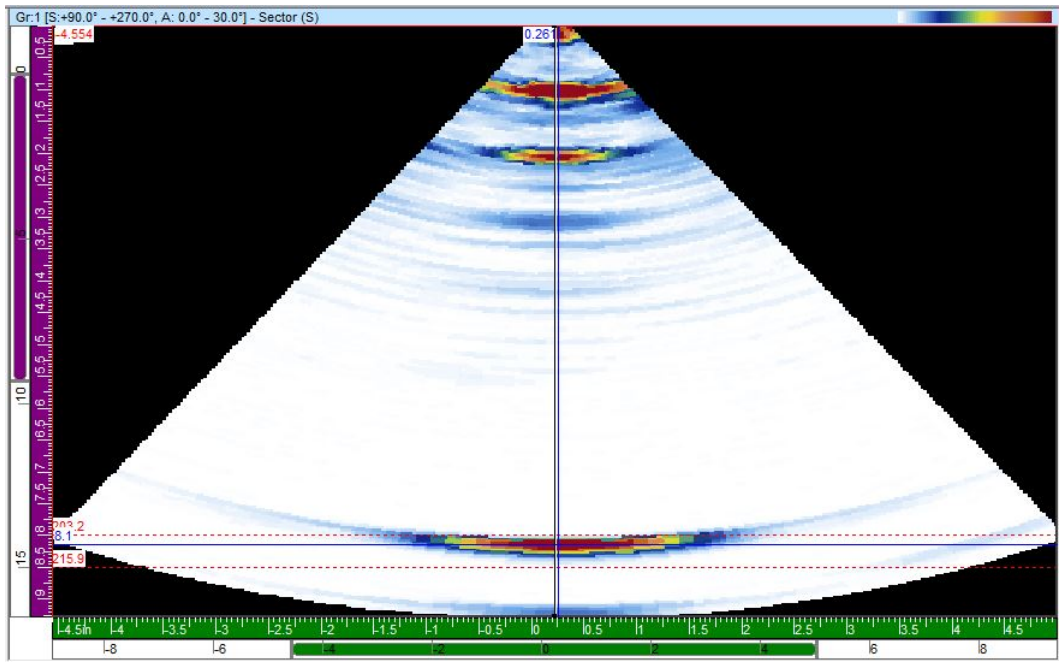

Figure B.16: File0145 S-scan of Exterior Edge with calibrated PMMA Case II (Testing I.1.2).

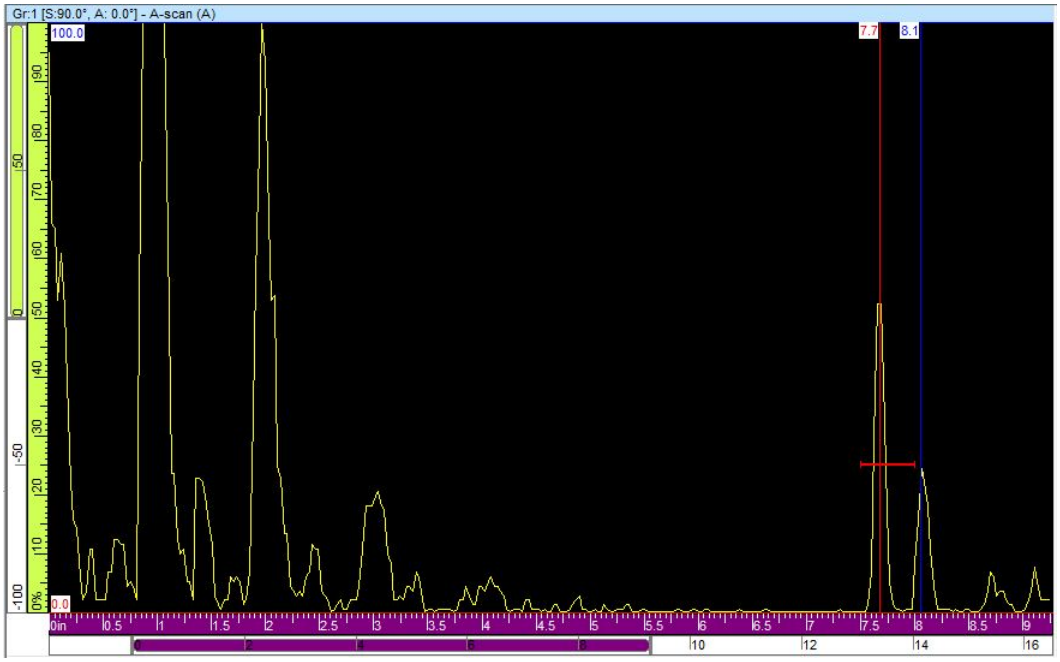

Figure B.17: File0144 A-scan of Keyhole 1 with calibrated PMMA Case II (Testing I.2.2).

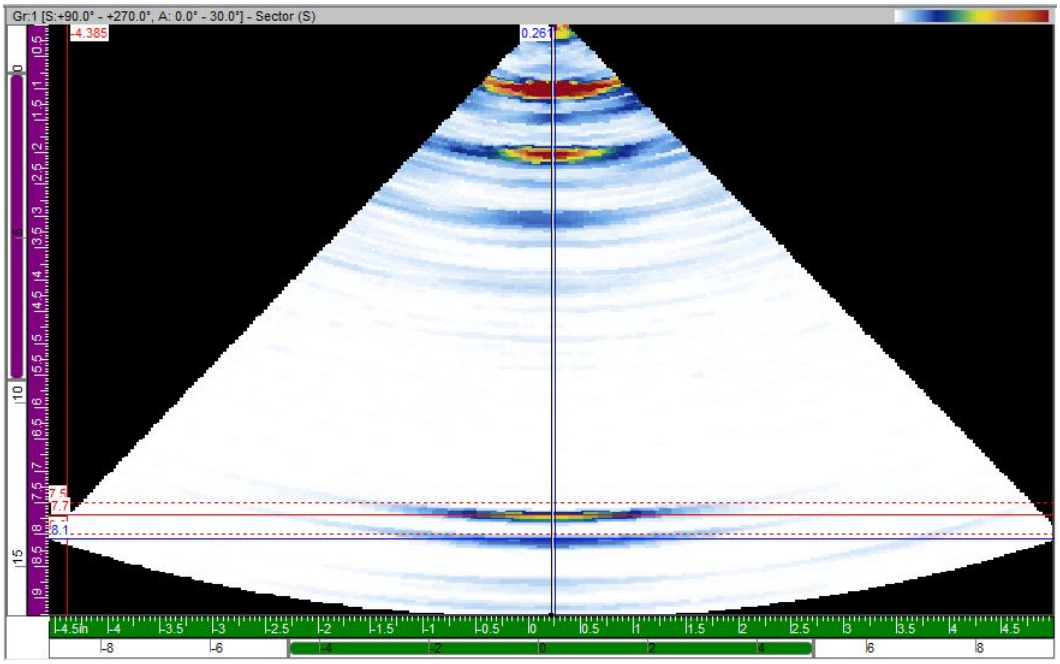

Figure B.18: File0144 S-scan of Keyhole 1 with calibrated PMMA Case II (Testing I.2.2).

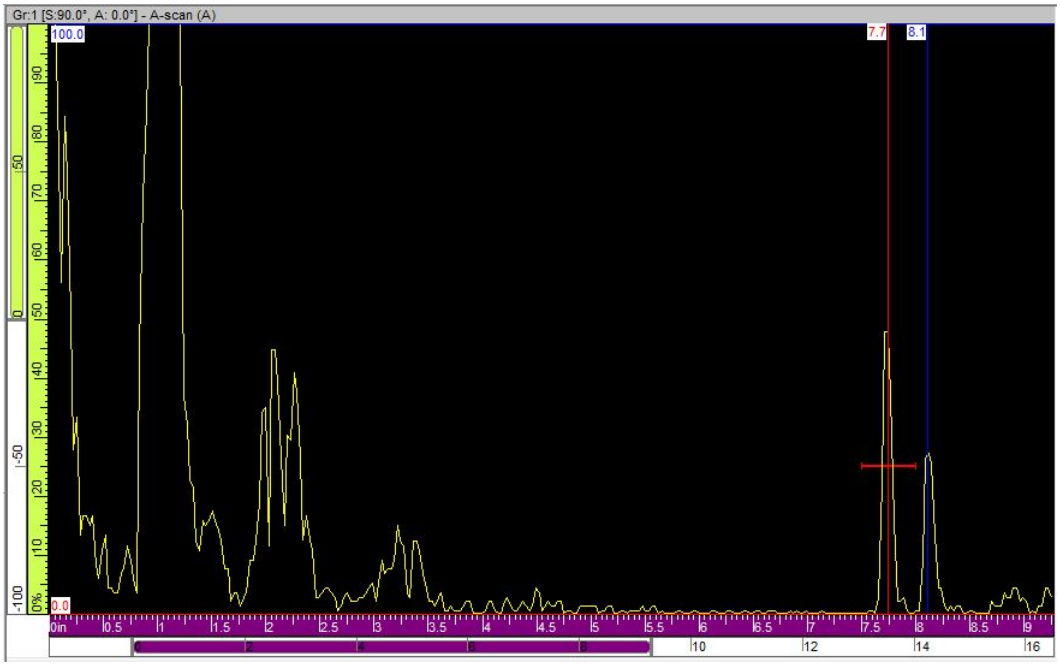

Figure B.19: File0143 A-scan of Keyhole 2 with calibrated PMMA Case II (Testing I.2.2).

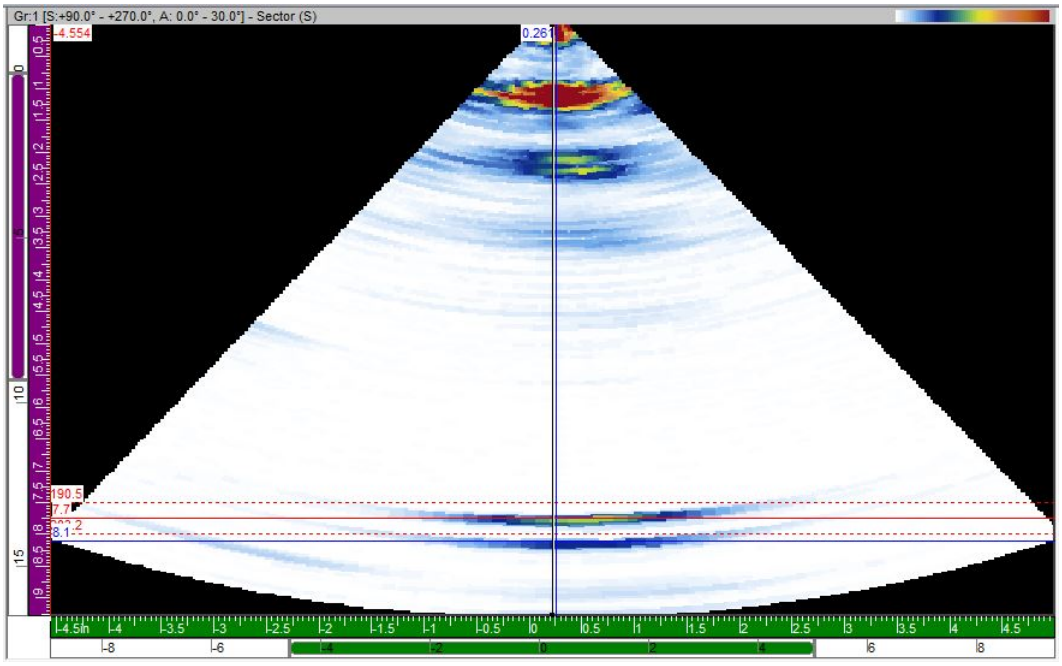

Figure B.20: File0143 S-scan of Keyhole 2 with calibrated PMMA Case II (Testing I.2.2).

B.3 Wedge Calibration

Table B.5: Testing I.1.2 for PMMA Case II Using a 0.44 in. Wedge Height.

Trial	Reading (in.)	dB
1	8.34	40
2	8.355	40
3	8.325	40
4	8.32	40
5	8.369	40
6	8.374	40
7	8.32	40
8	8.327	40
9	8.288	40
10	8.335	40
Average	8.335	in.
Target	8.565	in.
% Error	2.68	%

Table B.6: Testing I.2.2 for PMMA Case II Using a 0.44 in. Wedge Height.

Trial	Reading (in.)	dB	KH
1	7.979	40	1
2	7.924	40	1
3	7.938	40	1
4	7.941	40	1
5	7.927	40	1
6	7.97	40	2
7	7.931	40	2
8	7.935	40	2
9	7.949	40	2
10	7.938	40	2
Average	7.9432	in.	
Target	7.943	in.	
% Error	3.01	%	

Table B.7: Wedge Height Calibration Analysis Testing the Exterior Edge, Using a 40dB gain.

Wedge Height (in.)	Reading (in.)
0.69	7.941
0.19	8.895
0.35	8.521
0.4	8.435
0.38	8.503
0.34	8.575
0.65	7.935
0.6	8.03

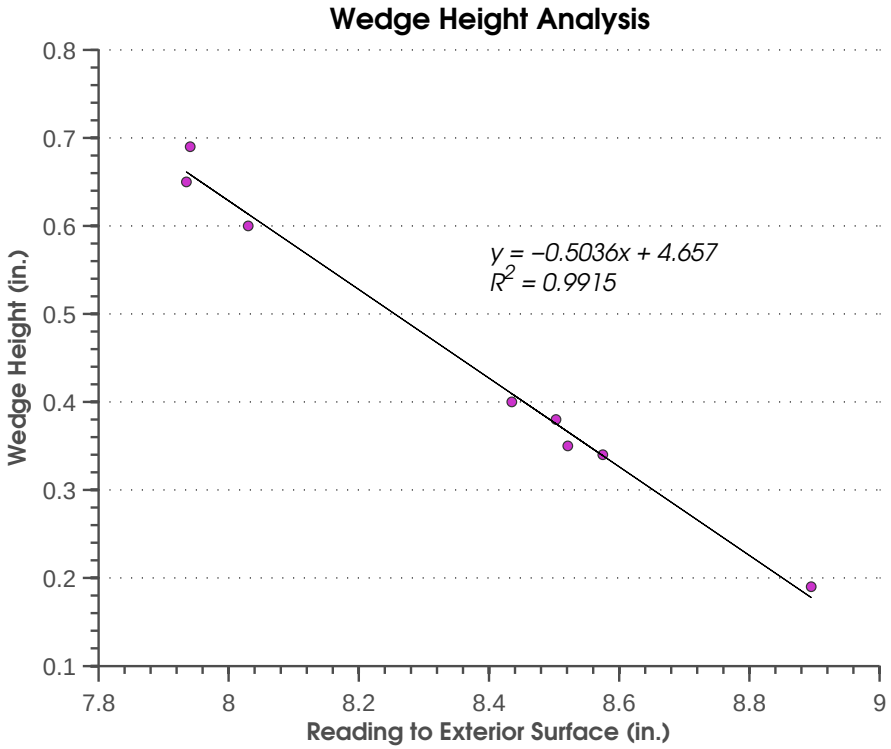

Figure B.21: Wedge Height Relationship Analysis.

APPENDIX C

FIELD TESTING

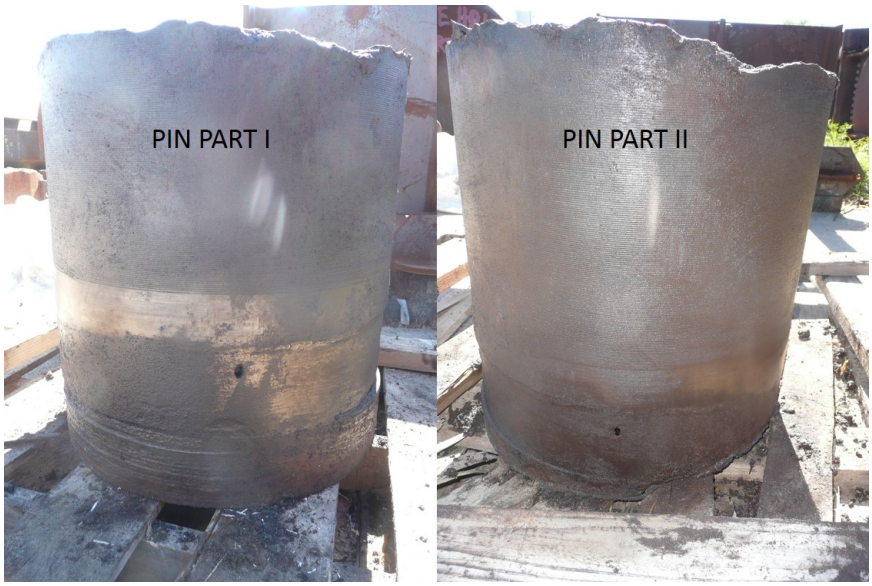

Figure C.1: Grease holes in both Pin Parts I and II during the visual inspection.

Table C.1: Testing I.1.3 for Pin Part I, from Omniscan (55dB).

Depth (in.)	Polar (deg)	A-scan reading (in.)
9.75	45	8.137
9.25	20	8.114
11	300	8.135
13	335	8.1
9	210	8.133
14	250	8.135
10.5	140	8.105
9.5	120	8.122
12.5	170	8.103
13.5	0	8.146
Average	8.123	in.
Target	8.125	in.
% Error	0.02	%

Table C.2: Testing I.1.3 of Pin Part II, from Omniscan (55dB).

Depth (in.)	Polar (deg)	A-scan reading (in.)
8	125	8.015
9.5	170	8.002
7.5	60	8.091
8.5	80	8.08
7	0	8.254
8	310	8.22
7.25	210	8.018
8	250	8.175
9.5	185	8.02
7.75	380	8.152
Average	8.1027	in.
Target	8.125	in.
% Error	0.27	%

Table C.3: Exterior Edge Readings (Testing I.1.3) from top 3.5 in. of Pin Part I, from Omniscan (55dB).

Depth (in.)	Polar (deg)	A-scan reading (in.)
2.5	0	6.889
	330	6.91
	235	7.075
	200	7.01
	160	6.958
	130	6.925
	60	6.94
	80	6.891
	20	6.928
	70	6.972
	90	7.049
Average	6.959	in.
Target	6.935	in.
% Error	0.34	%

Table C.4: Testing 1.2.3 of Pin Part I, from Omniscan (55dB).

KH	Depth (in.)	Polar (deg)	A-scan reading (in.)
1	2.5	320	6.55
1	2.5	320	6.545
1	2.5	320	6.527
1	2.5	320	6.537
1	2.5	320	6.525
1	2.5	320	6.541
1	2.5	320	6.528
1	2.5	320	6.512
1	2.5	320	6.545
1	2.5	320	6.504
		Average	6.5314

Table C.5: Testing I.2.3 Keyhole 2 Readings of Pin Part I, from Omniscan (55dB).

KH	Depth (in.)	Polar (deg)	A-scan reading (in.)
2	2.5	150	6.64
2	2.5	150	6.623
2	2.5	150	6.61
2	2.5	150	6.68
2	2.5	150	6.675
2	2.5	150	6.654
2	2.5	150	6.652
2	2.5	150	6.625
2	2.5	150	6.65
2	2.5	150	6.608
		Average	6.6417

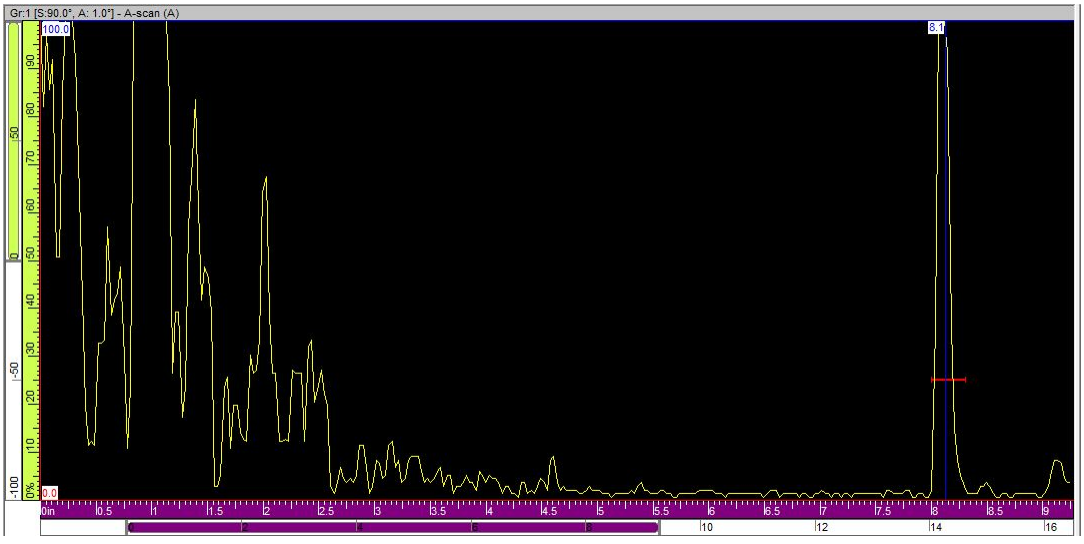

Figure C.2: File146 A-scan showing the exterior edge for Pin Part I (Testing I.1.3).

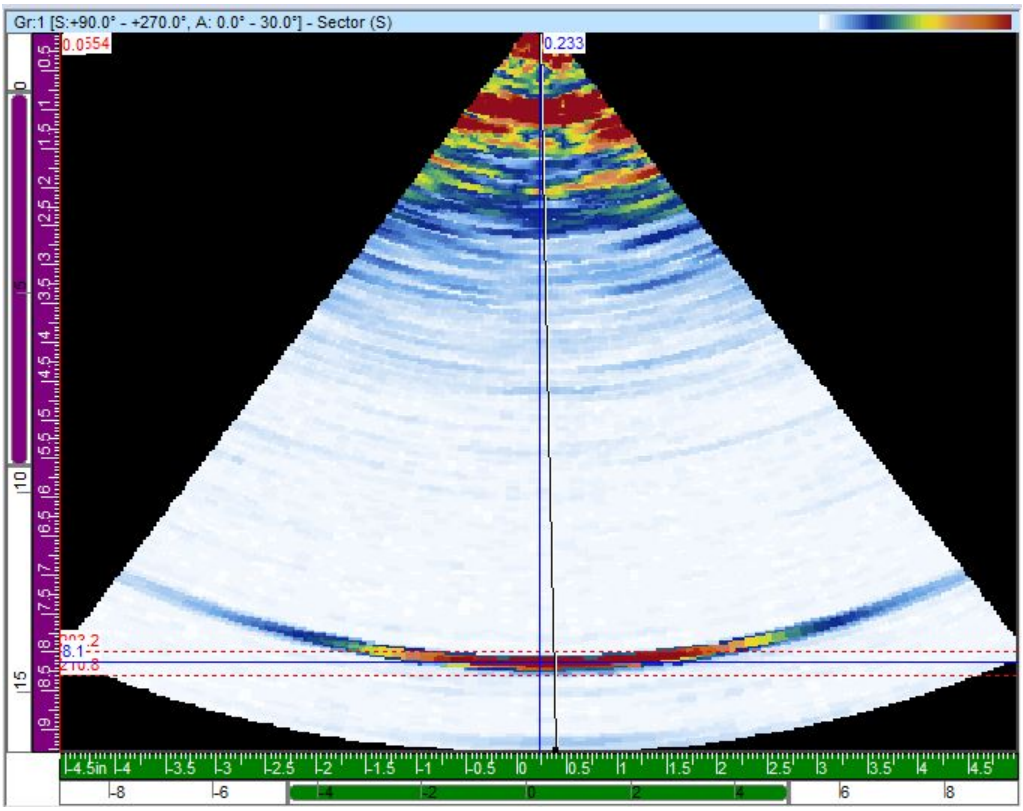

Figure C.3: File146 S-scan showing the exterior edge for Pin Part I (Testing I.1.3).

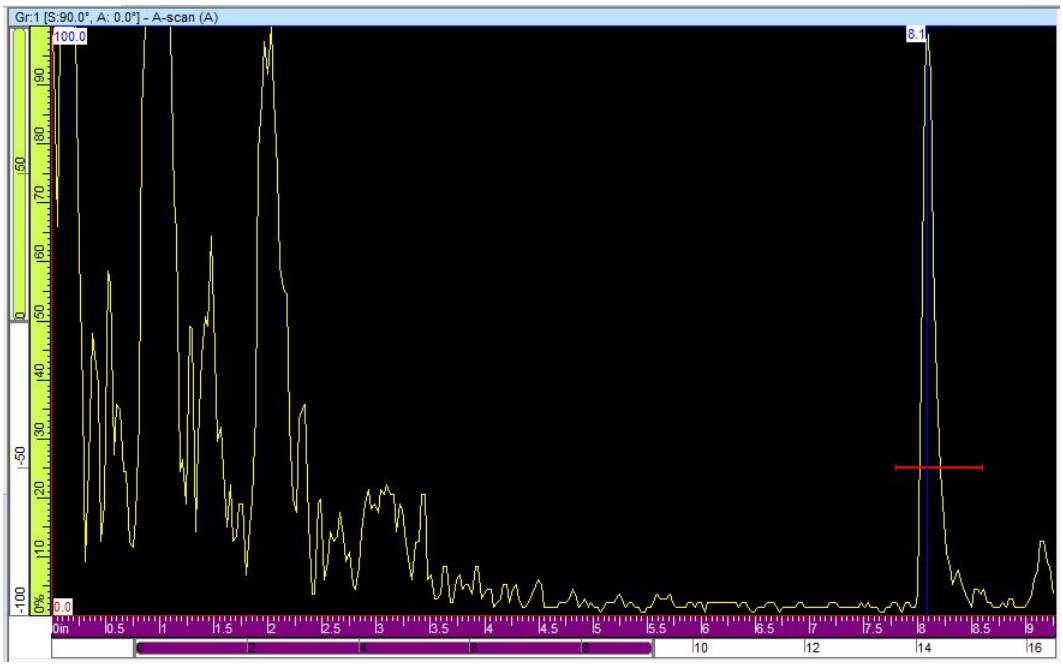

Figure C.4: File154 A-scan showing the exterior edge for Pin Part II (Testing I.1.3).

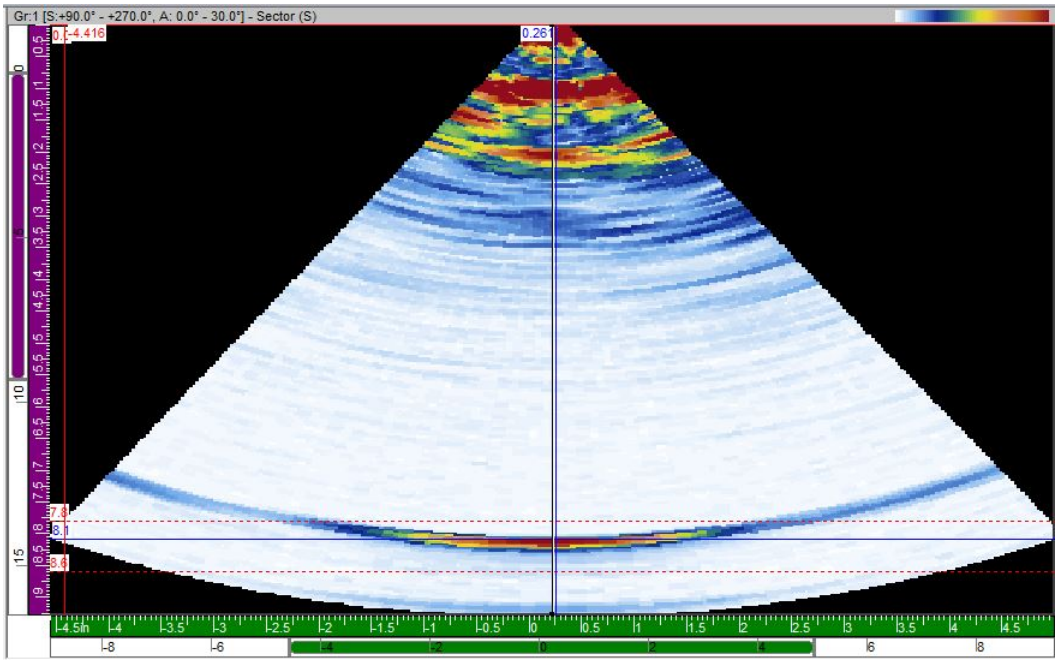

Figure C.5: File154 S-scan showing the exterior edge for Pin Part II (Testing I.1.3).

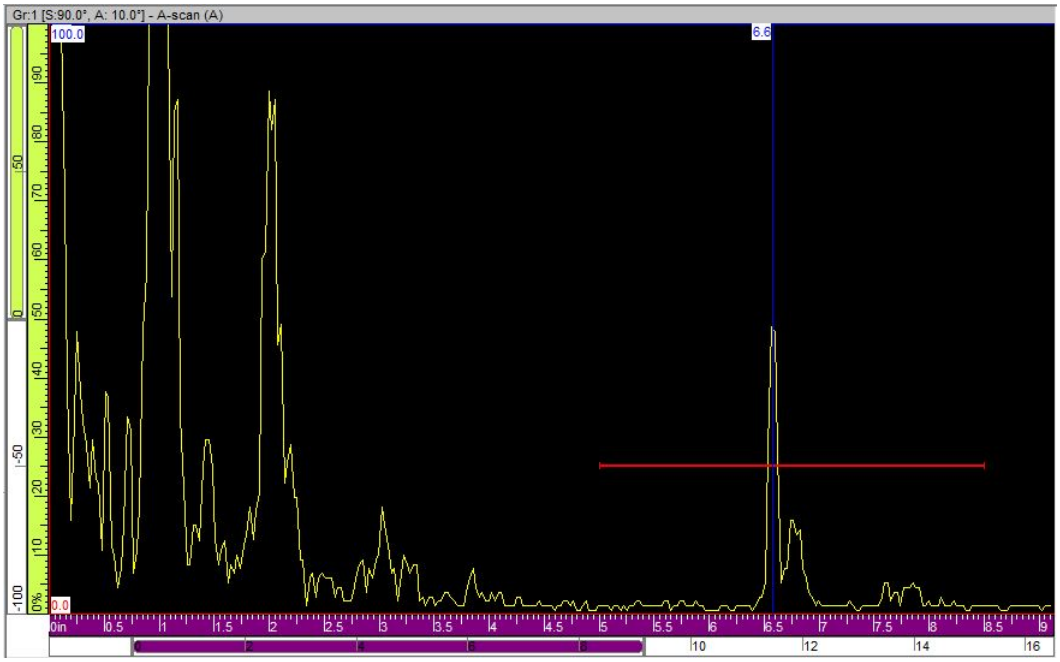

Figure C.6: File156 A-scan showing the exterior edge for the top 3.5 in. of Pin Part I (Testing I.1.3).

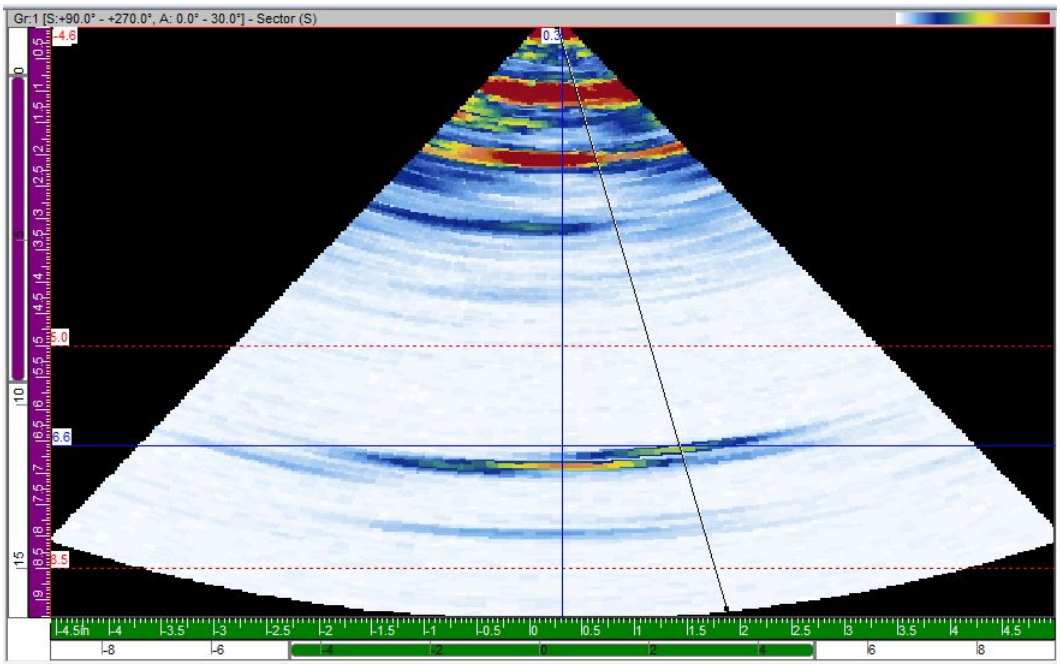

Figure C.7: File156 S-scan showing the exterior edge for the top 3.5 in. of Pin Part I (Testing I.1.3).

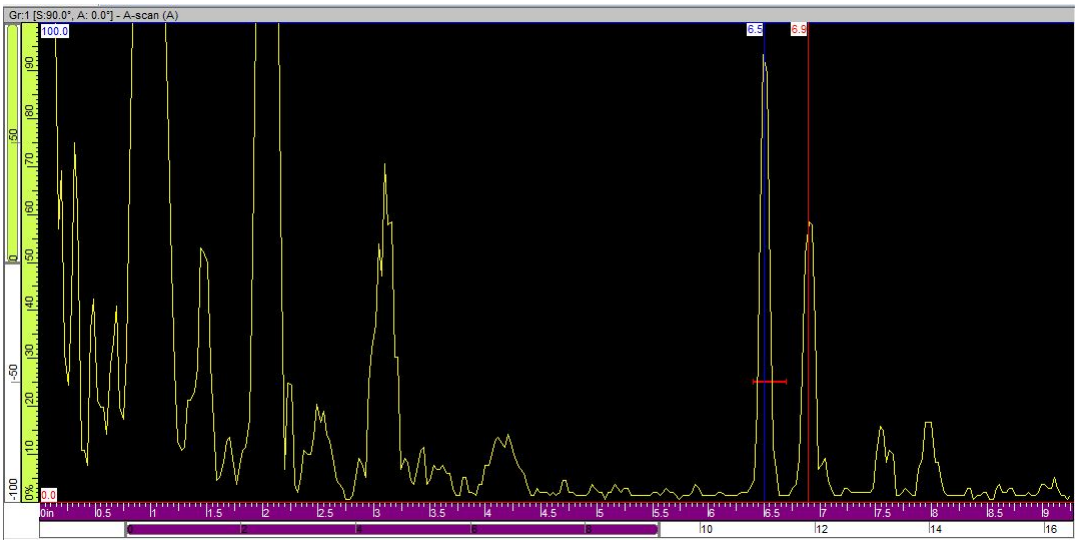

Figure C.8: File165 A-scan for Keyhole 1 of Pin Part I (Testing I.2.3).

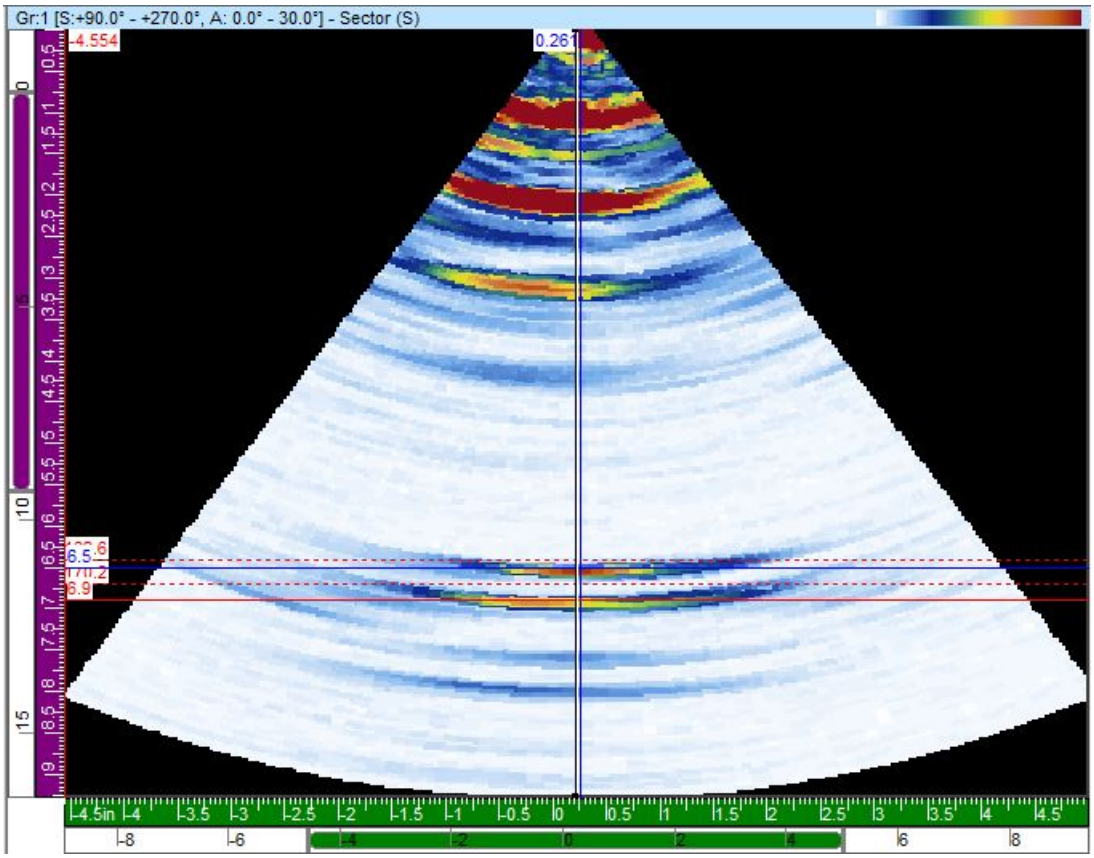

Figure C.9: File165 S-scan for Keyhole 1 of Pin Part I (Testing I.2.3).

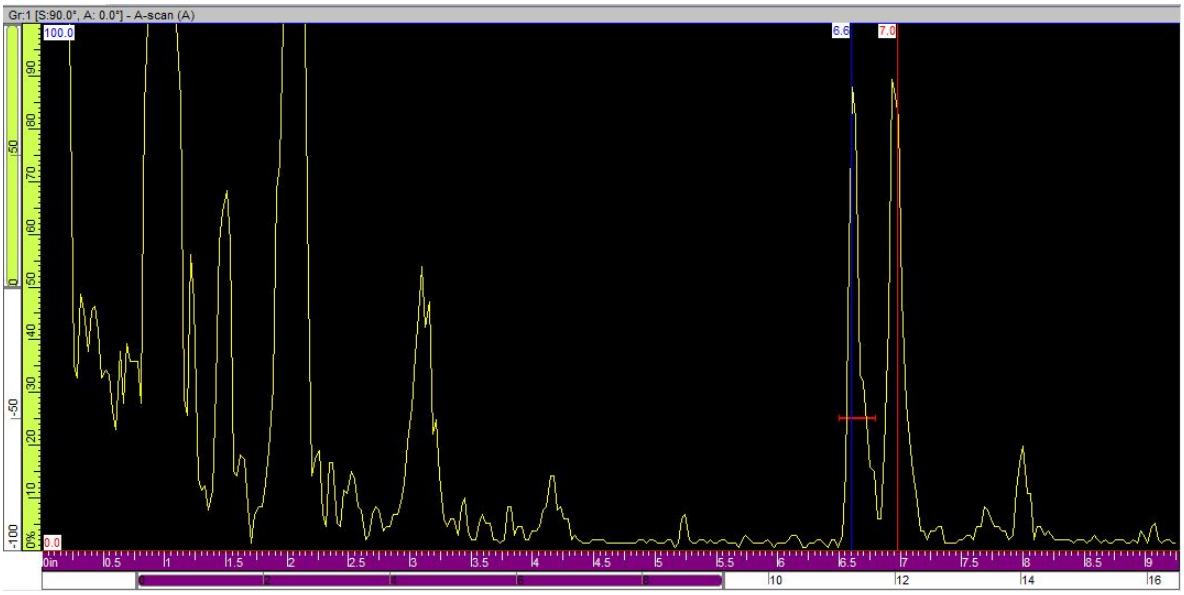

Figure C.10: File163 A-scan for Keyhole 2 of Pin Part I (Testing I.2.3).

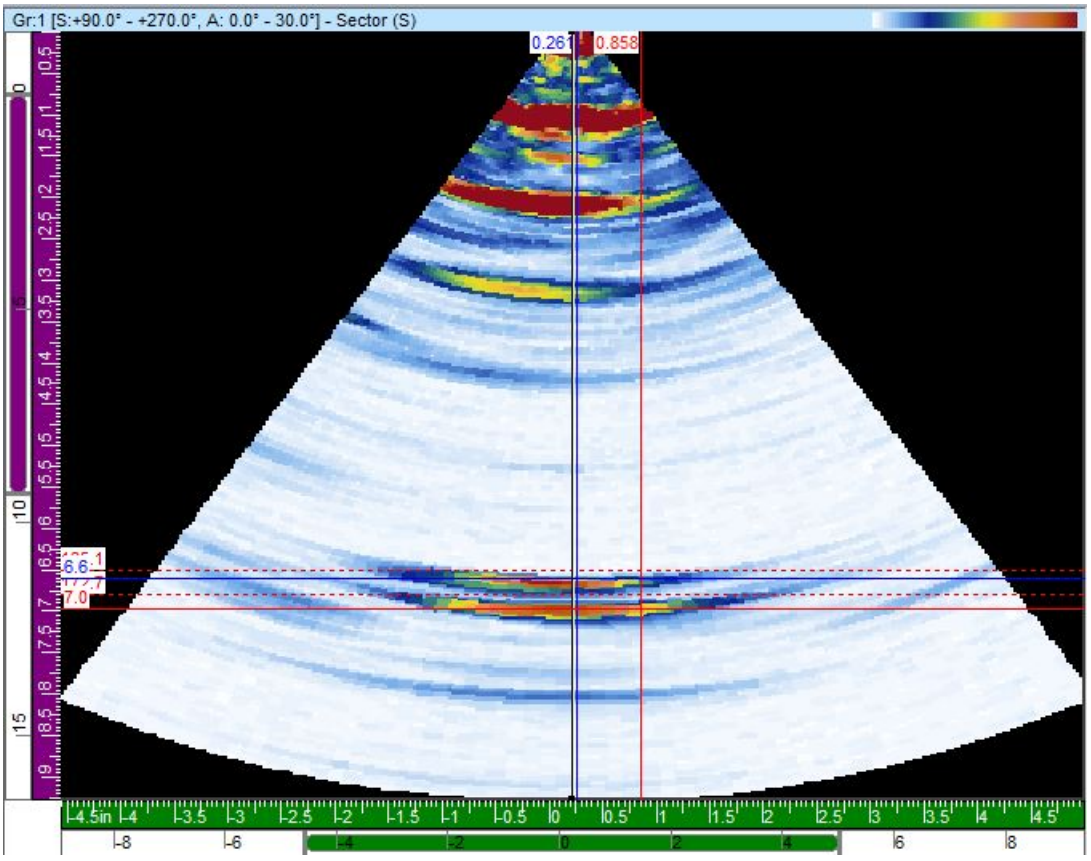

Figure C.11: File163 S-scan for Keyhole 2 of Pin Part I (Testing I.2.3).

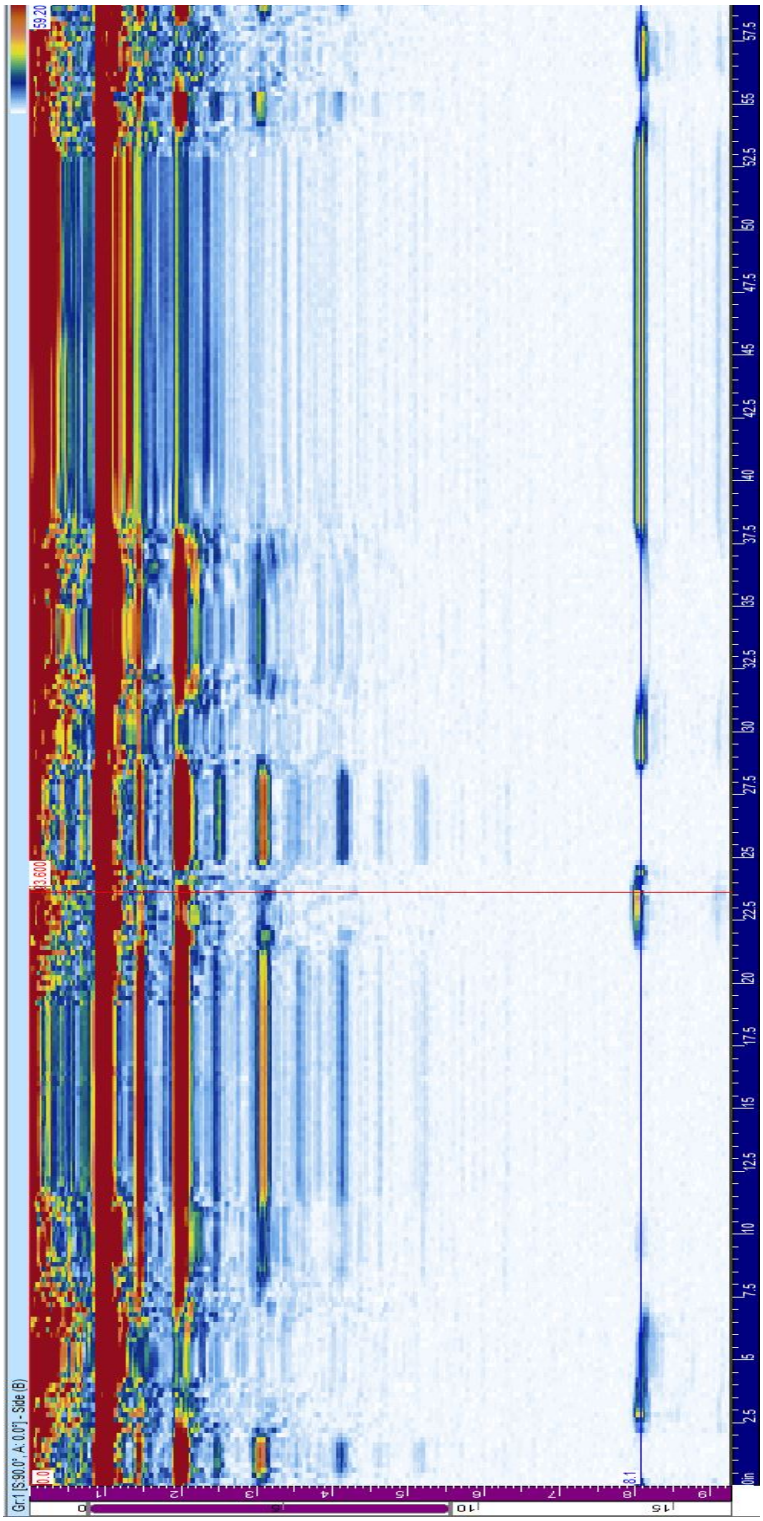

Figure C.12: File174 showing the 360 degree of Pin Part II (Testing I.4).

APPENDIX D

MATLAB CODES

This MATLAB program was used to depict the readings from the exterior inspections using a SA5-N60S 5L32 wedge and probe. The transducer location is taken from the S-scan.

D.1 Matlab Parameters

The parameters used for the MATLAB program are shown in Table D.1.

Table D.1: Parameters used for MATLAB run.

Parameters	Values
Y	-5.5 in.
Z	-2.25 in.
Beam Angle	45°
Slope, tanθ	1
Z-intersection, b	-3.25 in.

D.2 Matlab script: Hole_Inspection.m

Hole_Inspection.m

```
clear; clc;
% -------------- Hole Inspection Program ------------------- %
% Used to detect location of hole from S-scan.               %
%                                                            %
% Roldan, A.                                                 %
% Last Modified: 7/9/13                                      %
% ---------------------------------------------------------- %

% Hole Info
int_hole = [0,0,0];
ext_hole = [-8,0,-8.5];

xhole = int_hole(1):-0.1:ext_hole(1);
yhole = linspace(int_hole(2),ext_hole(2),length(xhole));
zhole = (ext_hole(3)/ext_hole(1)).*xhole;

% Transducer Location
% Tx = input('Transducer x-loc: ');
% Ty = input('Transducer y-loc: ');
% Tz = input('Transducer z-loc: ');
Tx = -5.5; Ty=-5.5;Tz=-2.25;

transducer_loc = [Tx,Ty,Tz]; clc

%Dce = input('Distance from Transducer to Hole Inspection: ');
%T_angle = input('Angle of Inspection, or 0 if none: '); clc;

% Transducer Location - Angle Calc
Dist_trans = Distance(Tx,Ty,Tz,int_hole(1),...
    int_hole(2),int_hole(3));

xtheta = acosd( Tx/Dist_trans);
ytheta = acosd(Ty/Dist_trans);
ztheta = acosd(Tz/Dist_trans);

```

```
    % Transducer Beam path
    % 25 deg
    DEG = 25;
    Z1 = -2.25:-0.1:-8;
    [m,b,Y1] = transducer_beam(DEG,Ty,Tz,Z1);
    X1 = ones(1,length(Z1))*Tx;
    % 75 deg
    DEG = 75;
    Z2 = -2.25:-0.1:-5;
    [m,b,Y2] = transducer_beam(DEG,Ty,Tz,Z2);
    X2 = ones(1,length(Z2))*Tx;


    % Trans INSPECTION
    T_angle = 45; % degrees
    Z = -2.25:-0.1:-9;
    [m,b,Y] = transducer_beam(T_angle,Ty,Tz,Z);
    X = ones(1,length(Z))*Tx;

    % Plotting Pin
    ang = 0:0.01:2*pi;
    R1 = 6; R2 = 9.625;
    z = ones(length(ang)); z = z(1,:);
    xp1 = R1*cos(ang); yp1 = R1*sin(ang); ...
        x1 = z*1.6875; zp1=z*2.25;
    xp2 = R2*cos(ang); yp2 = R2*sin(ang); ...
        x2 = z*1.4115; zp2=z*-2.25;
    zp3 = z*-22;
    % Pin_LVL1 = [xp1;yp1;zp1]; Pin_LVL2 = [xp2;yp2;zp2];
    figure(1)
    plot3(xp1+x1,yp1,zp1,'k'); hold on;
    plot3(xp1+x1,yp1,z*-2.25,'k')
    plot3(xp2+x2,yp2,zp2,'k');
    plot3(xp2+x2,yp2,zp3,'k');

    grid on

    % Plotting Hole
    plot3(0,0,0,'r.')
    plot3(ext_hole(1),ext_hole(2),ext_hole(3),'r.')

    % TRANSDUCER PLOT
    plot3(Tx,Ty,Tz,'g*')
    plot3(xhole,yhole,zhole,'r-') % hole line
    plot3(X1,Y1,Z1,'g'); plot3(X2,Y2,Z2,'g')

    plot3(X,Y,Z)


    % hole -- from calculations
    plot3(-7.29,0,-7.75,'go')

    % plotting options
    xlabel('X')
    ylabel('Y')
    zlabel('Z')
    % Plotting Specifications
    line_width = 1;
    font_size = 14;
    mkr_size = 6;
    set(0,'DefaultLineLineWidth',line_width);
    set(0,'DefaultAxesFontSize',font_size);
    set(0,'DefaultLineMarkerSize',mkr_size);
```

D.3 Matlab function: Transducer_Beam.m

transducer_beam.m

```
function[m,b, Y] = transducer_beam(trans_angle, y,z, Z)
% trans_angle should be in DEGREES
 % (y,z) should be location of transducer
 % Z is an array to calculate Y points to plot

 m = -tand(trans_angle);
 b = y - m*z;

 Y = m*Z+b;
```

D.4 Matlab function: Distance.m

Distance.m

```
function [D] = Distance(x1,y1,z1,x2,y2,z2)

 D = sqrt( (x1-x2)^2 + (y1-y2)^2 + (z1-z2)^2 );
```